Development of novel nanostructured drug carrier systems for targeting of human macrophages for inhalation treatment

Dissertation

zur Erlangung des Grades

des Doktors der Naturwissenschaften

der Naturwissenschaftlich-Technischen Fakultät

der Universität des Saarlandes

von

Thorben Fischer

Saarbrücken

2021

Tag des Kolloquiums: 09. September 2021

Dekan: Prof. Dr. Christian Motz

Berichterstatter: Prof. Dr. Marc Schneider
Prof. Dr. Alexandra K. Kiemer

Vorsitz: Prof. Dr. Andriy Luzhetskyy

Akad. Mitarbeiter: Dr. Stefan Boettcher

''Persistence is very important. You should not give up

unless you are forced to give up.''

Elon Musk, 2019

Table of contents

I   Summary

The modification of the particle shape for drug delivery systems to address the lungs offers a new field in the development of inhalable therapies. By using aspherical forms, advantageous properties are generated, which can be used for the treatment of various lung diseases. Thereby, the efficient and targeted transport of drugs with a modification of the uptake rate of immunologically active cell populations as well as an increased loading capacity due to the larger surface area compared to spherical particles, are in focus.

In the present work, a nanostructured, cylindrical particle system in the micrometre range was developed, which was loaded with a specific small interfering RNA (siRNA) for inhibition of tumour necrosis factor alpha (TNF-α) to generate an anti-inflammatory effect in alveolar macrophages. In a first step, the obtained microparticles were characterized with respect to their aerodynamic properties. The measured results showed positive aerodynamic properties, which indicates a possible pulmonary application. Furthermore, both alveolar epithelial cells and macrophages showed good particle tolerance. Additionally, *in vitro* tests demonstrated that a significant inhibition of TNF-α could be induced by the particle system. These results could be further improved by modifying the delivery system to load an additional drug to enhance the anti-inflammatory effect, making the formulation developed in this thesis a possible carrier system for pulmonary administration.

II   Zusammenfassung

Die Modifizierung der Partikelform von Arzneistoffträgersystemen zur Applikation der Lunge eröffnet ein neues Feld in der Entwicklung von inhalativen Therapien. Durch die Verwendung asphärischer Formen werden positive Eigenschaften generiert, welche für die Behandlung verschiedener Lungenerkrankungen genutzt werden können. Dabei steht besonders der effiziente und gezielte Transport von Arzneistoffen im Fokus, der zudem, aufgrund der Form, auch die Aufnahmegeschwindigkeit durch immunologisch aktive Zellen verändert.

In der vorliegenden Arbeit wurde ein nanostrukturierter, zylindrischer Wirkstoffträger im mikropartikulären Größenbereich entwickelt. Dieser wurde mit einer spezifischen siRNA zur Inhibition der TNF-α Sekretion beladen, um eine anti-inflammatorische Wirkung in Makrophagen zu erzeugen. Die erhaltenen Mikropartikel wurden in einem ersten Schritt hinsichtlich ihrer Flugeigenschaften charakterisiert. Die Messergebnisse wiesen positive aerodynamische Eigenschaften auf, was eine pulmonale Applikation möglich macht. Außerdem zeigten sowohl alveolare Epithelzellen als auch Makrophagen eine gute Partikelverträglichkeit. *In vitro* Testungen haben weiterhin gezeigt, dass eine signifikante Inhibition von TNF-α durch das Partikelsystem und damit eine Hemmung der inflammatorischen Eigenschaften, hervorgerufen werden konnte. Die Kombination aller Ergebnisse zeigt, dass die in dieser Arbeit entwickelte Formulierung ein mögliches Trägersystem zur pulmonalen Administration darstellt.

III   Abbreviations

ACI	Andersen cascade impactor
AR	aspect ratio
bPEI	branched polyethyleneimine
CF	cystic fibrosis
CFTR	cystic fibrosis transmembrane conductance regulator
CLSM	confocal laser scanning microscopy
COPD	chronic obstructive pulmonary disease
DAPI	4',6-diamidino-2-phenylindole
DCE	dichloroethane
Dex. Sulph.	dextran sulphate
DMSO	dimethyl sulphoxide
DNA	deoxyribonucleic acid
DPI	dry powder inhalers
dsRNA	double stranded RNA
dTHP-1	differentiated macrophage-like THP-1 cells
ELISA	Enzyme Linked Immunosorbent Assay
EMA	European Medicines Agency
FCS	fetal calf serum
FDA	Food and Drug Administration
FPF	Fine Particle Fraction
GSD	Geometric Standard Deviation
ICP-MS	inductively coupled plasma mass spectroscopy
ICRP	International Commission on Radiological Protection
IgA	Immunoglobulin A
IL	Interleukin
LDH	lactate dehydrogenase
LPS	lipopolysaccharide
MDI	metered dose inhalers
MMAD	Mass Median Aerodynamic Diameter
MTT	3-(4,5-Dimethylthiazol-2-yl)-2,5-diphenyltetrazoliumbromid
NC	negative control

NF-κB	nuclear factor 'kappa-light-chain-enhancer' of activated B-cells
NGI	Next Generation Impactor
nt	nucleotide
PBS	phosphate-buffered saline
PC	positive control
Ph. Eur.	European Pharmacopoeia
PMA	phorbol 12-myristate 13-acetate
RISC	RNA-induced silencing complex
RNA	ribonucleic acid
RNAi	RNA interference
SDS	sodium dodecyl sulphate
SEM	scanning electron microscopy
shRNA	short hairpin RNA
siRNA	small interfering ribonucleic acid
SNP	silica nanoparticle
TAM	tumour-associated macrophage
THF	tetrahydrofuran
TNF-α	tumour necrosis factor alpha
WHO	World Health Organization

1.   Introduction

Respiratory diseases are among the most common diseases worldwide because of their broad distribution in the human population and a mortality rate of 20% [17, 18]. Thereby, a distinction can be made between acute and chronic forms. An acute illness of the lungs is an infection with a pathogenic germ such as bacteria, viruses, or fungi, which subsides after successful treatment. In contrast, the symptoms of a chronic course extend over a longer period of time without any improvement. The most common representatives for this clinical pattern are asthma bronchial, chronic obstructive pulmonary disease (COPD) cystic fibrosis (CF) and chronic bronchitis [19-21]. These diseases can be addressed by different types of application, including inhalativ, oral or intravenous. However, for pulmonary diseases the last two application routs named combine different disadvantages like low drug availability in the target tissue caused by the first-pass metabolism as well as possible side effects [22, 23]. For these reasons, a pulmonary application is preferred. Since the airways are often narrowed in chronic lung diseases and chronic inflammation of the bronchial tubes and deep lungs predominates, glucocorticoids and β-agonists are used as standard therapy [24, 25]. However, the choice of inhalation device for the patient is of high importance and influences the therapeutic success [26]. Therefore, many research groups are pursuing to develop new drug delivery systems for pulmonary administration [27-30]. In the following thesis, cylindrical, nanostructured microparticles loaded with a RNA sequence against pro-inflammatory cytokines will be developed. The delivery of oligonucleotides in particular is associated with many hurdles, as both the chemical structure and the low stability in biological media result in low bioavailability [31]. Therefore, it is important to use suitable drug delivery systems that specifically address the lungs in order to transport the drug directly to the target tissue and the associated cells. This allows the therapy to be more efficient and, due to the combination of local application and increased quantity of loading from aspheric delivery system caused by the higher surface area, lower amounts of the formulation are required to achieve the same dose of drug.

In the following chapters, the scientific background of pulmonary applications, including aspheric drug delivery systems, will be explained in more detail. Thereby,

a focus is also placed on the biological processes that occur after the successful deposition of the oligonucleotides.

1.1. Physiological aspects and principles of pulmonary administration

The lungs represent the organ of the human body responsible for the gas exchange of oxygen and carbon dioxide. In this process, oxygen is absorbed from the air and transported to the cells in the body to maintain metabolism. Carbon dioxide is produced as a by-product, which is cleaned from the body by exhalation. The transport medium of these gases in the body is the blood. This is supplied with oxygen in the pulmonary alveoli by diffusion and pumped through the mitral valves into the left ventricle, from where it enters the systemic circulation. There, gas exchange occurs in the tissue capillaries, releasing oxygen into the surrounding cells and absorbing carbon dioxide by the blood. The deoxygenated blood is then pumped in the venous system to the right atrium and transported via the pulmonary artery to the lungs where, due to the prevailing concentration gradient, oxygen is again taken up with the release of carbon dioxide. The respiratory cycle is completed by exhaling the carbon dioxide [32].

To manage this cycle of gas exchange, the lungs have defined regions with different functions to accomplish their task. These areas are divided in the extrathoracic, the tracheobronchial and the alveolar region, as illustrated in Figure 1 [11]. During the inhalation process, air first passes through the conducting airways, which consist of the nasopharynx, the larynx with its narrowest part, the glottis, and the trachea [33]. The trachea passes tubularly in the direction of the lungs and is held in shape by horseshoe-shaped curved cartilaginous clasps with smooth muscle fibres between. At the level of the fifth thoracic vertebra, the trachea bifurcates into the two main bronchi, which enter the lobes of the lung at the hilus. These large bronchi divide into smaller branches, increasing their cross-sectional area [34]. The small bronchi pass into the bronchioles and these into the terminal bronchioles. From the 17th generation of division onwards, the *bronchioli respiratorii* follow, in the walls of which some alveoli are already present. With the 20th generation, the *ductuli alveolares* begin, which are densely occupied with alveoli, increasing the cross-sectional area and slowing down the air movement to enable the most effective gas exchange possible [35].
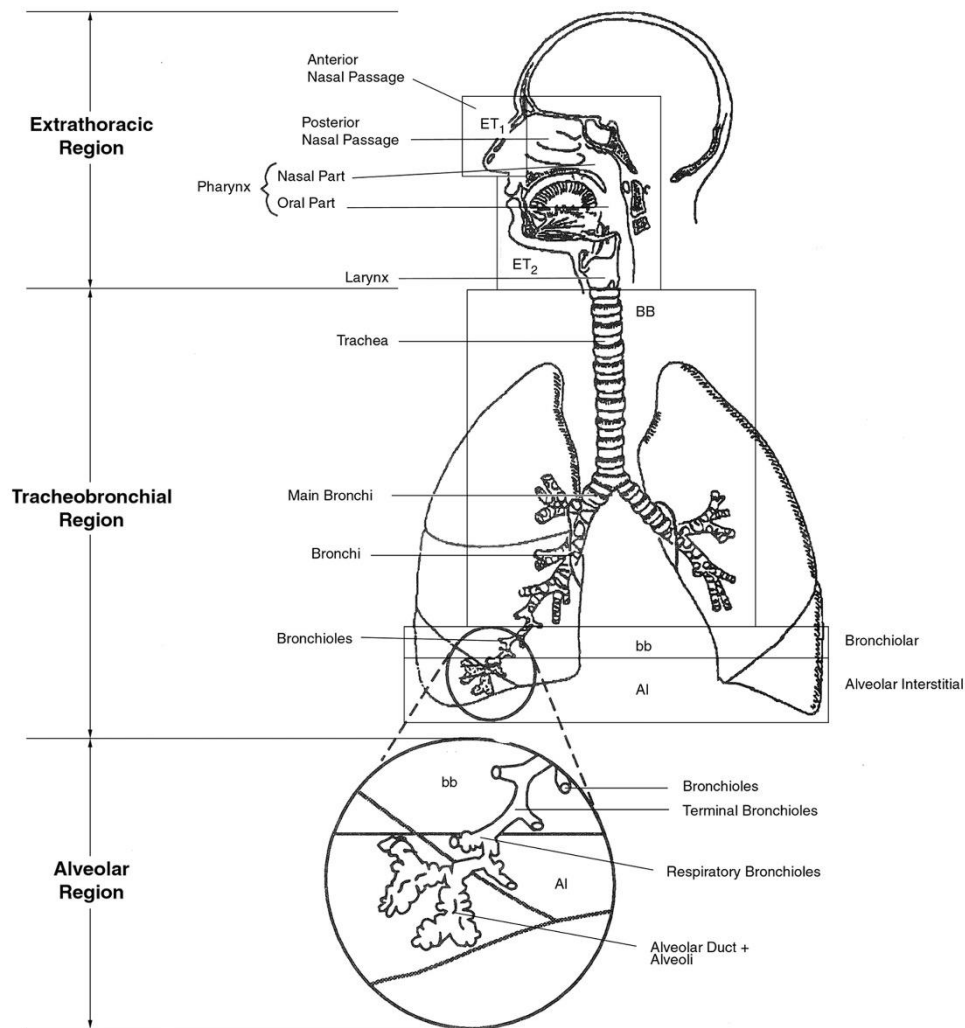
Figure 1: Schematic structure of the anatomical regions of the human respiratory tract. The extrathoracic region forms the first area of the respiratory tract and opens into the trachea and thus the beginning of the tracheobronchial region. Here the trachea branches into the bronchi and from the 3rd to the 15th generation into the bronchioles. From the 16th branching, the terminal bronchioles begin, which flow into the respiratory bronchioles and finally, in the 20th generation, into the alveolar duct and alveoli. Here, a specific surface area from up to 190 m^2 is present to ensure effective gas exchange. Reprinted with permission from [11], Copyright © 2011 Elsevier Ltd.

Although gas exchange occurs in the alveolar region with special types of cells, already on the way from the bronchi to that point there are epithelial cells involved in purifying, humidifying and warming the inhaled air [34]. This pseudostratified columnar epithelium from the conductive airways is formed mainly by ciliated, goblet, basal and brush cells as shown in Figure 2 [36]. The ciliated cells, which form about half of the tracheal epithelium and carry about 250 cilia per cell [37], as well as the brush cells are responsible for the removal of protective mucus, which intercepts contaminants of the inhaled air [33, 38]. The progenitors of the ciliated cells and of Club cells are the basal cells, which are located at the basement

membrane and therefore do not belong to the luminal surface of the epithelium [39]. These Club cells, together with the goblet cells, form the secretory cell types, which are mainly involved in the formation of the mucus layer due to the secretion of various molecules like antimicrobial molecules (defensins, lysozyme and IgA), immunomodulatory molecules (*e.g.*, cytokines) and glycoproteins (called mucins) [40, 41]. As illustrated in Figure 2, the thickness of the mucus layer depends on its location in the airways and varies from 10-30 µm in the tracheal and bronchial regions to 2-5 µm in the smaller bronchioles [5, 42]. The interaction of these different cell types and their functions serves to protect the lungs from inhaled contaminants and is also termed as mucociliary clearance [43].
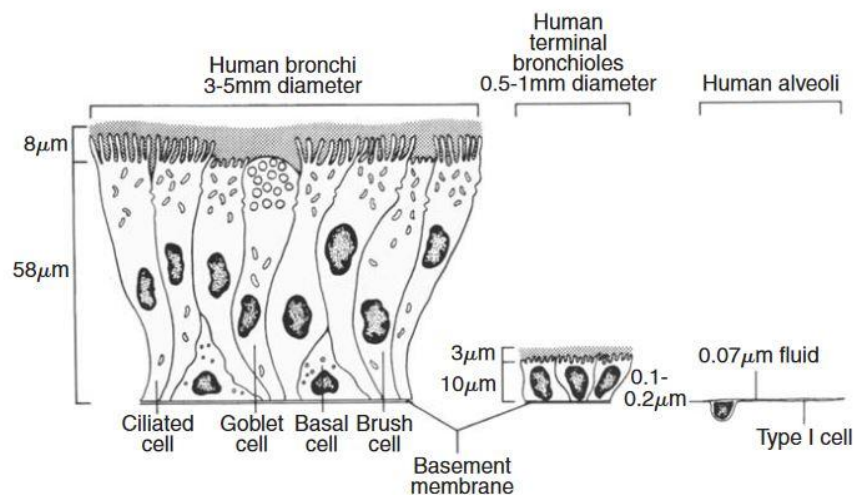
Figure 2: Morphology of different cell types from the bronchial and alveolar region of the human lung. This lateral view on the epithelial cells shows the decreasing thickness of the cells, as well as the mucus layer and cilia from the upper to the deeper lung to ensure an effective gas exchange by lowering the diffusion path. Reprinted with permission from [5], Copyright © 1996 Elsevier B.V.

The route of air in the inhalation process from the extrathoracic region to the deep lungs passes by different types of epithelial cells, which vary in their form and function, as well as in the composition and thickness of the coating fluid (Figure 2). In the deep lungs, which is also known as alveolar region, gas exchange takes place [35]. For this reason, no mucus is present in this area [34]. The epithelium located here consists of several hundred million air sacs, the alveoli. Due to their high degree of branching, they have a large surface area of 100-190 m^2. This allows an effective gas exchange [34]. Responsible for the gas exchange are the thin alveolar type 1 cells (0.1-0.2 µm in the periphery and 2-3 µm in the perinuclear region (Figure 2)), which represents approximately 90% of the alveolar surface and, together with

the capillary endothelium, form the so-called air-blood barrier [37, 44]. As shown in Figure 3A, blood and air are separated only by a thin layer of tissue. This so-called alveolocapillary membrane is composed of the flat alveolar epithelium of type 1 cells, the interstitium with intercalated elastic connective fibres and the capillary endothelium, with a thickness of less than 1 µm [8].

In the respiration process, the surface tension of the alveoli plays an important role. Since the alveoli are very small, a high surface tension would result, which could cause the alveoli to collapse [45]. To prevent this, surface-active substances are produced and released into the alveolar fluid (Figure 3B). This compound is called surfactant. These substances are formed by the alveolar type 2 cells and consists of a mixture of proteins, phospholipids and lecithin derivatives that reduce surface tension and facilitating alveolar re-expansion [15].
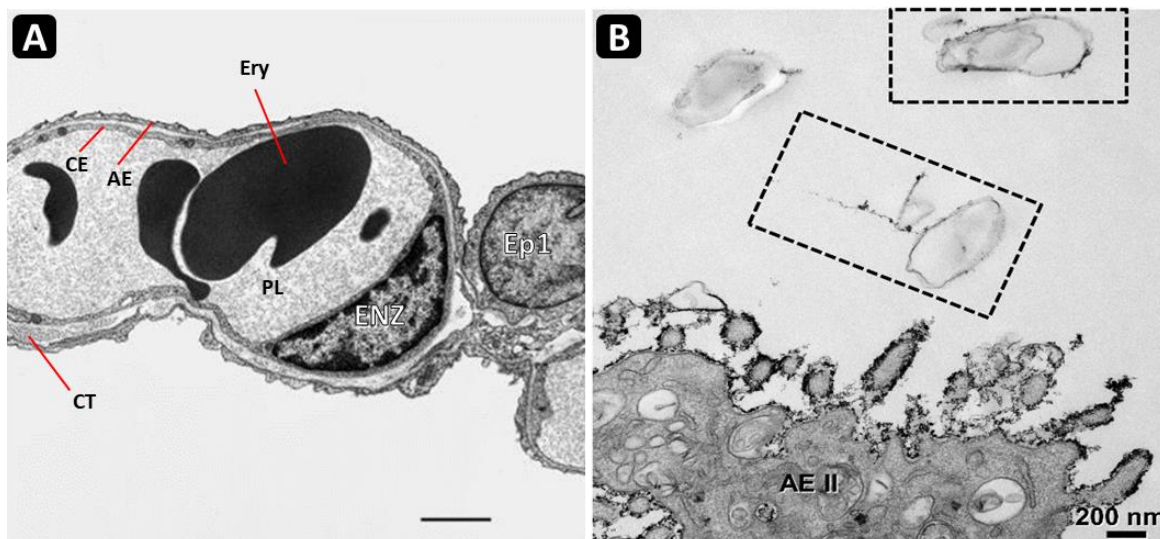
Figure 3: Electron microscope image of the capillary in the alveolar wall (A) and from alveolar type 2 cells (AE II) (B). In (A), the capillary with the endothelial cell (ENZ) and the alveolar type 1 cell (Ep1) build the diffusion barriers in the lung. CT: connective tissue fibres; CE: capillary endothelium; AE: alveolar epithelium; Ery: erythrocyte; PL: plasma. (Scale bar represents 2 µm). In (B), the surfactant released by AE II in the airspace of an alveolus is visualised by thorium dioxide (boxed areas). Reprinted with permission from [8] (A) Copyright © 2016 Springer-Verlag and [15] (B) Copyright © 2020 MDPI.

Since not only air but also contaminants can enter the deep lungs during the inhalation process, which can hinder gas exchange, the alveolar region has a special cell type for clearance, the alveolar macrophages [46]. These cells phagocyte particles in the range of 1-5 µm, but can also absorb and remove nanoparticulate contaminants from the lungs [47-49]. Alveolar macrophages are

also responsible for immunological and inflammatory processes through the formation and release of messenger substances, as well as interaction with antigen-presenting cells [50, 51]. However, because these processes are disrupted in some diseases, favouring chronic inflammation, alveolar macrophages provide a target cell type for drug delivery [52-54]. Due to its high importance, this cell type with its cellular processes will be described in more detail in chapter 1.3 (Human pulmonary macrophages as target for drug delivery).

In order to reach the alveolar region, special particle parameters are required to ensure successful transport. For this reason, different inhalation systems have been developed to generate inhalable particles. The major systems in this context represent nebulizers, metered dose inhalers (MDI) and dry powder inhalers (DPI) [55]. Nebulizers are used in groups of patients who, due to different lung diseases, are not able to inhale quickly and deeply enough to generate sufficient airflow [56]. In this process, the drugs are usually aerosolized through a vibrating mesh to generate high delivery efficiency, low residual dose and lack of requirement for external gas power [57, 58]. But also, other methods for aerosolization like jet and ultrasonic nebulizers are used. However, these methods lead to a change in temperature, making the use of temperature-sensitive drugs unsuitable [59]. In contrast to nebulizers, MDIs use a propellant gas, where the drug is suspended or dissolved, to form an aerosol [60]. This simplifies inhalation and, with the use of spacers, prevents side effects and increases effectiveness, especially for children [61]. As MDIs are easy to use and show good and high efficiency, they are the most widely sold inhalers in the world, but on a similar scale to DPIs [62]. The use of dry powders for inhalation offers the advantage of improved physical stability due to the solid state [63], as well as a lower risk of microbial growth [64]. Here, the drug can be formulated in different ways to generate an effective aerosol: as a mixture with large inert powder like lactose (interactive mixture), as agglomerate of micronized drug (soft pellets) or as spray-dried powder [62].

All described inhaler classes have in common, despite different techniques, to generate particles with an aerodynamic diameter of 1-5 µm to reach the deep lungs [65]. In Figure 4, the correlation between aerodynamic diameter and the deposition in different regions of the lungs is presented. These regional deposition differences

as a function of particle diameter have been studied in detail in the ICRP (International Commission on Radiological Protection) deposition model [66].
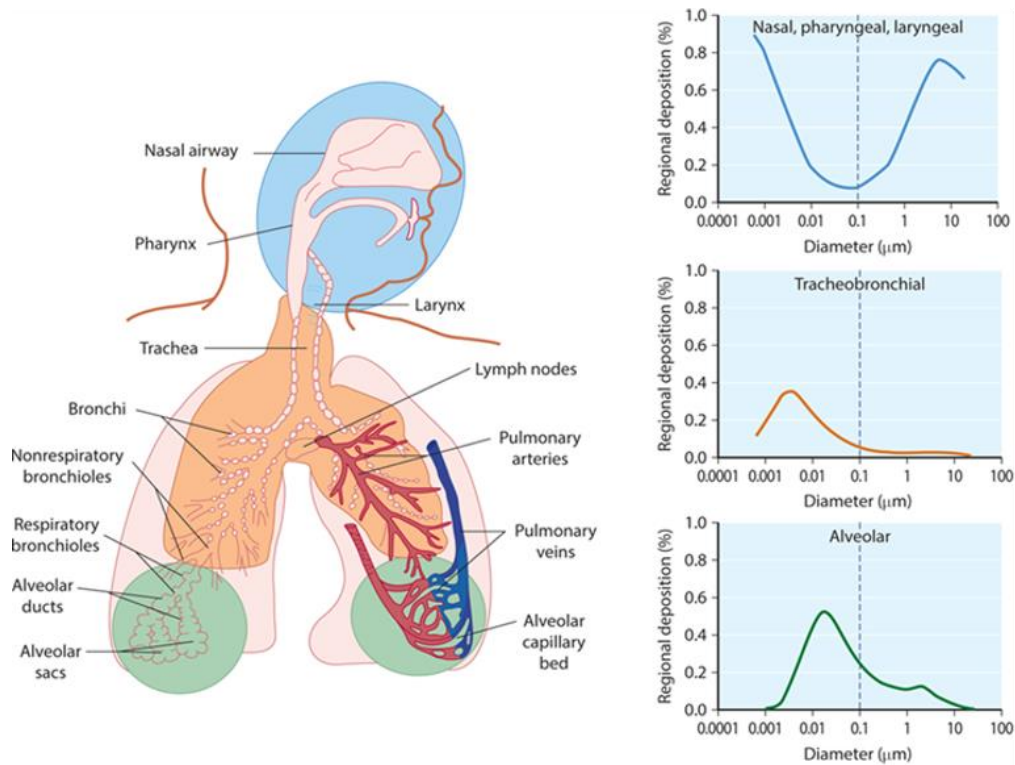
Figure 4: Statistical deposition distribution of inhaled particles on dependency of their aerodynamic diameters for the nasal (blue), tracheobronchial (orange), and alveolar (green) region of the respiratory tract based on data from International the Commission on Radiological Protection. Reprinted with permission from [2], Copyright © 2015 McGraw-Hill Education.

As the efficacy of pulmonary administration is proportional to lung deposition, two size ranges are revealed, which would be suitable for lung application [67]. One peak is in the lower nanoscale range, the other in the range between 1-5 µm. This second peak in the microparticulate size range is consistent with the target size in the production for inhalation devices and the described size optimum [65, 68]. However, the peak in the nanometre range is surprising, since increased exhalation is expected for sizes < 0.5 µm [69-71]. This can be explained by the fact that nanoparticles can reach the deep lungs by diffusion, but due to their small size, they are not able to sediment and impacted, which leads to a fast exhalation [66]. However, since microparticulate particles involve increased sedimentation and impaction, these particle systems are preferred for pulmonary delivery [34].

During the development of a new delivery system for lung application, the characterization of the aerodynamic properties is of high importance, because the

flight properties are not only influenced by the geometric diameter, also density and shape play an important role [72]. These parameters are described in more detail in the next chapter (1.2 Drug delivery of aspherical particles to the lungs). To classify a formulation for pulmonary application, impactors are used to simulate the probability of deposition into different areas of the lungs. Subsequently, conclusions about the aerodynamic properties of the powder mixture can be drawn [73]. To determine these properties, the European Pharmacopoeia (Ph. Eur.) has listed the Next Generation Impactor (NGI) [3], which is defined by a horizontal structure (Figure 5) and thus differs from other Ph. Eur. approved impactors with an horizontal setup, such as the Andersen cascade impactor (ACI) [74]. In the present work, the flight properties of the developed formulations were characterized using NGI, since this device is established at a wider range of flow rates compared to ACI [75].
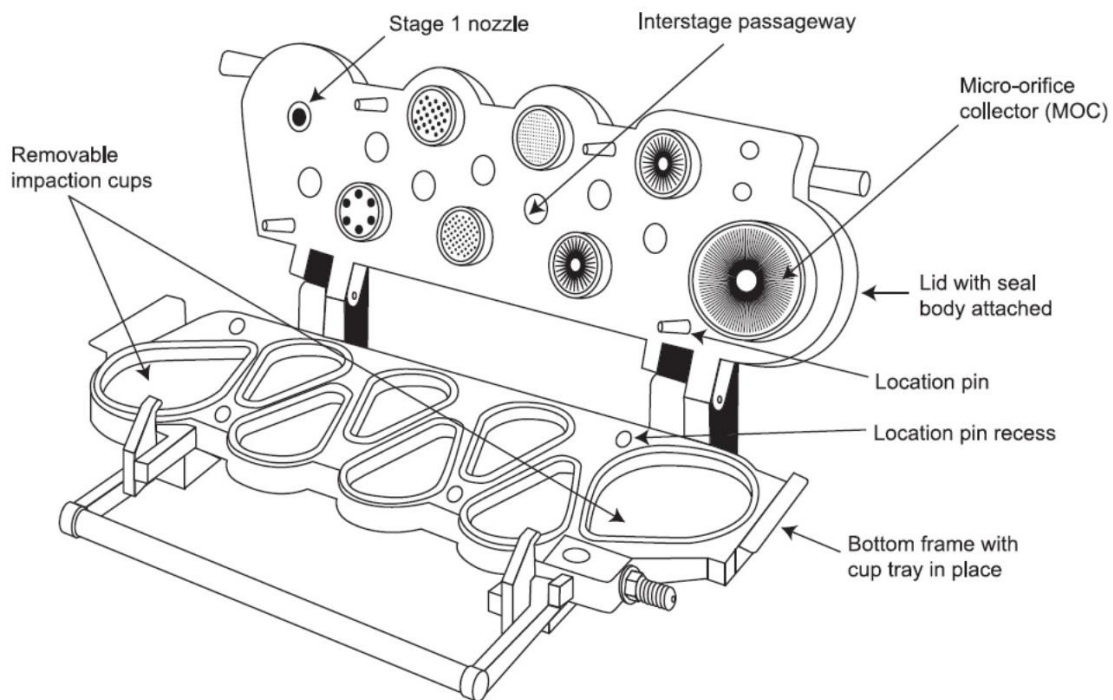
Figure 5: Structure of the inside of the Next Generation Impactor. Here, the different nozzle size for each stage is illustrated, which spilt the investigated powder in terms of its aerodynamic properties. Reprinted with permission from Ph. Eur. 10.0 [3], Copyright © 2020 EDQM.

As shown in Figure 5, the NGI is built up of eight removable impacting cups, representing different air flows, which results in impaction of distinct particle sizes. The eighth stage, also called micro-orifice collector, represents the final filter. During the experiment, the powder mixture to be analysed is aerosolized by a vacuum pump with a defined air flow to enter the NGI by a 90° angle through the induction

port, which mimics the throat. This is followed by the pre-separator, which separates larger particle aggregates before the powder reaches the interior [9]. When the powder reaches the inner chamber, it follows the prevailing air flow through the nozzles of the individual stages. Each stage has its own nozzle pattern with different diameters, which become smaller as the number of stages increases, resulting in a higher air flow. Due to this enhanced flow, the inertia of the particles increases, so that above a certain air flow they can no longer follow the stream and impact instead [9]. The powder retained in each stage can then be quantified and used to determine the mass median aerodynamic diameter (MMAD), fine particle fraction (FPF) and geometric standard deviation (GSD) to characterize the flight properties. The calculation and implementation are further explained in chapter 5.4.3 (Aerodynamic particle size analysis by Next Generation Impactor).

1.2. Drug delivery of aspherical particles to the lungs

In the development of new drug delivery systems, the design of particle shape has become increasingly important in recent years. This is demonstrated by the number of newly developed methods for the formation of aspherical particles, where a controlled change in size, shape, functionality, spatial arrangement and composition is feasible [76-81]. The resulting particles in the nano- or micrometre dimension have an anisotropic shape and can additionally be designed anisotropic in chemistry [13]. A selection of different shape designs of non-spherical particles is shown in Figure 6.
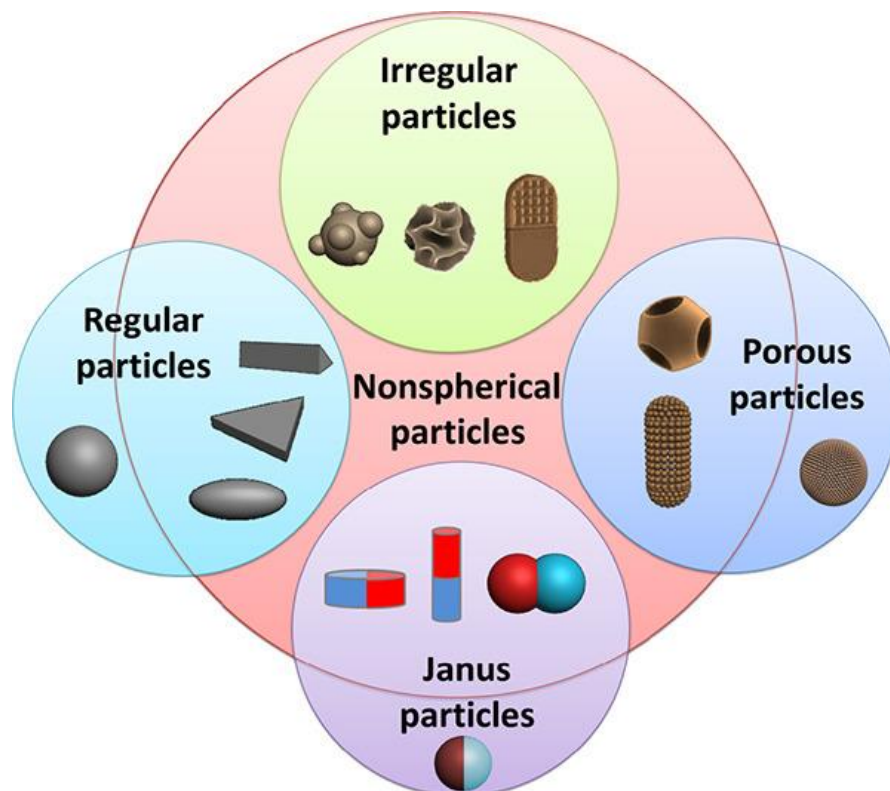
Figure 6: Illustration of different particle designs. Here, irregular and regular particles, as well as porous and Janus particles are illustrated as examples. By changing the morphology, structure or shape of particles, the biological interactions and physical properties are modified. This allows various parameters of a drug delivery system to be specifically modified to improve the transport of drugs. Reprinted with permission from [13]. Copyright © 2018 Elsevier B.V.

By using different shapes, the intrinsic properties of the particles can be specifically modified. This fact is of interest for the development of carrier systems, as the degradation, as well as the drug release of polymer particles can depend on particle shape [14, 82]. In addition, the shape of the particle system affects the rheological properties of suspensions [83], as well as the electrophoretic behaviour [84, 85]. All

these characteristics influenced by the geometric structure can be considered for the development of new carrier systems [86, 87].

Various techniques, such as seeded polymerization, clusterization, microfluidic techniques, ion etching, electrohydrodynamic jetting and template-assisted methods, can be employed for the production of non-spherical particles [13]. These particles can be used to improve delivery for specific administration routes [14], but not all of them are suited for lung delivery. This is due to the fact that the developed particle system requires an aerodynamic diameter of 1-5 µm to reach the deep lungs [65]. However, this diameter does not only depend on the geometric diameter, but is also influenced by shape and density, as described in equation 1 [88, 89]:

$$d_a = d_{ve} \sqrt{\frac{1}{\chi} \frac{\rho_p}{\rho_0} \frac{C_c(d_{ve})}{C_C(d_a)}}. \qquad \text{(equation 1)}$$

d_a: aerodynamic diameter

d_{ve}: volume equivalent diameter

χ: dynamic shape factor

ρ_p: particle density

ρ_0: standard density

$C_c(d_{ve})$: Cunningham slip correction factor of the volume equivalent diameter

$C_c(d_a)$: Cunningham slip correction factor of the aerodynamic diameter

The shape is described by the dynamic shape factor (χ), which is always $\chi > 1$ for aspherical particles and $\chi = 1$ for spheres. This factor describes the ratio of the resistance force of aspherical particles to their volume-equivalent spheres when both particle systems move with the same relative velocity in a gas [88]. In addition, the air resistance changes with different particle systems. If the relative velocity of a gas at the particle surface is non-zero, the drag is reduced during the flight of the particles [89]. Because this reduced drag influences the aerodynamic flight properties, Allen and Raabe introduced the Cunningham Slip Correction Factor C_c [90, 91]. Since C_c is not selectively changeable and the standard density ρ_0 is also given, the shape factor and the particle density can be changed specifically. With χ in the denominator below the root, increasing this factor lowers the aerodynamic

factor, keeping the rest of the parameters constant. For particle density ρ_p, it is exactly the opposite. Here, d_a and ρ_p are proportional, so that a reduction in density also causes a reduction in aerodynamic diameter. Thus, ρ_p and χ offer important parameters in the development of drug delivery systems for pulmonary administration.

Among the different shapes and the associated pulmonary mobility, the rod shape in form of the asbestos has been particularly prominent, as this substance has been found to reach the deep lungs and to cause lung cancer, mesothelioma and fibrosis (asbestosis) [92]. The elongated shape of the rods, which by definition has a length greater than 5 µm and an aspect ratio (AR, ratio of length to width) greater than 3 [93, 94], allows them to align to the airflow and thus reach the deep lungs [92]. Here, they enter the alveoli and small non-ciliated airways, where clearance is only achieved by alveolar macrophages, which is hindered by the elongated shape [93, 95]. Since due to its chemical composition, asbestos does not disintegrate in the lungs the residence time increases, resulting in high toxicity [92, 93]. All these properties of the rod shape of asbestos, except toxicity due to chemical properties, represent an interesting design for the development of a drug delivery system for pulmonary administration. Therefore, it is in the scope of different working groups [96-98].

For the determination of the dynamic shape factor of cylindrical particles, the AR is of great importance. As shown in Figure 7, χ increases slowly up to an aspect ratio of about 100, but exponentially thereafter [6]. Orientation in the air stream plays a decisive role here. In Figure 7, the dotted line represents an arrangement parallel to the airflow ($\chi//$), the dashed line represents a perpendicular alignment ($\chi \perp$), and the solid line represents a random orientation (χr).
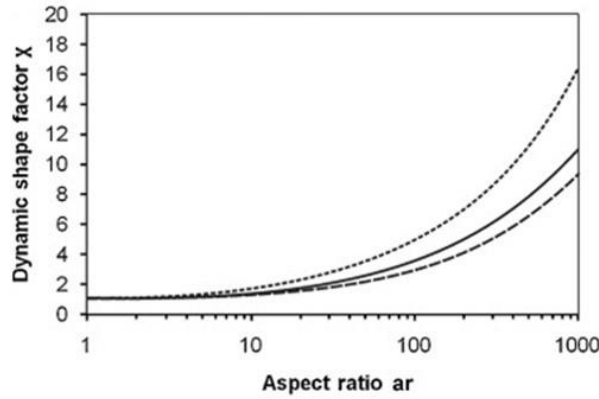
Figure 7: Dependence of the aspect ratio to the dynamic shape factor χ. By increasing the aspect ratio, χ increases slowly at first, but exponentially from an AR of about 100. The arrangement of the particles to the air stream also plays an important role. This is illustrated in this graph by the three different lines. The dotted line represents an parallel arrangement $\chi//$, the dashed line a perpendicular arrangement $\chi \perp$ and the solid line a random orientation χr. Reprinted with permission from [6], Copyright © 2014 Elsevier B.V.

To determine the appropriate shape factor for a specific AR and a specific alignment in the gas flow, Robert Sturm has created different mathematical formulas for calculation [6]. Since not all rods are oriented parallel to the airflow (equation 2), the orientation perpendicular to the airflow must also be considered (equation 3).

$$\chi// = \frac{\frac{4}{3}(ar^2-1)ar^{-\frac{1}{3}}}{\left[\frac{2ar^2-1}{\sqrt{ar^2-1}}\right]\ln\left(ar+\sqrt{ar^2-1}\right)-ar} \qquad \text{(equation 2)}$$

$$\chi \perp = \frac{\frac{8}{3}(ar^2-1)ar^{-\frac{1}{3}}}{\left[\frac{2ar^2-3}{\sqrt{ar^2-1}}\right]\ln\left(ar+\sqrt{ar^2-1}\right)+ar} \qquad \text{(equation 3)}$$

These two formulars are used to calculate the shape factor for a random orientation in the air flow (equation 4), which represents an approximation of the shape factor for a cylindrical particle system.

$$\frac{1}{\chi r} = \frac{1}{3\chi //} + \frac{1}{3\chi \perp}$$ (equation 4)

ar: aspect ratio

$\chi //$: shape factor with an arrangement parallel to the air flow

$\chi \perp$: shape factor with an arrangement perpendicular to the air flow

χr: shape factor with a random arrangement to the air flow

For very high aspect ratios (AR ≈ 1000), only an alignment to the airflow occurs, which causes equation 3 to be disregarded for such particle systems, resulting in $\chi r = \chi //$ [92, 93, 99].

In order to produce cylindrical particle systems with defined AR and narrow size distribution, the use of templates has proven to be a suitable method. Here, the PRINT® technology (Particle Replication in Non-Wetting Templates) represents an interesting technique, where aspherical nanoparticles with a narrow aerodynamic diameter (low GSD) can be produced for the transport of small molecules and biological therapeutics [30, 100]. For the preparation of cylindrical microparticles, track-etched membranes served as templates for shaping the microrods, which are composed of nanoparticles. These can be stabilized in the pores by various methods, such as the Layer-by-Layer technique, in order to maintain the shape after release from the membrane [81, 96]. The preparation by this method is described in detail in chapter 3 (Preparation of cylindrical nanostructured microparticles).

To evaluate the described properties of the cylindrical particles for pulmonary application, various experiments were performed both *in vitro* and *in vivo*. Since transport to the lungs is possible [94], the influence of oligonucleotide-loaded microrods on macrophages was investigated. It was found that a significant reduction of pro-inflammatory cytokines is possible *in vitro* without causing cytotoxicity [101]. The use of cylindrical microparticles was also shown *in vivo* by Möhwald *et. al.*, where a transfection of BALB/c mouse macrophages was successful after seven days [96]. This retarded biological response *in vivo* suggests that, first, the release of the drug is prolonged and, second, phagocytosis of the elongated particles is delayed. This perturbation of macrophage uptake toward aspheric particles was evaluated and resulted in a change in uptake rate as a

function of shape [95]. In addition, the increase in AR slows phagocytosis [102], which is mainly influenced by the point of attachment, where the macrophage starts to internalize the rods (Figure 8) [14].
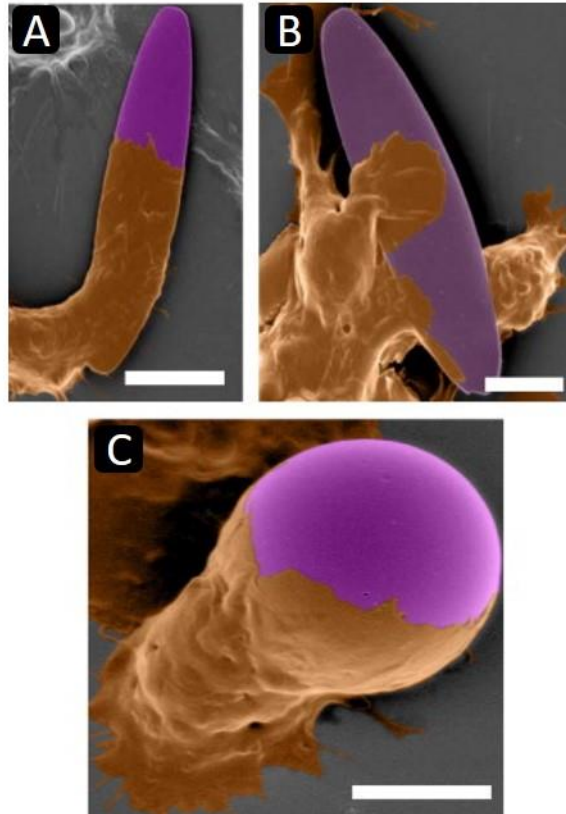
Figure 8: The importance of the point of attachment for the phagocytosis of aspherical particles. These illustrations show SEM images of alveolar macrophages (brown) while phagocyting different shaped particles (purple). (A) The macrophage started to internalize the elliptical disk at the pole, increasing uptake rate. (Scale bar represents 10 μm). (B) Here, the absorption of the particle starts in the middle of the flat side, which hinders the internalization and thus prolongs the uptake speed (Scale bar represents 5 μm). (C) For spherical particles, the point of attachment does not affect the velocity, due to the symmetrical structure (Scale bar represents 5 μm). Reprinted with permission from [14], Copyright © 2007 Elsevier B.V.

Thus, for two elongated particles of the same size, the uptake can be significantly affected. The beginning of internalization at the pole end can take a few minutes until uptake (Figure 8A), whereas macrophages attached at the middle part of the particle causes uptake of several hours (Figure 8B). In comparison, spherical particles can be internalized equally from all sides due to their symmetry, which does not influence the uptake rate (Figure 8C) [14].

The described properties show that the shape of a particle system varies different parameters, which may be of interest for the development of new particle systems. Especially for pulmonary application, rod-shaped particles have emerged as a possible design to generate a more efficient lung administration. For this reason, in

the present work, a cylindrical microparticulate system was characterized with respect to its properties as an inhalation product.

1.3. Human pulmonary macrophages as target for drug delivery

The immune system is an important barrier to protect the human body from infections. A distinction can be made between the innate immune response, which is the initial defence reaction, and the adaptive immune response, which specifically targets pathogens that have not been eliminated by the innate immune system [103]. Here, both immune responses have specific immunologically active cell types and barriers, as shown in Figure 9 [7]. An adapted immune response is characterized by antigen specificity, whereby specific protein structures are recognized to target these pathogens. This immunological memory is primarily addressed in vaccinations, where the acquired immune system is activated in such a way that pathogens can be directly recognized and eliminated [104, 105].
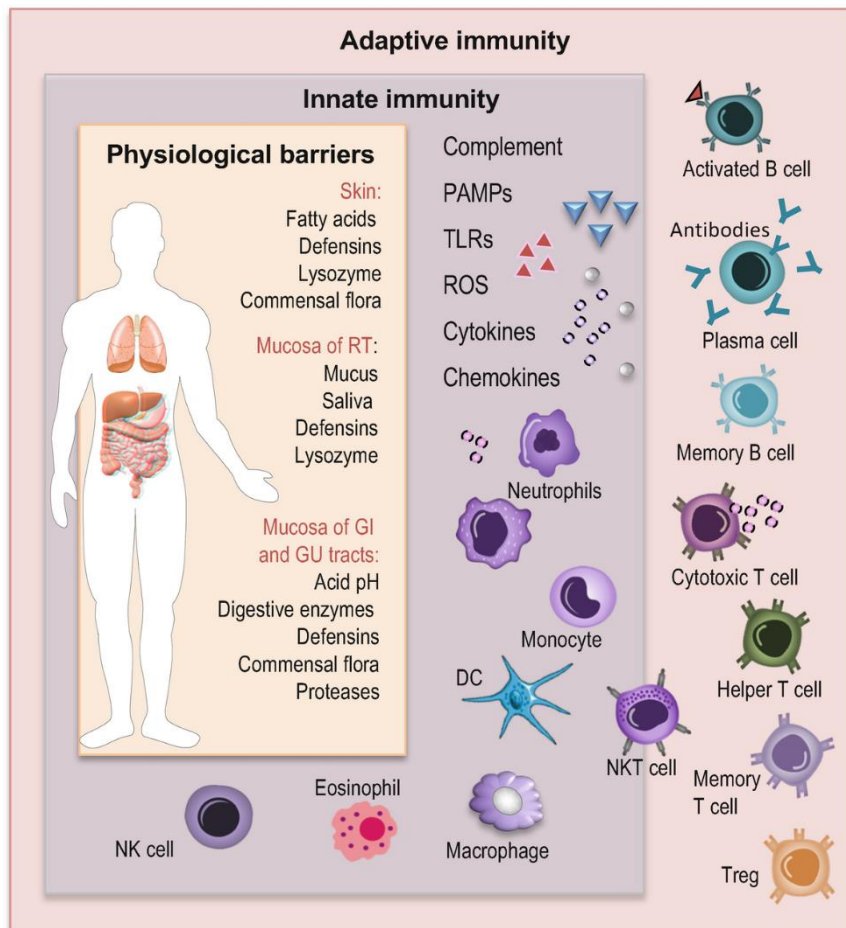
Figure 9: Overview of the different cell types and barriers of the innate and adaptive immune system. The first defence line is represented by the physiological barriers, which prevent pathogens from entering the human body. If pathogens overcome this barrier, the cells of the innate immune system start to remove the exogenous particles. If this pathogen has already passed the human body before and the immune system has reacted to it, the adaptive immune system can quickly recognize and remove it. Reprinted with permission from [7], Copyright © 2019 Springer Nature Singapore Pte Ltd.

However, the first defence line is represented by the innate immune system, which consists of physiological barriers (epithelia), immune cells and various plasma proteins Figure 9 [7]. The skin, as well as the mucous membranes of the gastrointestinal tract, the urogenital tract, and the respiratory tract, not only serve as a physical barrier, but can also produce antibacterial peptides, various enzymes and opsonins [106]. Of particular note are the surfactant proteins A and D, which coat the lung epithelia and, due to their surface activity, can attach themselves to the surface of the pathogens. They act as opsonins, thus facilitating the phagocytosis of the pathogens [107, 108]. If pathogens still overcome this physical barrier, macrophages will recognize and phagocytose them. This causes the release of chemokines from macrophages, which attract neutrophils from the blood and vessel walls that assist in phagocytosis [106]. In this process, messenger substances such as tumour necrosis factor-α (TNF-α) and interleukin 1 (IL 1) are released, which modulate the transcription factor NF-κB, resulting in an inflammatory response (Figure 10) [4].
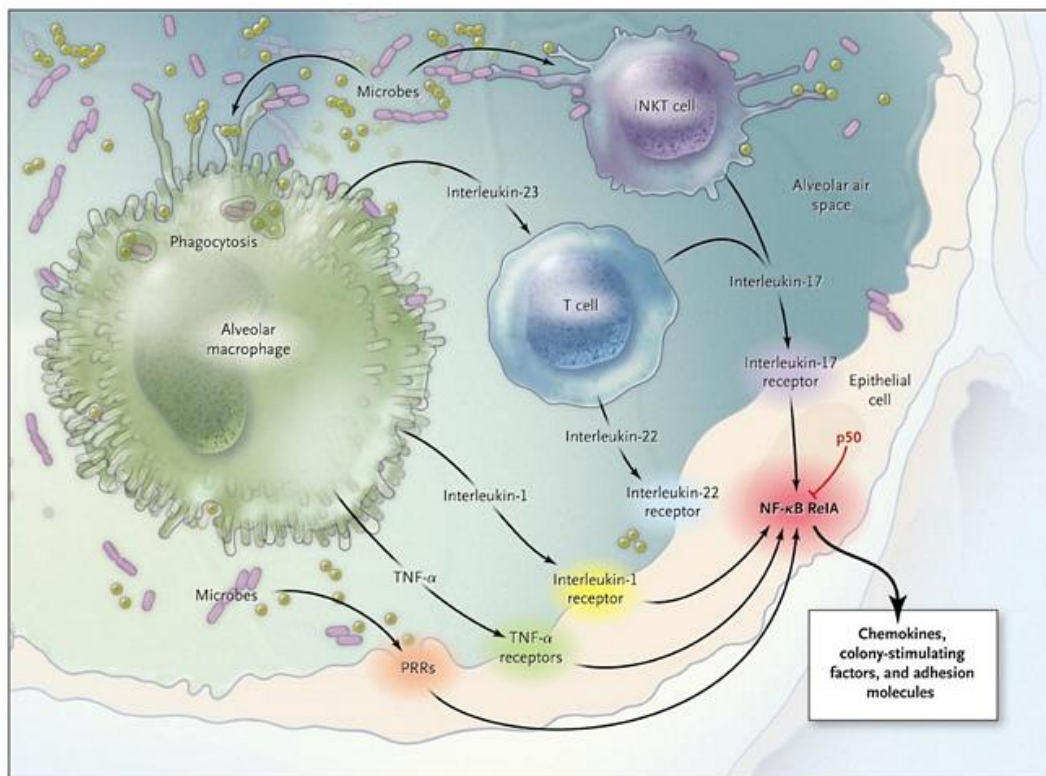
Figure 10: Activation of the innate immune system by microbes. The macrophages start to internalize these pathogens and to release pro-inflammatory cytokines (TNF-α, IL 1) to promote the immune reaction. Reprinted with permission from [4], 2008 Copyright © Massachusetts Medical Society.

Due to this regulatory function of macrophages, disruption of their activity can lead from acute to chronic inflammatory responses, as well as cancer diseases [109].

The disease profile depends on the polarization of the macrophages. They are classified into two subtype classes, the M1 and M2 macrophages (Figure 11) [110]. M1 macrophages are responsible for inflammatory processes as they produce pro-inflammatory cytokines and reactive oxygen species, which serve both to defend against pathogens and tumour cells, whereas M2 macrophages release anti-inflammatory mediators and promote angiogenesis, inhibiting tumour cell targeting and enhance metastasis [111]. In addition to these two polarization types, there is a third group of macrophages, the tumour-associated macrophages (TAMs). These TAMs are the major component of the tumour microenvironment and act as stimulators to promote tumour growth by releasing growth factors, cytokines, inflammatory substrates and proteolytic enzymes (Figure 11) [1].
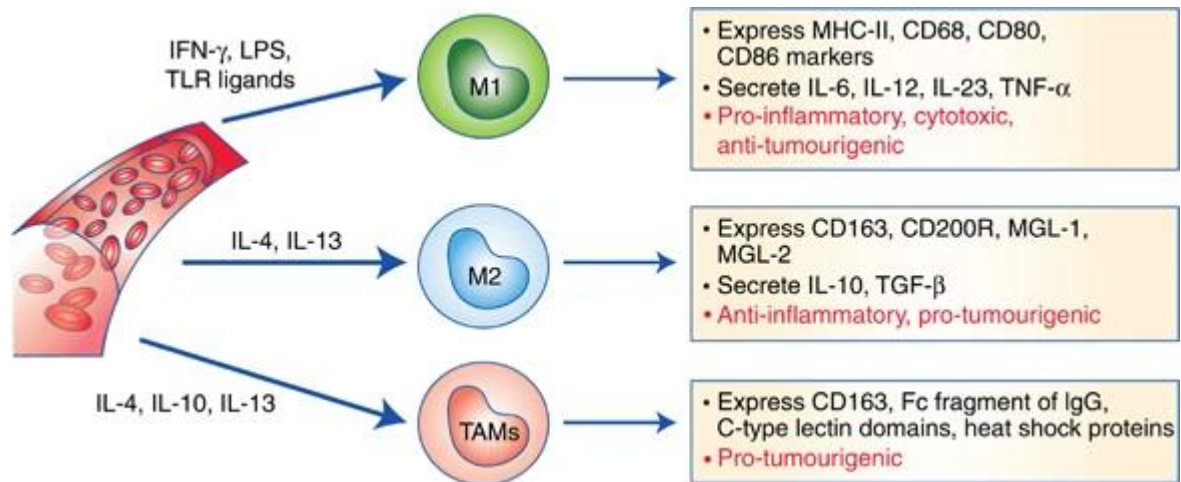
Figure 11: The different types of macrophage polarization and their role in tumorigenesis and inflammation. Reprinted with permission from [1], 2017 Copyright © BJC, Aras and Zaidi.

Due to these different polarization possibilities and the associated disease patterns, macrophages represent an important target for the treatment of various diseases [112-114]. One of the most affected organs are the lungs. According to the World Health Organization (WHO), chronic respiratory diseases are among the most common diseases worldwide, with a high mortality rate [115]. Even if the course of the disease is not fatal, lung function is permanently affected [116]. The most common representatives are CF, COPD and asthma [117]. In all of them a disruption of macrophage activity is present, leading to an increased release of pro-inflammatory cytokines like TNF-α [118].

To restore the disbalance of macrophage activity, new therapeutic strategies are still being developed to generate the most efficient immune response [119-121]. The use of genetic material like plasmid DNA, as well as oligonucleotides like siRNA or mRNA to specifically modify the formation of messenger substances has proven to be a very efficient method [122, 123]. Nevertheless, these developed therapeutics also need to be delivered to their target and overcome the specific hurdles of biological barriers and immunological defence mechanisms [124-126]. This specific issue serves as a topic for the following thesis.

1.4. Challenges of oligonucleotide delivery to immunologically active cells

Oligonucleotides form a relatively new class of drugs with the potential to treat a wide spectrum of diseases [127]. From the first identification of DNA in the 1860s by Swiss chemist Friedrich Miescher, the understanding and use of DNA building blocks (nucleotides) has changed significantly [128]. These nucleotides consist of three building blocks, as shown in Figure 12: a nitrogenous base, a five-carbon sugar (ribose) and a phosphate group. Here, a distinction can be made between DNA (deoxyribonucleic acid) and RNA (ribonucleic acid). While in double-stranded DNA the ribose at the 2' position is deoxidized and the bases consist of cytosine, thymine, adenine and guanine, single-stranded RNA has a hydroxy group at the 2' position and uracil instead of thymine as a base [128].
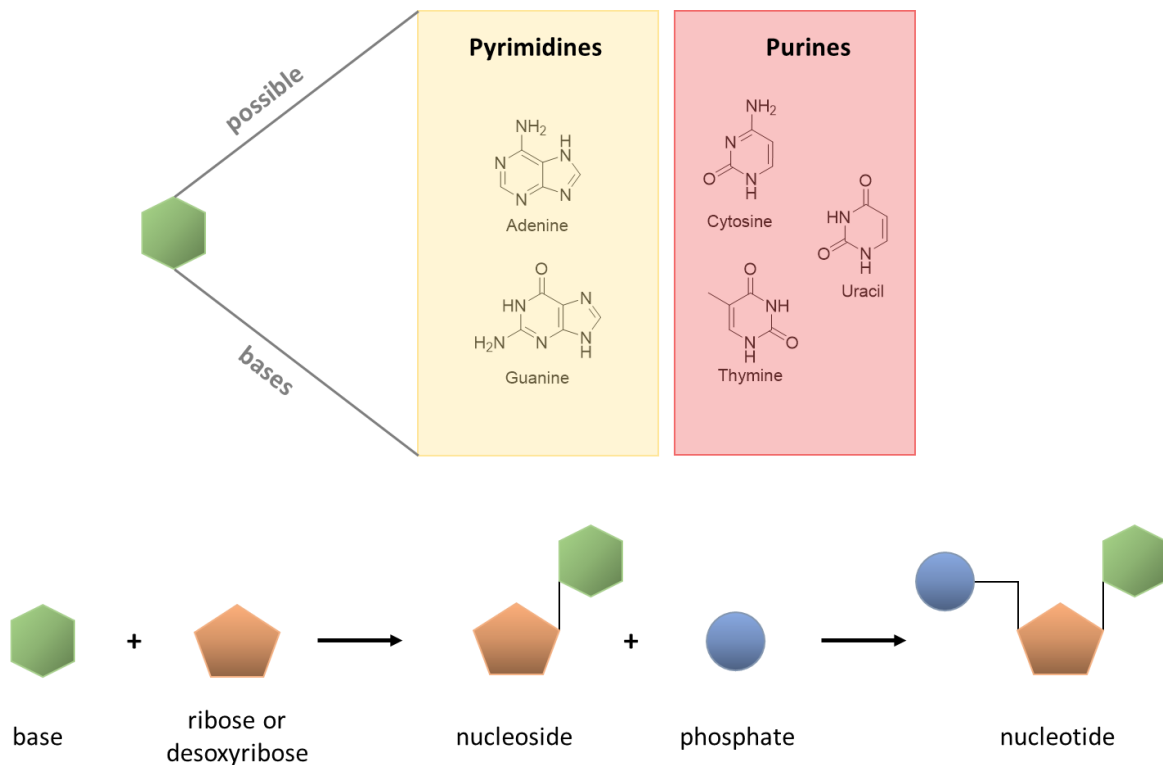
Figure 12: Chemical structure of a nucleotide consisting a pyrimidine or a purine base, as well as a five-carbon sugar and a phosphate group. The sugar (ribose) in DNA is deoxidized at the 2' position with cytosine, thymine, adenine or guanine, whereas RNA has a hydroxyl group at the 2' position and the thymine is replaced by uracil.

By definition, oligonucleotides are short DNA or RNA chains consisting of approximately 8-50 nucleotides [129]. In 1978, the first effective inhibition of a virus replication by a 13 nucleotides oligonucleotide was demonstrated [130]. This was the first step in the development of oligonucleotide therapeutics, which introduced

this new class of drugs to the market in 1998 with the first Food and Drug Administration (FDA) approval of an oligonucleotide named Fomivirsen (Vitravene®) [131, 132]. With the development of new sequences in the past 20 years, ten oligonucleotide therapeutics are FDA and European Medicines Agency (EMA) approved by January 2020 [133, 134]. Here, different variants of oligonucleotides can be used to inhibit the production of messenger substances or to protect against various diseases, which also allows patient-specific sequences to be addressed to treat rare diseases [135].

Currently, the most popular oligonucleotides are some of the recently FDA and EMA approved vaccines against COVID-19 [136], which contain an mRNA sequence to form the spike protein of the viral shell, triggering the body to produce specific antibodies against the virus [137-139]. This new application of mRNA vaccination against a virus is based on the experience already gained in the development of mRNA vaccines against cancer, where a boost of cancer-specific T cells is generated and immunological memory is induced to prevent metastasis and recurrence of cancer cells [140, 141].

The counterpart to the mRNA, which is required for the formation of proteins, is the siRNA. This oligonucleotide manages the pathway of RNA interference (RNAi) to induce sequence-specific post-transcriptional gene silencing. In this process, degradation of mRNA is initiated, resulting in an inhibition of protein formation (Figure 13) [10]. There are different ways to trigger the RNAi experimentally in a targeted cell: once by short hairpin RNA (shRNA), which is expressed by a plasmid, also with long double stranded RNA (dsRNA) or by synthetic siRNA [142]. As shown in Figure 13, the dsRNA (and also the shRNA) must first be cleaved by the enzyme complex Dicer [143] to generate strand separation of the resulting siRNA by the RNA induced silencing complex (RISC) in the next step [144]. After separation, the sense strand is degraded by nucleases, whereas the non-sense strand directs the RISC complex to the base-complementary mRNA sequence [145]. Binding of activated RISC to mRNA results in cleavage by the endonuclease Argonaute, silencing gene expression and thereby inhibiting protein formation [146].
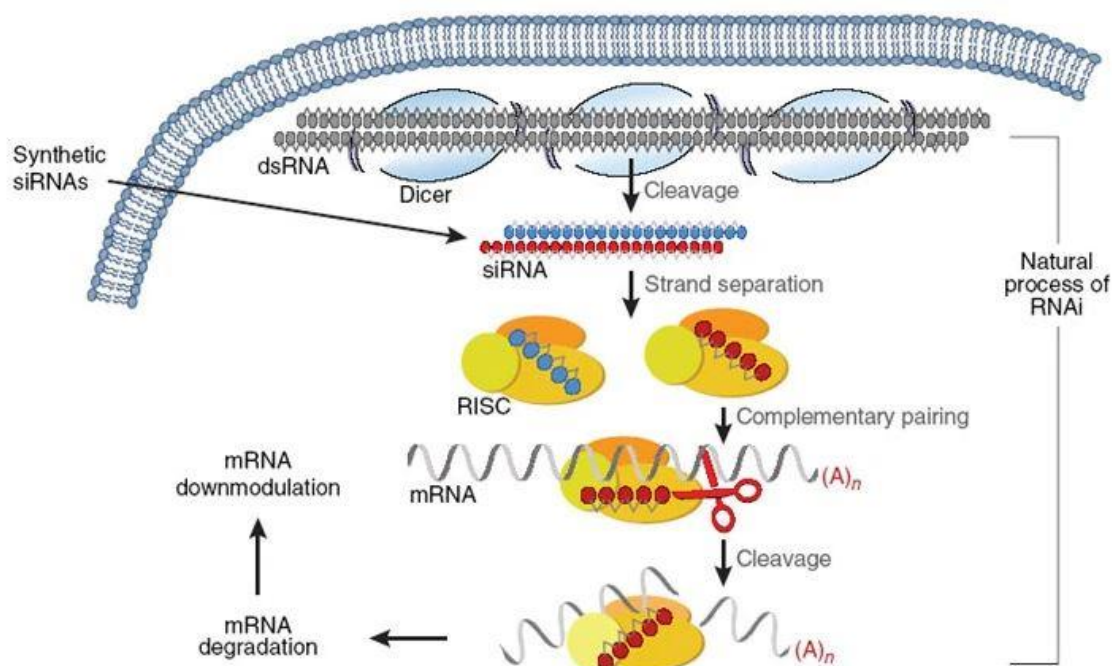
Figure 13: Process of RNAi in eukaryotic cells. The long double stranded RNA gets in the first step cleaved by the enzyme Dicer into smaller fragments (siRNA). These fragments are then separated by the RNA-induced silencing complex (RISC) under the degradation of the sense strand by nucleases. The RISC complex containing the non-sense strand is directed to the base-complementary mRNA sequence, which gets cleaved by the endonuclease Argonaute to silence gene expression. Reprinted with permission from [10], 1969 Copyright © Nature Publishing Group.

Since oligonucleotides have a high potency and thus form a suitable drug class, a closer look at their transport into the target tissue follows. Considering the chemical structure, a high instability is evident especially for single-stranded sequences, due to the easy degradation of intracellular nucleases [31]. This is particularly problematic with regards to the oligonucleotides already approved by the FDA and EMA, as approximately half of them are based on single-stranded sequences [133, 134]. Furthermore, the negative charge of unmodified oligonucleotides makes it difficult to be taken up by cells [146]. This complicates transport to the desired tissue, as the sequence must enter the correct intracellular compartment to induce an effect [147]. This is also associated with the high dose requirement needed to enable efficient therapy [148].

To address these problems, modifications can be made either to the chemical structure of the oligonucleotide, *e.g.,* by replacement of phosphate groups to increase stability [149], or by conjugation with functional ligands and polymers to avoid clearance from cells of the reticuloendothelial system [147], as well as by

encapsulation in a carrier system [150, 151]. These delivery systems are mostly in the nanoparticulate range and serve to protect the active ingredient, but also to ensure targeted transport [147]. The most commonly used carrier system for oligonucleotides represents lipid nanoparticles [152, 153]. Especially for the transport of siRNA positive results have been achieved [154], also for clinical trials [155]. But also, the use of other polymers like chitosan, poly-methacrylates. polyethylenimine and derivates, poly-l-lactic-co-glycolic acid and inorganic materials, for RNA delivery are described in literature [142]. Even though nanoparticles are good vehicles for many drug delivery purposes, not all application routes are suitable for them [156, 157]. This is especially the case for pulmonary applications, where the delivery system must fulfil specific characteristics in order to reach the deep lung, like described in chapter 1.1 (Physiological aspects and principles of pulmonary administration). However, nanoparticles can also be processed in terms of their flight properties by various techniques. On one hand, the particles can be spray-dried to influence the geometric diameter and thus the aerodynamic properties [158], and on the other hand, the shape and size can also be adapted by, for example, a template-assisted approach [81], to generate advantages of aspherical particles for pulmonal application, as described in Chapter 1.2. Delivery of a specific RNA sequence against TNF-α with a cylindrical, nanostructured delivery system was already shown with a significant reduction of TNF-α release [159].

In general, oligonucleotides represent a highly potent class of drugs that currently are used primarily in cancer therapy, vaccination against viruses, and regulation of pro-inflammatory diseases. However, due to the chemical properties and associated instability in biological environments, modification of the chemical structure, or innovative drug delivery systems must improve transport into tissues and intracellular compartments to ensure effective therapy.

2. Aims of the thesis

The present thesis aims to develop and characterize a nanostructured, cylindrical delivery system for the targeted transport of specific oligonucleotides into the deep lungs and specifically address different cell types located there. To discuss this topic in more detail, several objectives were defined and performed to gain an accurate overview of the properties of the particle system described. These chapters were defined as follows:

I) Investigation of flight properties of nanostructured, cylindrical microparticles

II) Oligonucleotide delivery and interaction of cylindrical microparticles with macrophages

III) The influence of silica nanoparticles to alveolar epithelial cells

IV) Mesoporous silica nanoparticles as drug delivery system for co-delivery of two anti-inflammatory drugs

The first question that arises when using cylindrical microparticles for pulmonal delivery is the resulting flight characteristics and whether the target tissue can be reached. For this reason, the first section of the work deals with the flight properties of cylindrical microparticles with different aspect ratios and the comparison to their spherical counterparts.

In the second part, the loading of a specific oligonucleotide sequence to inhibit TNF-α will be analysed and quantified using various techniques, followed by observation of the biological response of macrophages *in vitro*. Not only cell viability is considered, but also inhibition of proinflammatory cytokines and uptake behaviour after different time points.

The third chapter of the thesis deals with interaction between the particle system and alveolar epithelial cells. Here, the focus is particularly on the uptake characteristics of the nanoparticles that have been released from the disintegrated microrods in the biological environment.

In the fourth section, the cylindrical microparticles are constructed from mesoporous silica nanoparticles and simultaneously loaded with two anti-inflammatory drugs. Here, the chosen active ingredients represent two different classes with different

chemical structures and special physicochemical characteristics: the hydrophobic curcumin and a hydrophilic oligonucleotide sequence against TNF-α. The focus was on both the characterization of the newly developed carrier system and the biological response, especially with respect to the simultaneous transport of two drugs with different properties.

3.   Preparation of cylindrical nanostructured microparticles

3.1.   Template-assisted approach for the fabrication of cylindrical microparticles

This section is taken from the following publication:

siRNA delivery to macrophages using aspherical, nanostructured microparticles as delivery system for pulmonary administration
(**Chapter 2.2 Particle preparation)**

Thorben Fischer[1], Thomas Tschernig[2], Franziska Drews[3], Kristina Brix[4], Carola Meier[2], Martin Simon[3], Ralf Kautenburger[4], Marc Schneider[1*]

Affiliations
[1]Department of Pharmacy, Biopharmaceutics and Pharmaceutical Technology, Saarland University, Campus C4 1, 66123 Saarbrücken, Germany
[2]Anatomy and Cell Biology, Medical Faculty, Saarland University, building 61, 66421 Homburg, Germany
[3]University of Wuppertal, Molecular Cell Biology and Microbiology, Department of Chemistry and Biology, Gaußstr. 20, 42097 Wuppertal, Germany
[4]Institute of Inorganic Chemistry – WASTe-Elemental Analysis Group, Campus C4 1, 66123 Saarbrücken, Germany

For the preparation of cylindrical nanostructured microparticles, a template–assisted approach was used [81, 96] as illustrated in Figure 14.
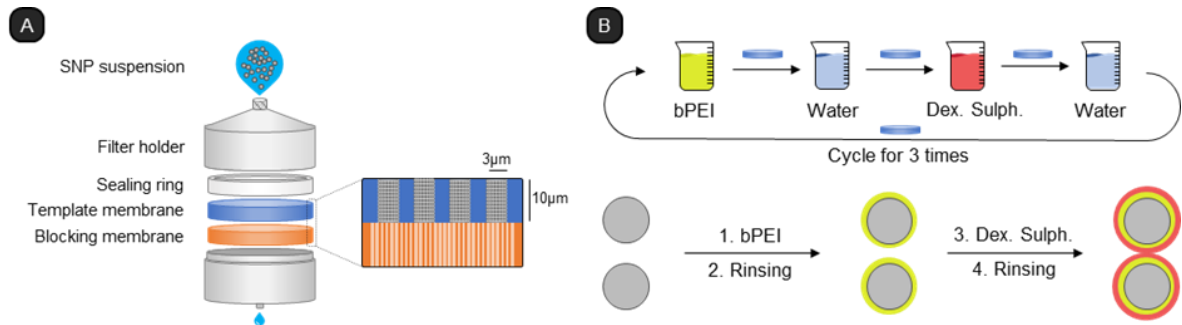
Figure 14: (A) Template-assisted approach for the preparation of cylindrical, nanostructured microparticles. A filter holder is used for this process, which inside consists of a sealing ring, a template membrane and a blocking membrane. The template membrane is the shaping membrane with a pore diameter of 3 µm and a pore length of 10 µm. To prevent the SNP from flowing through this membrane, the blocking membrane with a pore diameter of 0.1 µm is located underneath. Thus, the SNPs arrange themselves in the template membrane to form cylinders of defined size and will not flow through the blocking membrane. This filter holder is infiltrated in 3 steps of 500 µL each of a suspension of SNPs (d=200 nm) with a concentration of 1.5 mg/mL using a syringe pump. The filled template membrane is then removed from the filter holder and stabilized by the layer-by-layer technique. (B) To stabilize the nanoparticles in the cylindrical pore, the template membrane gets alternatingly floated with a polycationic and polyanionic polymer solution for 12 min each to increase the ionic forces between the nanoparticles. The membrane is also immersed in water between the polymer solutions for 12 min to remove excess polymer. This layer cycle must be repeated at least 3 times to generate a stable formulation. In the siRNA-loaded formulation, the Dex. Sulph. is replaced by an siRNA solution in the last layer step.

As model substance amorphous silica nanoparticles (SNP) with a diameter of 200 nm were used, which were infiltrated into a template membrane with a defined length of 10 µm and a width of 3 µm. A filter holder system was applied to fill the pores of the template membrane, as shown in Figure 14. This system contains a sealing ring, the template membrane and a blocking membrane with a pore diameter of 0.1 µm. When the membrane got infiltrated with SNP suspension, the nanoparticles cannot leave the pores and arrange themselves according to the shape of the pore. For complete filling, the membrane was infiltrated three times with 500 µL of a 1.5 mg/mL SNP suspension using a syringe pump (kd Scientific, Holliston, US). Afterwards, the template membrane was removed from the filter holder and stabilized using layer-by-layer technology to stabilize the cylindrical arrangement of the SNPs in the pores [81, 96, 160, 161]. As layer solutions, branched polyethyleneimine (bPEI) served as polycationic and dextran sulphate (Dex. Sulph.) as polyanionic compound. The reason for using bPEI as a stabilizing polymer is that the high buffering capacity of bPEI causes an osmotic swelling of the

lysosome, leading to leakage of the vesicle's membrane. This destabilization of the membrane caused by the so-called ''proton sponge effect'' leads to a release of the siRNA into the cytoplasm [162]. The membrane loaded with nanoparticles was first immersed in a 2% bPEI solution for 12 min because silica is negatively charged. After a 12 min washing step in water, the membrane was submerged in a 2% Dex. Sulph. solution in order to adsorb the polymer on the surface through electrostatic interactions. After a further 12 min cleaning step in water, the polycationic solution was started again. Between every coating step, the membrane was cleaned with a lint-free tissue to remove polymer residues on the membrane. This cycle was repeated three times to achieve a stable formulation. In the last step, the Dex. Sulph. solution was replaced by a 0.05% siRNA solution, as polyanionic compound. To release the microparticles from the template, the filled polycarbonate membrane was dissolved with tetrahydrofuran (THF), leaving only the formulation residue, as both the SNPs and the polymers are insoluble in THF. In a final step, the THF was evaporated to obtain a dry formulation. The entire manufacturing process was performed under aseptic conditions to ensure stability of the oligonucleotide and allow *in vitro* cell culture experiments. After preparation, the formulation was stored in a freezer at -20 °C to prevent decomposition of the oligonucleotides.

3.2. Modification of cylindrical microparticles to improve flight characteristics

This section is taken from the following publication:

siRNA delivery to macrophages using aspherical, nanostructured microparticles as delivery system for pulmonary administration
(**Chapter 2.3 Aerodynamic particle size analysis by Next Generation Impactor**)

Reprinted with permission from Elsevier (© 2020 Elsevier B.V.):

The particles titled "formulation" in the following paragraph refer to the manufactured cylindrical microparticles described in section 3.1 (Template-assisted approach for the fabrication of cylindrical microparticles).

To improve the flight properties, the formulation was coated with L-leucine. Therefore, an exact mass of the rods was weighed and redispersed in an L-leucine solution with a concentration of 0.4% of the rod mass. This suspension was then lyophilized to ensure homogeneous coating of the formulation.

4. Comparison between the aerodynamic properties of cylindrical, aspherical microparticles and their spherical counterparts using Next Generation Impactor

This section refers to the following publication:

Thorben Fischer, Aljoscha Koenneke, Marc Schneider[*]

Affiliations

Department of Pharmacy, Biopharmaceutics and Pharmaceutical Technology, Saarland University, Campus C4 1, 66123 Saarbrücken, Germany

(submitted)

4.1 Abstract

The use of innovative shapes of drug delivery systems offers new possibilities for the targeted transport of genes and drugs into the human body. Especially when addressing specific cell types in the lung, aspheric microparticles can provide a potential advantage and improve the current therapy. In addition, a higher drug quantity can be loaded in comparison to the spherical counterparts. However, particles for pulmonary application must fulfil certain aerodynamic criteria to reach the target organ.

In this work, a cylindrical drug delivery system based on hierarchical organized nanoparticles for pulmonary application was investigated analysing the aerodynamic characteristics by Next Generation Impactor. For this, several formulations with different length width ratios (aspect ratios), were produced. Here, the length of the rods was constantly set to 10 µm, only the width was changed to 2, 3 and 5 µm covering aspect rations from 2 - 5. We could show that the mass median aerodynamic diameter was reduced by the cylindrical shape with an increase in fine particle fraction compared to similar spherical counterparts. This underlines the interesting aerodynamic properties of the microrods to potentially serve as a new class of pulmonary drug delivery systems.

4.2 Introduction

The lung represents one of the most important application routes in the human body, which is why many particle systems have already been developed for this application. The most common inhalation systems are provided by nebulizers, metered dose inhalers (MDI) and dry powder inhalers (DPI) [55]. In MDIs and nebulizers, propellant gases or vaporizers are used to form droplets to be deposited in the lungs [60, 163]. DPIs form solid aerosols, which are in the same aerodynamic size range as the droplets of MDIs and nebulizers [164, 165]. The incorporation of biopharmaceuticals in spray dried powders for inhalation is usually considered as challenging [166], although recently progress is made regarding this [167]. Although improvement in dry powder formulation and preparation techniques have already occurred, delivery of therapeutics through the respiratory tract can be improved, as the physical properties of the powders and the devices used for inhalation represent

critical factors [168]. For the physical properties, not only the shape and surface morphology of the particles is of high importance for lung deposition [169], also hygroscopicity [170] and the electrostatic surface charge are influencing aerosolization [171].

By changing the shape, previous studies have shown, that cylindrical, nanostructured microparticles can be loaded with biopharmaceuticals and are able to reach the lungs *in vivo* [96]. In addition, flight studies of rod-like microparticles have shown that an FPF of >30 % can be achieved with an aerodynamic diameter < 3 µm [172]. This shape is interesting because the uptake kinetics of immunologically relevant cell types can be modified by changing the aspect ratio [173, 174]. In addition, the nanostructure and loading of the surface with active ingredient means that every fragment of the carrier system is loaded with drug [81], so that even if the microrods disintegrate, the resulting nanoparticles can still address immunologically active epithelial cells [175]. All these advantages indicate that nanostructured rod-like microparticles are an attractive drug delivery system for pulmonary application.

In this work, we are focusing on the flight characteristics of cylindrical microparticles and their spherical counterparts. For this purpose, different microrod formulations with different widths at the same length were analysed regarding their flight properties using Next Generation Impactor and subsequently compared with spherical microparticles. These spheres had a diameter equal to the length or width of the microrods as well as the same volume. The results obtained from the particle populations were compared and flight characteristics were evaluated in terms of shape.

4.3 Materials and Methods

4.3.1 Materials

Fluorescently labelled silica nanoparticles (green) with a diameter of 200 nm and green, fluorescent silica microparticles with a diameter of 3; 5 and 10 µm were purchased from Kisker Biotech (Steinfurt; Germany). Branched polyethyleneimine with a mass of 25 kDa and L-leucine were purchased from Sigma Aldrich (Steinheim, Germany). Highly sulphated dextran sulphate 10 HS was purchased from TdB Labs (Uppsala, Sweden). Tetrahydrofuran was obtained from Thermo Fisher Scientific Inc. (Darmstadt, Germany). Nuclepore® Track-Etched membranes with a pore size from 0.1; 2; 3 and 5 µm and a thickness of 10 µm were purchased from Whatman plc (Kent, UK).

4.3.2 Production of the cylindrically shaped microparticles

The aspherical, cylindrical microparticles were produced using a template-assisted approach [81, 96, 172]. This method makes use of the defined shape and dimensions of membrane pores. These pores with a fixed length of 10 µm and a variable width of 2; 3 and 5 µm were infiltrated with amorphous silica nanoparticles with a diameter of 200 nm. The layer-by-layer technique was used to stabilize the nanoparticles in the cylindrical voids [160]. In this process branched polyethyleneimine (bPEI) as polyanionic and dextran sulphate as polycationic polymer's electrostatic interactions were exploited to link the nanoparticles. The microrods were then released by dissolving the polycarbonate membrane in tetrahydrofuran. The resulting formulation was then surface-coated with L-leucine to reduce the hygroscopicity and increase the roughness of the surface which leads to a more flowable powder [176, 177]. For coating, the microrods were redispersed in an aqueous L-leucine solution and then freeze-dried. The amount of L-leucine was 0.4% of the mass of the rods.

4.3.3 Morphology analysis by Scanning Electron Microscopy

In order to characterize the manufactured formulations and the spherical microparticles with respect to their morphology, scanning electron microscopy was used. For this analysis we applied a Zeiss Evo HD 15 Electron Microscope (Carl Zeiss AG, Jena, Germany) equipped with a Lanthanum hexaboride (LaB$_6$) cathode. The sample to be analysed was placed as a powder on a silica wafer and then coated with a gold layer about 10 nm thick to render the surface conductive, avoiding the accumulation of electrons. To generate the thin gold layer a Quorum Q150R ES sputter coater (Quorum Technologies Ltd., East Grinstead, UK) was used. The images were taken at a magnification of 10 and 1 kX at 5 kV.

4.3.4 Aerodynamic characteristics of spherical and aspherical microparticles

To estimate the deposition profile of the drug carrier systems in the lung after inhalation, the determination of the aerodynamic diameter is often applied. To generate this value for the developed formulation a Next Generation Impactor (NGI) (Copley Scientific, Nottingham, UK) was used. The experiment was performed with a setup described by Marple *et. al.* [9] at a flow rate of 60 L/min. The flow rate was adjusted by a M1A flowmeter (Copley Scientific, Nottingham, UK) to ensure efficient aerosol formation of the different formulations [178, 179]. To perform the experiment, approximately 3 mg of the formulation to be tested were filled into a capsule and then aerosolized with a HandiHaler® (Boehringer Ingelheim, Ingelheim, Germany) at an air flow of 60 L/min for 4 s, generated by a vacuum pump (Erweka, Langen, Germany). The concentrations of the individual stages of the NGI were then analysed fluorometrically using microplate spectrophotometer (TecanReader® infinite M200, Tecan, Männedorf; Switzerland). The results obtained were then used to calculate the Mass Median Aerodynamic Diameter (MMAD), the Fine Particle Fraction (FPF) and the Geometric Standard Deviation (GSD) according to Abdelrahim *et.al* [180] and as done before by our group [28, 181].

4.4 Results and Discussion

4.4.1 Aerodynamic properties of microrods

In this analysis three different microrod formulations were tested, which are shown in Figure 15.
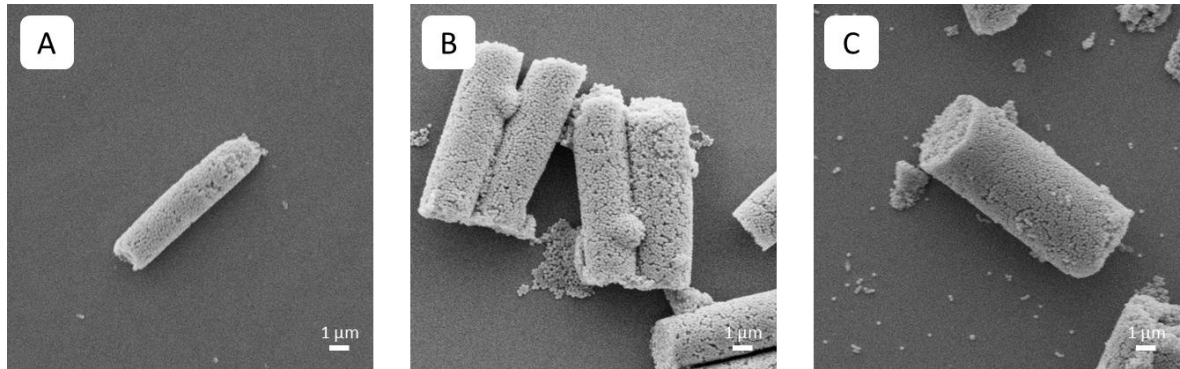
Figure 15: The three different microrod formulations are shown here using scanning electron microscopy. The length of the cylinders is identical in [A-C] with L=10 µm. The width of the particles varies between 2 µm in [A], 3 µm in [B] and 5 µm in [C]. All three formulations are coated with a thin layer of L-leucine to prevent agglomeration. The images clearly show the nanostructure that is created by the silica nanoparticles used in the production process. Magnification: 10 kX.

The length of the delivery system was kept constant at 10 µm whereas the diameter varied between 2 (µR 2), 3 (µR 3) and 5 µm (µR 5). To improve the flowability of the powder formulations and thus also to modify the flight properties, the surface of the particles was coated with L-leucine. This proteinogenic amino acid reduces the interactions between the microparticles, thereby reducing agglomerate formation, which should improve MMAD, GSD and FPF.

The results of the NGI analyses, which are listed in Table 1 show, that the aerodynamic diameter of the microrods is smaller than their geometric diameter. This trend is evident for all three formulations showing that the aerodynamic properties are strongly influenced by the shape.

Table 1 Results of the NGI experiments using the cylindrical microparticles. The three formulations have a length of 10 µm and differ only in their width. It is evident that the MMAD of the tested particles is smaller than their width and length which is caused by the shape factor χ. The GSD is slightly elevated in all three samples, which can be explained by agglomeration or disintegration of particles during the NGI experiment. The FPF, which represents the percentage of mass with a size < 5 µm [12] is for all three samples in a good range in comparison to DPIs [16].

	MMAD [µm]	GSD	FPF [%]
Rods (µR 2) d= 2 µm; L= 10 µm	1.87 ± 0.09	3.17 ± 0.37	35.72 ± 4.96
Rods (µR 3) d= 3 µm; L= 10 µm	2.53 ± 0.23	3.20 ± 1.22	33.94 ± 5.07
Rods (µR 5) d= 5 µm; L= 10 µm	4.76 ± 0.13	2.40 ± 0.17	27.81 ± 5.76

Therefore, this factor is also considered when calculating the aerodynamic diameter, which is called the dynamic shape factor χ. The equation for calculating the aerodynamic diameter is as follows [88, 89]:

$$d_a = d_{ve} \sqrt{\frac{1}{\chi} \frac{\rho_p}{\rho_0} \frac{C_c(d_{ve})}{C_C(d_a)}}.$$

Since χ is almost always greater than one for aspherical particles and equal to one for spherical particles [88], the quotient under the root becomes smaller for aspherical particles, which means that for the same volume equivalent diameter (d_{ve}) the aerodynamic diameter becomes smaller .For this case to occur, all other parameters in this equation like the particle density (ρ_p), the standard density (ρ_0) as well as the Cunningham slip correction factor of the volume equivalent diameter ($C_c(d_{ve})$) and of the aerodynamic diameter ($C_c(d_a)$) must be kept constant. If this is the case, the aerodynamic diameter of the microrods is not equal to the diameter or length of the particles, but smaller.

4.4.2 Comparison of cylindrical microparticles and their spherical counterparts regarding their aerodynamic properties

To compare the flight properties of cylindrical and spherical microparticles, the formulation µR 3 was investigated against its spherical counterparts, as this formulation was already used demonstrating successful loading of siRNA to reduce TNF-α secretion from macrophages [172]. For comparison spherical particles were chosen offering similar formulation-relevant parameters such as the diameter, the length and the volume. Therefore, particles with a diameter of 3 µm (width of the rods), with a diameter of 10 µm (length of the rods) and particles with a diameter of 5 µm (equal volume) were selected (Figure 16).
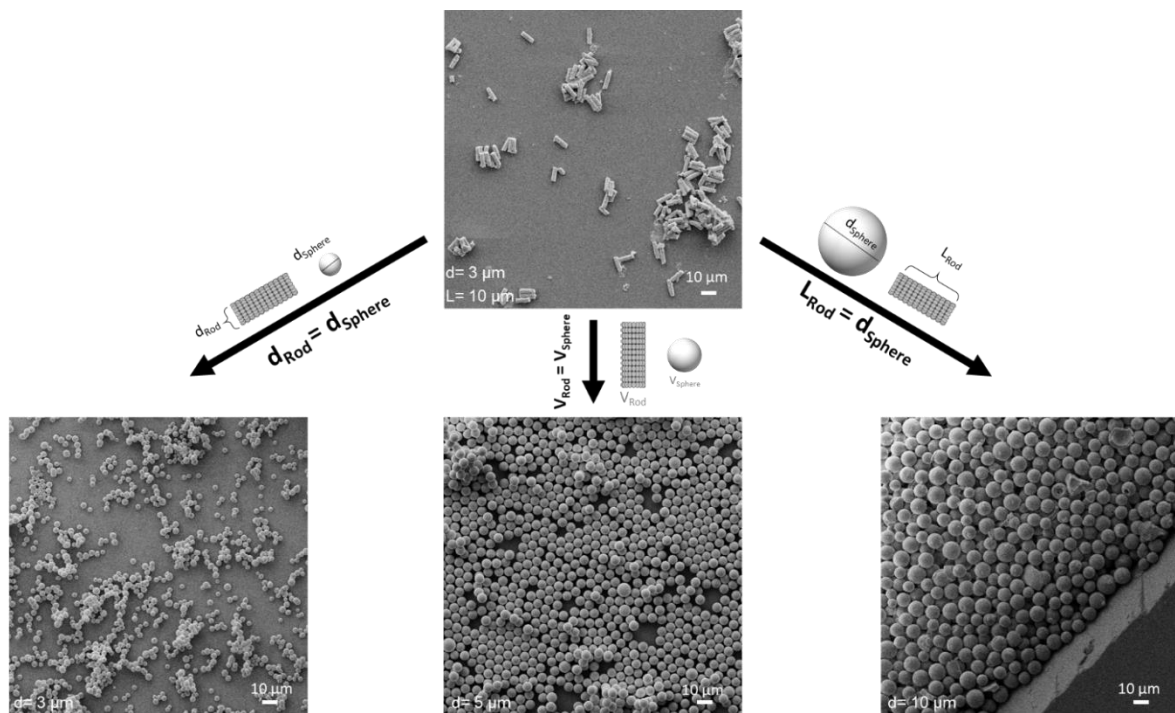
Figure 16: Scanning electron microscopy images of µR 3 (top) and the spherical counterparts (bottom). Three different diameters were used for the spherical microparticles from identical material. Diameters of 3 µm (bottom left) and 10 µm (bottom right) were used to represent the length and width of the rods. In order to use an equal-volume spherical particle, a diameter of 5.13 µm was mathematically determined, whereby silica particles with d=5 µm (bottom middle) were used to come close to this value. All four formulations shown are coated with L-leucine to keep the particle system as uniform as possible. Magnification: 1 kX.

Since in the present nanostructured drug delivery system the active ingredient is located on the surface, the diameter of a round particle with the same surface area was also calculated. Due to the internal surfaces of the nanostructured carrier this

value is with d=124.60 µm significantly higher than the size fraction that can reach the deep lung [182-184] and was therefore not analysed by NGI.

The results of the flight experiments are displayed in Table 2 demonstrating that the rods have smaller aerodynamic diameters compared to spheres with similar properties/sizes.

Table 2: Comparison between µR 3 and the spherical counterparts. The results obtained show that the rods have a smaller aerodynamic diameter than the spheres with the respective dimensions. The shift to larger MMADs for the round silica microparticles is due to the lower shape factor and the density, whereas the shape factor decreases the MMAD of the rods. When comparing the four particle formulations, it is obvious that µR3 has both the lowest MMAD and the highest FPF.

	MMAD [µm]	GSD	FPF [%]
Rods (µR 3) d= 3 µm; L= 10 µm	2.53 ± 0.23	3.20 ± 1.22	33.94 ± 5.07
Spheres d= 3 µm	4.72 ± 0.18	2.32 ± 0.17	24.19 ± 2.66
Spheres d= 5 µm	7.10 ± 0.01	2.10 ± 0.03	16.92 ± 4.51
Spheres d= 10 µm	10.95 ± 0.85	2.66 ± 0.10	14.34 ± 1.90

With an MMAD of 2.53 µm the aerodynamic diameter of sample µR 3 is smaller than the width as well as the length of the particles. This phenomenon can be attributed to the shape factor χ = 1.47 for µR 3 calculated according to Sturm [6]. The spherical particles show a shift of the aerodynamic diameter to larger values compared to their diameter caused by the density of the material (2.1-2.2 g/cm^3) [185]. Especially for an equal volume particle with d=5 µm the MMAD is 7.10 µm, which is 2.81-fold higher than µR 3. Additionally, the spheres with d=3 µm are already at the upper end of the respirable particle population with an aerodynamic diameter of 4.72 µm. These results show that cylindrical microparticles can provide better aerodynamic properties due to their shape than comparable round microparticles of the same dimensions.

4.5   Conclusion

Based on the obtained NGI results the shape of the drug delivery system has a significant influence on the aerodynamic diameter. When comparing two particle systems, where the material is identical and only the shape differs, an improvement of the flight characteristics of rod-like particles can be observed. With almost the same volume, the aerodynamic diameter of round particles is over 2.8-fold higher than the cylindrical counterpart allowing to transport potentially more drug. Looking at the surface, µR 3 has an area of 48,75 µm^2, which corresponds to a sphere with d=124.6 µm. This shows that the surface loading of µR 3 could be so large that no spherical reference sample can be generated for lung application. Thus, the developed formulation presents flight characteristics possible for a pulmonary delivery system.

5. siRNA delivery to macrophages using aspherical, nanostructured microparticles as delivery system for pulmonary administration

This section refers to the following publication:

siRNA delivery to macrophages using aspherical, nanostructured microparticles as delivery system for pulmonary administration

Thorben Fischer[1], Thomas Tschernig[2], Franziska Drews[3], Kristina Brix[4], Carola Meier[2], Martin Simon[3], Ralf Kautenburger[4], Marc Schneider[1*]

Affiliations

[1]Department of Pharmacy, Biopharmaceutics and Pharmaceutical Technology, Saarland University, Campus C4 1, 66123 Saarbrücken, Germany

[2]Anatomy and Cell Biology, Medical Faculty, Saarland University, building 61, 66421 Homburg, Germany

[3]University of Wuppertal, Molecular Cell Biology and Microbiology, Department of Chemistry and Biology, Gaußstr. 20, 42097 Wuppertal, Germany

[4]Institute of Inorganic Chemistry – WASTe-Elemental Analysis Group, Campus C4 1, 66123 Saarbrücken, Germany

5.1 Abstract

The delivery of oligonucleotides such as siRNA to the lung is a major challenge, as this group of drugs has difficulties to overcome biological barriers due to its polyanionic character and the associated hydrophilic properties, resulting in inefficient delivery. Especially in diseases such as asthma, chronic obstructive pulmonary disease and cystic fibrosis, where increased proinflammation is present, a targeted RNA therapy is desirable due to the high potency of these oligonucleotides. To address these problems and to ensure efficient uptake of siRNA in macrophages, a microparticulate, cylindrical delivery system was developed. In the first step, this particle system was tested for its aerodynamic characteristics to evaluate the aerodynamic properties to optimize lung deposition. The mass median aerodynamic diameter of 2.52 ± 0.23 µm, indicates that the desired target should be reached. The inhibition of TNF-α release, as one of the main mediators of proinflammatory reactions, was investigated. We could show that our carrier system can be loaded with siRNA against TNF-α. Gel electrophoreses allowed to demonstrate that the load can be incorporated and released without being degraded. The delivery system was found to transport a mass fraction of 0.371% [%w/w] as determined by inductively coupled plasma mass spectroscopy. When investigating the release kinetics, the results showed that several days are necessary to release a major amount of the siRNA indicating a sustained release. The cylindrical microparticles with an aspect ratio of 3.3 (ratio of length divided by width) were then tested *in vitro* successfully reducing TNF-α release from human macrophages significantly by more than 30%. The developed formulation presents a possible oligonucleotide delivery system allowing due to its internal structure to load and protect siRNA.

5.2 Graphical abstract
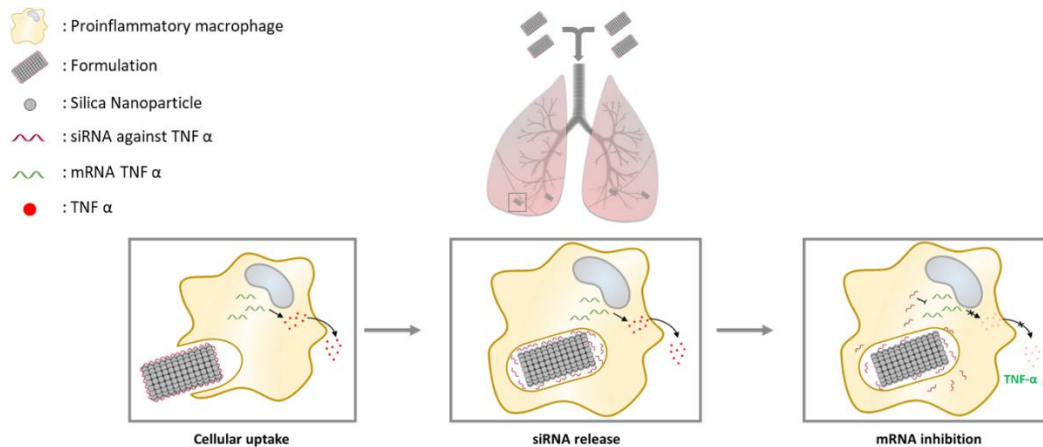
Figure 17: Graphical abstract from siRNA delivery to macrophages using aspherical, nanostructured microparticles as delivery system for pulmonary administration

5.3 Introduction

Chronic lung diseases are important due to their high mortality and morbidity rates as well as their broad distribution in the human population [19, 186]. Diseases like asthma, chronic obstructive pulmonary disease (COPD) and cystic fibrosis (CF) are the best-known representatives of this clinical pattern [20, 21]. Here, the innate immune system is no longer able to protect the lungs from pathogens due to various influences, which leads to an increased inflammatory reaction [187]. The cell population that contributes a large part to this inflammatory response are macrophages, as the first line of defence against inhaled harmful substances like air pollutants and pathogens [188, 189]. If these substances are not removed and the retention time in the lungs increases, the macrophages decompose them by phagocytosis, leading to an increased release of inflammatory mediators which enhances the activation of the immune system [190]. The most prominent mediator, which plays a central role in the inflammation process, is the tumour necrosis factor alpha (TNF-α). This cytokine not only induces an increased production of itself and other proinflammatory cytokines like interleukin-1 beta, it also activates further immunologically active cells, which enhance the inflammation status [191-193]. Therefore, specifically targeting macrophages is desirable in order to inhibit the inflammation cascade at its origin. However, in order to reach the regions of the lungs where this cell type is located, the aerodynamic diameter of the formulation

should have a value of 1–5 μm, to ensure that a large part of the delivery system arrives at its target [182-184, 194]. Commercial inhalation devices on the market produce spherical microparticles of defined size in this range to ensure transport to the lungs [195]. However, the transport of oligonucleotides, such as siRNA, across biological barriers is not easy to accomplish. This is caused by the negative charge and the associated hydrophilic properties, leading to an inefficient delivery [196-198]. Therefore, a specific transport into the desired cell population is important to improve the currently inefficient targeting of siRNA [199]. Especially in acute lung diseases, such as COVID-19-induced hyperinflammatory viral pneumonia, a targeted transport of inhibitory RNAs will be required to rapidly reduce inflammation. This approach to siRNA treatment is currently being considered as well as other drug classes [200-203]. To overcome this hurdle, the administration of siRNA should be non-invasive, since contact with serum proteins could cause siRNA degradation. Such proteins are not present on the apical side of the lung, resulting in delayed destruction [204]. In addition, the targeted delivery of siRNA into macrophages allows specific inhibition of cytokine release, thus reducing the risk of side effects [205]. In the interaction between particles and cells such as macrophages, it has already been shown that changing the geometry of the particle system influences the interaction [206]. This has already been shown for cylindrical microparticles evaluating that a change in aspect ratio can alter the uptake in macrophages [174]. In addition, the developed cylindrical microparticle system relies on drug surface loading allowing large amounts to be adsorbed. A spherical particle offering the same loading ability, would have a diameter >100 μm, which is not respirable. For production, a template-assisted approach was used to fill nanoparticles into the cylindrical pores of a template membrane with a specific pore size [81, 96]. Nanostructured particle stabilization in the pores was realized by the layer-by-layer technique [160]. For this method, the membrane is alternatingly placed in a solution with polycationic and polyanionic polyelectrolytes so that the polymers adhere to the surface and increase the ionic attraction. This formulation has several advantages that a spherical microparticle is unable to achieve. Due to the aspherical shape, the uptake of alveolar macrophages can be modified in comparison to their spherical counterpart [173]. This leads to a delayed availability of the cargo, which might lower the frequency of dosing. In addition, the individual nanoparticles are coated with

drug by the layer-by-layer procedure, whereby each fragment of the microparticles is loaded [81]. Thus, a targeted transport into immunologically active epithelial cells [207], which are also potential targets in various lung diseases such as asthma, COPD and CF [196], can also occur when the microparticles disintegrate into the individual nanoparticles before uptake by macrophages [175]. This decay allows a rapid uptake of the nanoparticles into the immunologically active epithelial cells [208, 209], which is particularly important in diseases such as non-eosinophilic asthma, where epithelial cells are mainly involved in the inflammation process [210]. Hence, this formulation is capable to address macrophages as well as epithelial cells, both of which induce a proinflammatory immune response [96, 175]. Thus, the sizes of the particles are the key parameter for uptake into different cell types. Phagocytosis is performed by macrophages and neutrophils and describes the uptake of particles >0.5 µm [211]. Particles <0.5 µm are absorbed by alveolar epithelial cells [212], but larger particles can also be taken up. Particles >1 µm are not taken up by these cells [213]. In addition, due to the rod shape, the deep lung can be reached as the aerodynamic properties are mainly attributed to the width of the particles allowing to reach the target cells [93, 214]. Previous studies have also shown that aspheric, nanostructured microparticles can successfully transfect alveolar macrophages both *in vitro* and *in vivo* [96]. The aim of this work was to incorporate siRNA against TNF-α into nanostructured microparticles for the passive targeting of macrophages and the inhibition of cytokine release of alveolar macrophages. For this delivery system, amorphous silica nanoparticles were used as model particles, since their physicochemical properties make them well-suited for formation of microparticles using layer-by-layer technique. However, this model would not be a first-choice system for human application because of the inflammatory properties in the respiratory tract [215, 216]. However, an exchange with biocompatible particle systems is possible [161], but complicates the production of the carrier system. The specific delivery of the developed microparticles should allow to silence the TNF-α expression. Thus, the continuous inflammation of the lung could be interrupted, potentially enabling new treatment options [190, 217].

5.4 Materials and methods

5.4.1 Materials

Rhodamine green-labelled silica nanoparticles with a hydrodynamic diameter of 220.2 nm ± 3.1 nm (ζ-potential = -42.1 mV ± 0.8 mV; PDI = 0.0173 ± 0.0054) were purchased from Kisker Biotech (Steinfurt; Germany). Branched polyethyleneimine 25 kDa and L-leucine were purchased from Sigma Aldrich (Steinheim, Germany). Dextran sulphate 10 HS was purchased from TdB Labs (Uppsala, Sweden). RPMI-1640 cell culture medium, Hanks' Balanced Salt solution, 4′,6-diamidino-2-phenylindol solution (DAPI), dimethyl sulphoxide (DMSO), phorbol 12- myristate 13-acetate (PMA), lipopolysaccharides from *Escherichia coli* (LPS), 3-(4,5-dimethylthiazol-2-yl)-2,5-diphenyltetrazolium bromide (MTT), lactate dehydrogenase (LDH) cytotoxicity detection kit and ethidium bromide solution were obtained from Sigma Aldrich Life Science GmbH (Seelze, Germany). Fetal calf serum (FCS) was purchased from Lonza (Basel, Switzerland). Alexa Fluor® 633, nuclease-free water, TNF-alpha Human ELISA Kit and tetrahydrofuran were obtained from Thermo Fisher Scientific Inc. (Darmstadt, Germany). SYBR® Gold nucleic acid gel stain was obtained from Invitrogen (Paisley, UK). IbiTreat® microscopy chambers for CLSM imaging were acquired from Ibidi® GmbH (Martinsried, Germany). Nuclepore® Track-Etched membranes with a pore size of 0.1 µm and 3 µm in diameter were purchased from Whatman plc (Kent, UK). Silencer® Pre-designed siRNA (Sequences: Sense (5′-GGACGAACAUCCAACCUUCtt-3′) Antisense (5′-GAAGGUUGGAUGUUCGUCCtc-3′)) was purchased from Ambion Inc (Austin, US). Silencer™ Select Negative Control No. 1 siRNA (Sequences: Sense (5′-UAACGACGCGACGACGUAAtt-3′) Antisense (5′-UUACGUCGUCGCGUCGUUAtt-3′)) used as negative control for siRNA (scrambled siRNA) was purchased from Invitrogen™ (Carlsbad, US). MicroRNA marker was purchased by New England Biolabs (Ipswich, US).

5.4.2 Particle preparation

This section was already described in chapter 3.1 Template-assisted approach for the fabrication of cylindrical microparticles.

5.4.3 Aerodynamic particle size analysis by Next Generation Impactor

In order to investigate the aerodynamic size distribution of the aspheric microparticles, a Next Generation Impactor (NGI) (Copley Scientific, Nottingham, UK) was used. The settings were the same as described from Marple *et al.* [9]: the air flow was adjusted to 60 L/min by a M1A flowmeter (Copley Scientific, Nottingham, UK) to generate an efficient aerosol of the formulation [178, 179]. The collection cups were not coated as this does not affect the measurement results [218]. To improve the flight properties, the formulation was coated with L-leucine. Therefore, an exact mass of the rods was weighed and redispersed in an L-leucine solution with a concentration of 0.4% of the rod mass. This suspension was then lyophilized to ensure homogeneous coating of the formulation. Approximately 3 mg of this powder was filled into a capsule, which was then placed in a HandiHaler® (Boehringer Ingelheim, Ingelheim, Germany) and punctured. An air flow of 60 L/min was then generated for 4 s using a vacuum pump (Erweka, Langen, Germany) to aerosolise the formulation. Subsequently, all components of the NGI were rinsed with defined volumes of water and collected for measurement by microplate spectrophotometer (TecanReader® infinite M200, Tecan, Männedorf, Switzerland) to determine the concentration of the microparticles for each stage. Mass Median Aerodynamic Diameter (MMAD), Fine Particle Fraction (FPF) and Geometric Standard Deviation (GSD) were then calculated as described from Abdelrahim *et. al.* [180] and as done already before [28, 181]. In addition, the emitted fraction (EF), which describes the powder fraction leaving the inhaler in relation to the recovered dose [219], was also determined to provide data for the efficiency of the aerosolization process.

5.4.4 Cell differentiation into macrophages (THP-1 -> dTHP-1)

For all the *in vitro* studies in this work, the human monocytic cell line THP-1 was used. Cells were differentiated into M0 macrophage-like cells. For that, phorbol 12-myristate 13-acetate (PMA) was added to RPMI 1640 medium with 10% fetal calf serum (FCS) to get a total concentration of 50 ng/mL. 200 µL of this mixture was then added to the wells, which contained $2*10^4$ cells each. The cells were incubated over three days in this differentiation medium in a humidified atmosphere of 5% carbon dioxide at 37 °C. After two washing steps with Hank's Balanced Salt Solution (HBSS), the medium was replaced by resting medium which does not contain PMA. At the end of this differentiation process, the morphology of the cells was checked by light microscopy. Here, the round, small undifferentiated cells showed a clear increase in volume, adhesion to the bottom of the well and additionally the shape of the cells changed to an asymmetric pattern, which was an indication for the successful differentiation to macrophage-like THP-1 cells (dTHP-1) [220].

5.4.5 MTT-Assay

For the 3-(4,5-dimethylthiazol-2-yl)-2,5-diphenyltetrazoliumbromid (MTT)–Assay, THP-1 cells were cultivated in 96–well plates and differentiated to M0 macrophage–like cells as described in the section above. Each well contained $2*10^4$ cells with 200 µL RPMI 1640 medium. The cells were incubated for 4, 24 and 48 h with a concentration of 100, 200 and 300 µg/mL of our formulation, dispersed in RPMI medium. Here, the formulation was tested once unloaded and once loaded with the oligonucleotide. Thereby 300 µg/mL of the loaded formulation was equivalent to 2.68 µg/mL siRNA, 200 µg/mL contained 1.79 µg/mL and 100 µg/mL included 0.89 µg/mL siRNA. The supernatant was then removed, and the cells incubated with MTT reagent for 4 h. After the reaction took place, the reagent was removed and changed through dimethyl sulphoxide (DMSO) to solve the formazan crystals. The absorption was measured at 550 nm after 20 min incubation using a microplate spectrophotometer. As positive control (PC) 1% Triton X was used, whereas pure RPMI medium was used as negative control (NC).

5.4.6 LDH-Assay

In parallel to the MTT-assay, a lactate dehydrogenase (LDH)-assay was performed to obtain a second measurement to determine toxicity evaluating the integrity of the cell membrane. In this experiment, 100 µL of the supernatant after incubation with the formulation from the MTT-assay were mixed with 100 µL of the LDH solution. After 5 min, the absorption was measured at 492 nm using a microplate spectrophotometer.

5.4.7 Gel electrophoresis for siRNA qualification

To qualify the used siRNA after loading into the formulation, gel electrophoresis was performed. First, the oligonucleotide had to be replaced from the rods. For this, the rods were heated at 94 °C for 3 min in Loading Dye, consisting of 95% formamide, 10 mM EDTA and 5% w/v bromophenol blue and afterwards centrifuged at 15.000 g for 10 min. The supernatant was then loaded onto a 17% urea denaturing polyacrylamide gel stained in SBYR® Gold. RNA size was estimated using the microRNA Marker (NEB). Additionally, 1 µL of the same sample was loaded on a Small RNA Bioanalyzer Chip and evaluated on a Bioanalyzer 2100 (Agilent).

5.4.8 Quantification of siRNA using Inductively Coupled Plasma – Mass Spectrometry

Inductively Coupled Plasma - Mass Spectrometry (ICP-MS) (7500cx, Agilent, Santa Clara, USA) was performed to determine the amount of the loaded siRNA cargo. For this purpose, the formulation was dissolved in nitric acid (69%, ultra-pure) for two weeks to detach the siRNA from the formulation. This solution is then heated to over 5000 °C by a high-frequency electric field in an argon gas stream, resulting in a plasma. This leads to an atomization and subsequently mono ionisation of the sample. The resulting ions can then be quantified by mass spectrometry. Since oligonucleotides are the only compounds in the formulation that contain phosphorus, quantification of siRNA can be executed by determining the amount of phosphorus in the formulation.

5.4.9 *In vitro* release of siRNA *via* fluorescence measurement

To characterize the release kinetics of siRNA in macrophages, a solution was prepared that reflects the milieu in the phagolysosome, the phagolysosomal simulant fluid [221]. This fluid consists of sodium phosphate dibasic anhydrous (Na_2HPO_4) 142.0 mg/L, sodium chloride (NaCl) 6650.0 mg/L, sodium sulphate anhydrous (Na_2SO_4) 71.0 mg/L, calcium chloride dihydrate ($CaCl_2 \cdot 2H_2O$) 29.0 mg/L, glycine ($C_2H_5NO_2$) 450.0 mg/L, potassium hydrogen phthalate (1-(HO_2C)–2-(CO_2K)–C_6H_4) 4084.6 mg/L and alkylbenzyldimethylammonium chloride 50 ppm. The formulation was dispersed in this solution and a concentration of 0.5 mg/mL was set. The resulting suspension was then divided into micro-reaction tubes with 500 µL each and incubated for a defined time at 37 °C while shaking. After the defined incubation times, the tubes were centrifuged at 20.000 g for 15 min to avoid possible measurement falsifications by nanoparticles. The supernatant obtained was then mixed with SYBR® Gold and the fluorescence at λ_{ex}= 485 nm and λ_{em}= 535 nm was analysed using a microplate spectrophotometer [222].

5.4.10 Enzyme Linked Immunosorbent assay (ELISA) for determination of TNF-α

To determine a possible change of TNF-α release after incubation with the siRNA-loaded rods, ELISA measurements were performed. Therefore 200.000 cells per well were seeded in a 96 well plate and differentiated with PMA. The dTHP-1 were then incubated with different rod concentrations from 100 to 300 µg/mL at 37 °C for 2 days followed by a treatment with 200 µg/mL lipopolysaccharide (LPS) from Salmonella typhimurium for 6 h to induce a polarization to M1 and a related cytokine release. The supernatant was centrifuged at 200 g for 10 min and analysed by ELSIA. As controls rods with scrambled siRNA, without any oligonucleotide as well as pure scrambled and non-scrambled siRNA were used. The dTHP-1 were stimulated with LPS for 6 h as positive control. Untreated dTHP-1 served as negative control.

5.4.11 Scanning electron microscopy for analysis of rod morphology

Scanning electron microscopy (SEM) was used to get a detailed impression of the produced microparticles and their nanoparticular structure. The microscope used was a Zeiss Evo HD 15 Electron Microscope (Carl Zeiss AG, Jena, Germany) equipped with a Lanthanum hexaboride (LaB$_6$) cathode. For sample preparation, some droplets of the formulation dispersed in water were placed on a silica wafer and left to dry. The surface was then coated with an approx. 10 nm thick gold layer using a Quorum Q150R ES sputter coater (Quorum Technologies Ltd., East Grinstead, UK) and afterwards analysed by SEM with a voltage of 5 kV and a magnification of 1 kX and 15 kX.

5.4.12 Cellular uptake investigated by confocal laser scanning microscopy

For analysing the *in vitro* uptake using the colocalization between formulation and macrophages, rhodamine green-labelled microrods were detected by confocal laser scanning microscopy (LSM710, Carl Zeiss AG, Jena, Germany), using an argon-ion-laser with λ= 488 nm. The siRNA was not stained separately in this experiment because the staining reagents could have caused a possible change in uptake. To visualize the dTHP-1 cell line, 4',6-diamidino-2-phenylindole (DAPI) with a concentration of 10 µg/mL was used to stain the cell nucleus whereas N-hydroxysuccinimide Alexa Fluor® 633 with a concentration of 5 µg/mL was used to stain the cell membrane. To detect the stained cell membrane, a helium-neon laser (HeNe633) with λ= 633 nm was applied. DAPI was visualized with a laser diode 405-30 utilizing λ= 405 nm. The measurement was performed in an ibidi® µ-Slide 8 well plate using a water-corrected objective M27 with a numerical aperture of 1.2 and a 40x magnification objective. For the uptake analysis, each well was seeded with 10^4 cells and differentiated like described in the section above. Subsequently, 200 µL of a 200 µg/mL rod-suspension was added to the cells and incubated for different time intervals. To quantify the uptake behaviour of macrophages, three individual measurements with 500 randomized chosen cells were performed at each time point and the percentage of cells that took up the formulation was determined. To evaluate whether an uptake has taken place, the Zen blue software (Carl Zeiss AG, Jena, Germany) was used to analyse the colour of the particles. In the case of

an uptake, the green fluorescent formulation was colocalized with the red stained cell compartments, resulting in a yellow staining. This was an indication for absorption.

5.4.13 Statistical evaluation

The significance was tested by two-sided Student´s t-test using Excel 365 software. A significant change in the data was assumed at $p < 0.05$.

5.5 Results and discussion

5.5.1 Particle characterization

For analysing the cytokine inhibition of the M0-like macrophages (dTHP-1), layer-by-layer stabilized microrods were fabricated with siRNA against TNF-α loaded on their surface. The polyanionic cargo was adsorbed and stabilized by electrostatic interactions with the underlying positively charged bPEI. Three double layers of polymer led to a stable formulation as shown in Figure 18. This was also confirmed by analysing the statistical size distribution by measuring the length of the particles from CLSM images using ImageJ software (Figure 24). The size distribution obtained shows that the majority of the formulation got a length between 8 and 10 µm. As in-process control, the sample was treated with ethidium bromide and analysed by CLSM to determine whether loading had occurred at the surface. As shown in Figure 18D, fluorescence at the specific excitation wavelength of ethidium bromide could be observed. However, unloaded microrods showed no ethidium bromide fluorescence. The number of the cylindrical carriers was determined by a Neubauer counting chamber leading to approximately 6×10^6 rods per membrane.
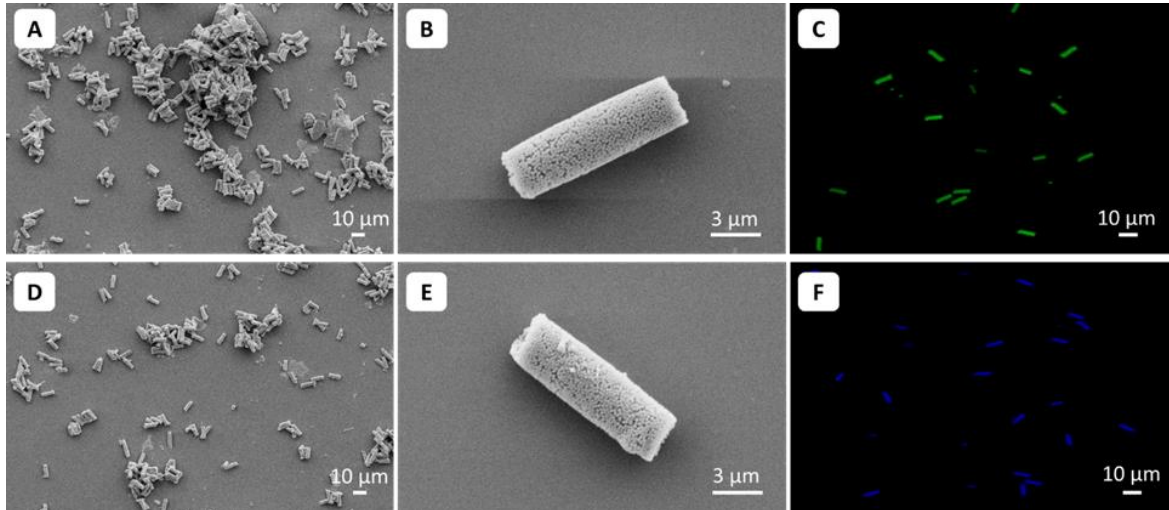
Figure 18: The manufactured microrod formulation illustrated by scanning electron microscopy (A), (B), (D), (E) and confocal laser scanning microscopy (C), (F). In figure (A), an overview of the formulation is shown, whereas in figure B the SEM image illustrates the nanostructured composition of a microrod, stabilized by bPEI and dextran sulphate. (C) The formulation is dispersed in water and visualized by CLSM (λ_{ex}= 485 nm, λ_{em}= 510 nm), since the nanoparticles are fluorescently labelled. (D), (E) and (F) show the microrods loaded with siRNA against TNF-α. (D) An overview of the formulation with siRNA on the surface, leading to a stable formulation. (E) At a higher magnification, the nanostructure of the microrods can also be seen here. (F) Here, ethidium bromide was added to the formulation from (D) and (E) to visualize the genetic material. λ_{ex}= 285 nm and λ_{em}= 590 nm were used to detect the fluorescent property. After ethidium bromide incubation, unloaded particles showed no fluorescence at these specific wavelengths. The microparticles are well dispersed and stable within weeks. The cylindrical shape, which is determined by the defined pore size of the template membrane, exhibits a length of 10 μm and a width of 3 μm. Representative sections were used for all images.

The characteristic shape as well as the dimensions are defined by the pores of the template membrane. The formulation chosen with a length of 10 μm and a width of 3 μm leads to an aspect ratio of 3.3 (ratio of particle length to particle width). An increase of the aspect ratio leads to a delayed uptake in macrophages as described in literature [102]. This delayed absorption offers advantages compared to spherical microparticles. These are degraded faster and more efficiently by the macrophages and removed from the target organ [95]. As a result, less active substance is available, thus reducing therapeutic success.

5.5.2 Flight characteristics

For a targeted transport of the active ingredient into the deep lung, the delivery system must have an aerodynamic diameter of 1–5 μm [183]. To ensure this property for the developed formulation, an NGI experiment was performed. The results obtained are listed in Table 3 and show that the cylindrical microparticles

with a length of 10 µm and a diameter of 3 µm exhibit an aerodynamic diameter of 2.52 µm. This value is in the range to allow deposition in the deep lung [223].

Table 3: Results from NGI analysis for the cylindric microparticles with a length of 10 µm and a width of 3 µm. The data obtained show, that the formulation displays properties that are suitable for deep lung delivery since the MMAD is < 5 µm. MMAD: mass median aerodynamic diameter describing the average size of particles, which reach the impactor [12]; GSD: geometric standard deviation, the sharpness of the collection efficiency described as the root of the quotient of $d_{84.1}$ and $d_{15.9}$. [224]; FPF: fine particle fraction providing the percentage of the mass with a size < 5 µm [12], EF: emitted fraction: the powder fraction leaving the inhaler in relation to the recovered dose [219].

MMAD [µm]	GSD	FPF [%]	EF [%]
2.52 ± 0.23	3.20 ± 1.22	33.94 ± 5.07	93.83 ± 1.99

Notably, the measured value is below the diameter of the rods and is in contrast to previous data from cylinders of soft materials such as gelatine [181]. This seems to be surprising at first glance but could be explained by the porous character of the rods due to the nanostructured architecture. For the gelatine nanoparticle-composed rods, the spaces between the nanocarriers were filled with mannitol thus not leaving voids. In combination with the surface stabilisation by the layer-by-layer technique the density of the cylinder might be modified accordingly due to the non-filled areas. However, such an explanation must consider the low standard deviations of the MMAD: this is most likely a result of the intact morphology of the rods after aerosolization. To confirm this hypothesis the individual stages of the NGI were visualized by SEM (Figure 25 and Figure 26). Here only a small fraction of the formulation was found in stages 5 to 8 (Figure 26), representing an MMAD < 0.94 µm [9], which shows that no breakage took place caused by the experimental conditions. This is also supported by the CLSM data after application to the cells; the rods were not corrupted in length and yielded a homogeneous morphology and size. Besides the rod shape which reduces obviously the deposited amount we also face an issue with double structures. Those are a consequence of the membrane structure, lowering the EF and FPF. Many double pores can be seen, which will be filled but cannot easily separated afterwards. But in general, this should be able to be solved. The obtained results with a FPF of almost 34% and an EF of over 90% indicate, that the flight properties are in an acceptable range for an inhalable system [225]. Thus, the aerodynamic properties of the developed

formulation show that the formulation displays properties that are suitable for deep lung delivery.

5.5.3 Uptake kinetics for different time points

To determine the uptake rate of the formulation in macrophages, microrods were incubated with dTHP-1 cells for 4, 24 and 48 h and visualized by CLSM. The results after staining the individual cell components are shown in Figure 19. After 4 h, it is evident that the macrophages begin to internalize the particles, but many rods are still on the surface, outside of the cells. This is obvious looking at the particles colour. Uptaken particles have overlapping own (green) fluorescence with the fluorescence of the stained actin (red) resulting in yellow merging the channels. Furthermore, no disintegration of the microrods is visible yet. After 24 h most of the formulation is internalized and furthermore a decomposition of the microparticles is detectable. This result shows that these properties enable macrophages as well as immunologically active epithelial cells to be addressed, both of which cause a proinflammatory reaction [196, 207]. The uptake of the released nanoparticles from the microparticles was already shown in A549 epithelial cells [175]. Within 48 h, all microrods are absorbed and only fragments are visible in the macrophages. This disintegration in the macrophages increases the surface area of the carrier system, thus accelerating the release of the drug. The obtained CLSM images from Figure 19 also correlate with the measurement results of the quantification of the uptake. Here, we observed that for 4 h incubation time $59.20 \pm 7.75\%$ of the cells, for 24 h $85.40 \pm 3.47\%$ and for 48 h $93.00 \pm 1.78\%$ of the cells took up the formulation. This shows that a longer incubation time favours an increased uptake of the formulation. This series of experiments showed that after 48 h of incubation, over 90% of the human macrophages had internalized microparticles and that disintegration took place after several hours, which increases the surface area and thus changes the release kinetics as well as enabling the addressing of different cell types.
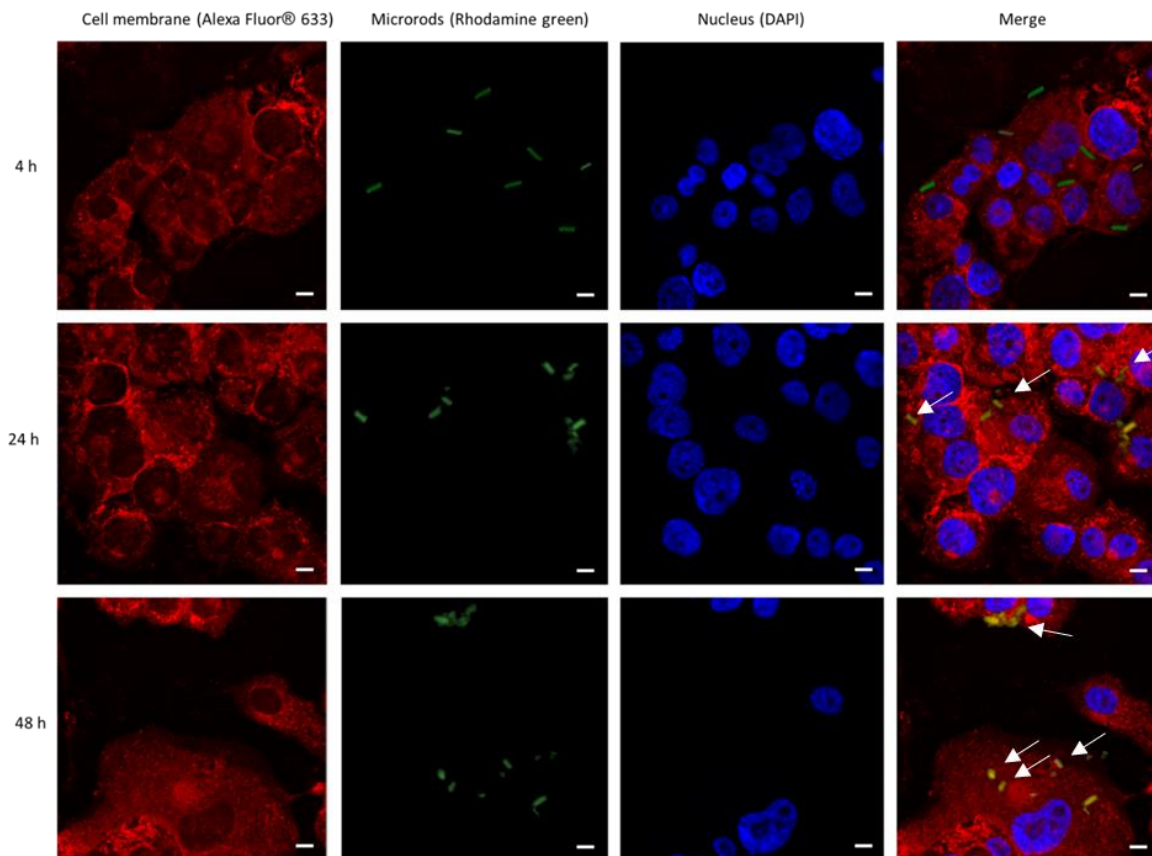
Figure 19: Cell uptake kinetics after 4, 24 and 48 h visualized by CLSM. For this experimental setup, microrods with a length of 10 µm and a width of 3 µm were incubated with the macrophage model cell line dTHP-1. After 4 hours of incubation, only a small part of the formulation was absorbed without any disintegration. By increasing the incubation time up to 24 h or 48 h, most of the microrods are taken up. Furthermore, a disintegration of the formulation is apparent (marked with arrows). These results show that most the formulation was taken up by the alveolar macrophages within 48 h. The scalebar represents 10 µm. All the images shown are representative.

5.5.4 Cell viability

In order to obtain a first impression of how the formulation behaves *in vitro*, a cytotoxicity measurement was performed. Especially regarding later cytokine release experiments, the data of this experiment are very important for estimating which stress factor the cells are exposed to after incubation with the formulation. High mortality rates would lead to increased cytokine release. To verify this, both an MTT-and an LDH-assay were performed. Therefore dTHP-1 were incubated for up to 48 h with a concentration of 100 to 300 µg/mL which later represents the maximum concentration in the cytokine release assays. As can be seen in Figure 20, no concentration shows a high decrease in cell viability.
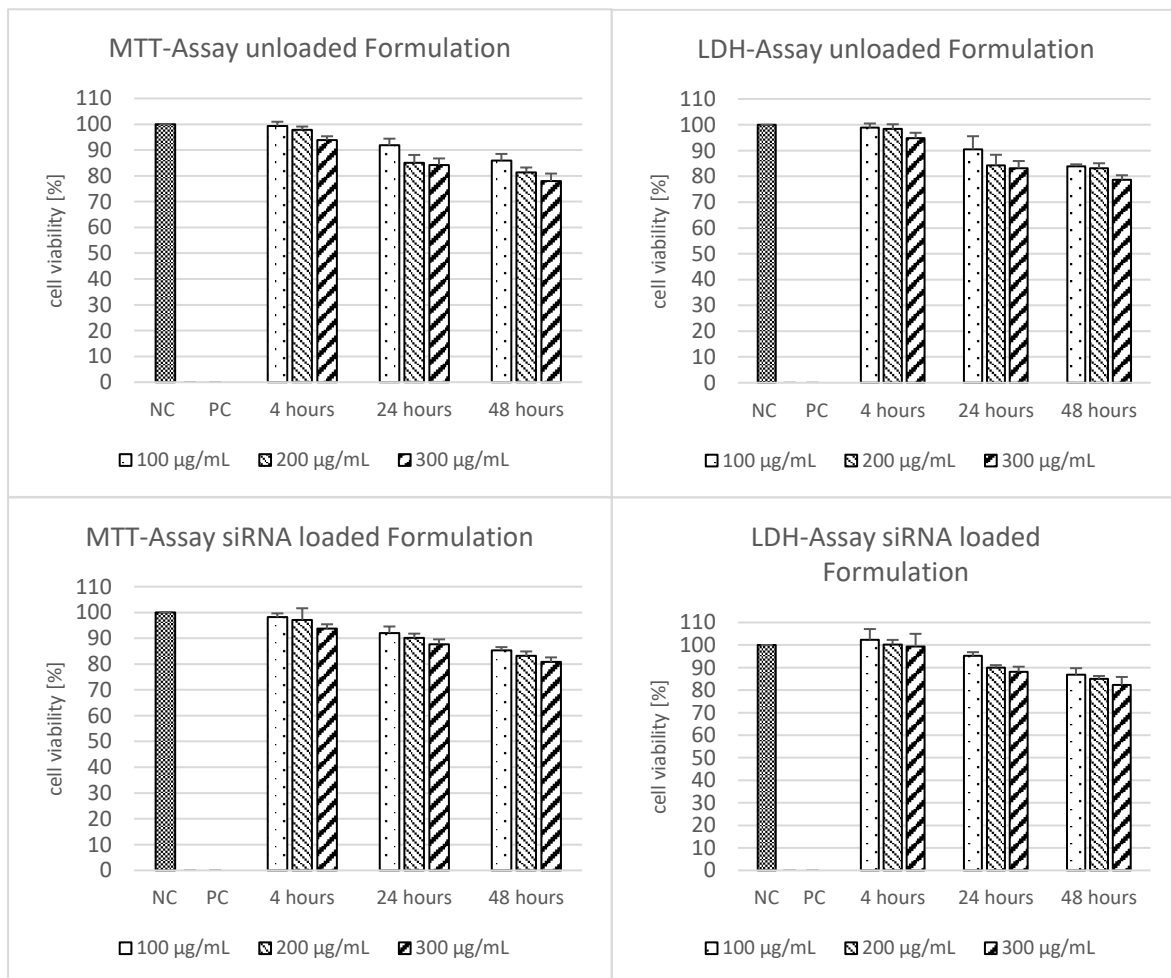
Figure 20: Determination of cytotoxicity by MTT-assay (left side) and LDH-assay (right side). The concentrations of 100 to 300 µg/mL were examined after an incubation period of up to 48 hours. The upper graphs show the toxicity data of the unloaded formulation, whereas the lower ones represent the formulation loaded with siRNA. When comparing the two formulations, it is clear that none of the tested formulations exhibits strong cytotoxicity. Additionally, the loaded one shows a slightly lower toxic potential. This shows that, based on the cytotoxicity tests, no strong cytokine release is to be expected.

5.5.5 Cargo qualification *via* gel electrophoresis

The cytokine inhibition experiments focused specifically on TNF-α as it is one of the most prominent cytokines, which is involved in the inflammatory cascade. Therefore, siRNA specifically targeting human mRNA of TNF-α was used, which is double-stranded and has a length of 21 nucleotides (nt). Before the formulation was used *in vitro*, it had to be ensured that the siRNA was intact after loading guaranteeing a release of functional material. If the siRNA was disintegrated during production, this would lead to a loss of effectiveness and it would not be possible to know whether the formulation or the degraded siRNA is the reason for the low effectiveness of the *in vitro* results. To address this aspect of stability, we extracted the siRNA from the formulation and analysed the integrity on a denaturing gel. SYBR® Gold was used to stain siRNA as this staining agent is on one hand much more sensitive than ethidium bromide and on the other hand also able to detect single-stranded RNA or DNA [226]. These properties are important conducting this experiment as the double-stranded siRNA is divided into two single strands upon extraction with the loading buffer and therefore cannot be detected with all staining agents for double-stranded oligonucleotides. In addition to standard gel electrophoresis, we loaded the extracted siRNA onto a Small RNA Bioanalyzer Chip to detect small RNA species <200 nt which were not visualized on the gel due to their low abundancy.

The results from Figure 21 show that no decomposition of the siRNA occurred during loading of the formulation. The band of siRNA extracted from the rods is at the same level as the 21 nt marker and the electropherogram of the bioanalyzer shows a peak of the same size with now smaller peaks appearing. If a degradation would have taken place, a staircase pattern in the direction of smaller bands would have been the result. Since this is not the case, the loading is not affecting the potential activity of the siRNA. Thus, the formulation can be used for further testing.
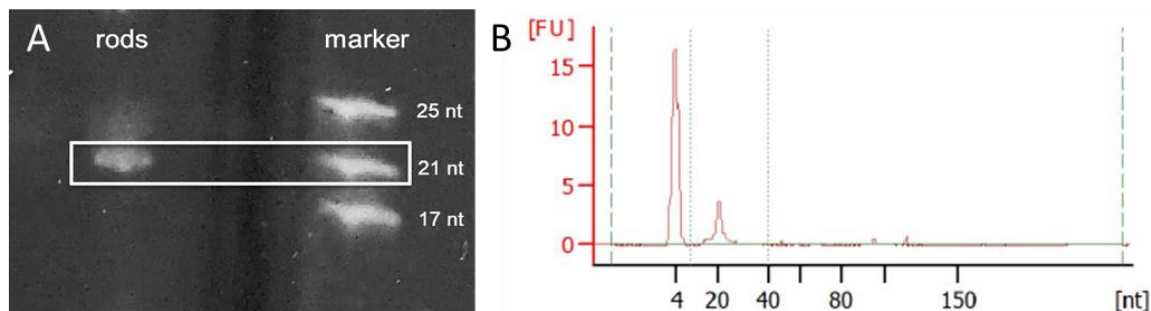
Figure 21: Analysis if the integrity of the loaded siRNA coupled to the rods is still intact after loading. (A) The siRNA was extracted from the formulation by heating in loading dye and afterwards applied to a gel stained with SYBR® Gold. The siRNA against TNF applied is double stranded with 21 nt per strand. Therefore, different markers of 25, 21 and 17 nt were loaded in parallel. (B) Extracted siRNA was then also analysed on a Small RNA Bioanalyzer chip which is suitable for separation and measurement of RNAs smaller than 200 nt. A clear 21 nt peak is visible corresponding to the siRNA detected on the gel (4 nt peak is an internal marker). Both figures clearly show no decay of the RNA because no staircase pattern in the direction of the lower nucleotide number is present. The band of the formulation is at the same level as the 21 nt marker and a clear 21 nt peak is visible in the bioanalyzer electropherogram. Thus, it can be summarized that the siRNA is not influenced during preparation.

5.5.6 Quantification of siRNA using inductively coupled plasma – mass spectrometry

Determination of the exact drug concentration is an indispensable step in the characterization of the developed formulation allowing to correlate the obtained *in vitro* data with the amount of cargo used. There are various methods for determining the active ingredient content. On the one hand, indirect content determination can be performed, like quantifying the layer solution before and after layering process determining the different amounts [227] or directly in the formulation. The direct method was used to quantify the formulation as it is more precise and less susceptible to interferences. ICP-MS was used to determine the phosphorus content of the formulation, since this element only occurs in the siRNA and thus conclusions can be reached about the loading. The results revealed a phosphorus content of: P [%w/w] = 0.034% and thus a siRNA content of: siRNA [%w/w] = 0.371%, which means that 1 mg rod formulation contains 3.71 µg siRNA. Loading corresponds to expectations and can be increased by multiple layering with the cargo [96].

5.5.7 *In vitro* release of siRNA *via* fluorescence measurement

Qualification by gel electrophoresis has already shown intact siRNA to be detached from the microrods. In this method, very harsh conditions were used which did not reflect the physiological conditions in the macrophages. Therefore, the next step was to analyse the release of siRNA under relevant, more physiological conditions. Since the formulation reaches the phagolysosome after uptake into the macrophage and releases the active ingredient there, this environment was simulated. The salt mixture was produced after Stefaniak *et al.* yielding a pH of 4.55 [228, 229]. In this solution, the formulation was incubated at 37 °C under gentle shaking and samples were taken at different time points over 15 days. As shown in Figure 22, siRNA is released from the rods under physiological conditions. The release profile shows no burst release and a slow increase in the siRNA concentration in the first days. After about 10 days the release levels off and a plateau is reached. Since *in vitro* experiments are carried out over shorter periods of time, this sustained release must be taken into consideration. The performed cytokine inhibition experiments were incubated for 2 days. Thus, it can be estimated that only about 530 ng/mg formulation is available at this time point.
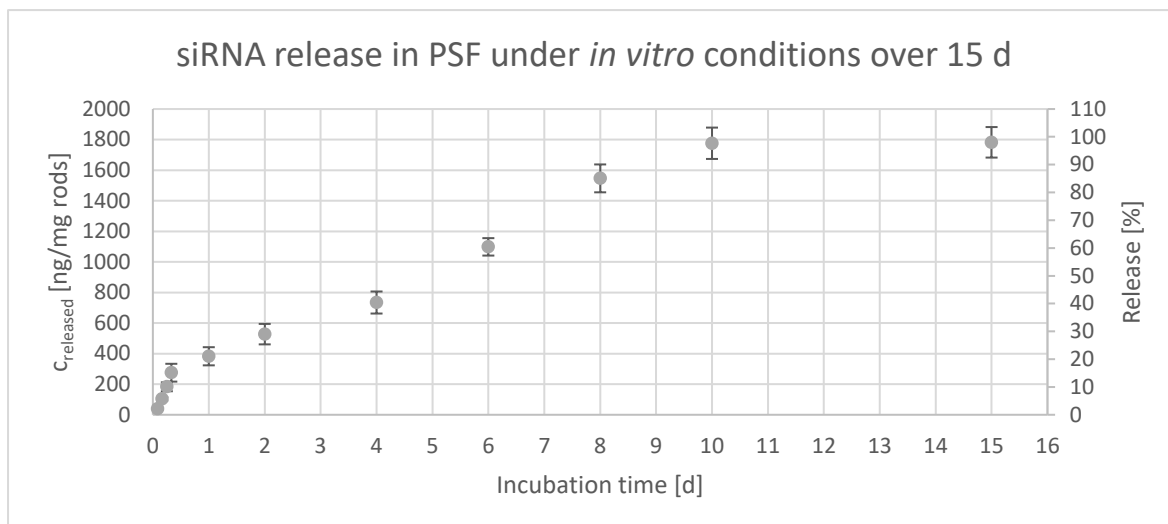
Figure 22: *In vitro* release of the formulation in PSF. For this, the formulation was incubated for 15 days at 37 °C under gentle shaking and analyzed after staining with SYBR® Gold. The results show that the release of siRNA reaches a plateau after about 10 days This plateau is formed by a continuous liberation and has no burst release. Looking at the 2-day value, which also represents the time period of the ELISA experiments, it becomes clear that only about 530 ng/mg rods were released at this time. This result must be taken into account when considering the ELISA data, as the complete load is not released and therefore lower siRNA concentrations are present. For each measuring point three individual tests were performed and the mean values, as well as standard deviation was determined (n=3).

5.5.8 Enzyme Linked Immunosorbent assay (ELISA) for determination of TNF-α

After the formulation was tested for loading, release and quality, its *in vitro* activity regarding cytokine release was evaluated. Therefore, dTHP-1 cells were grown in 96-well plates, incubated with different samples and the cytokine release was quantified by ELISA. As positive control the cells were stimulated for 6 h with LPS only whereas untreated dTHP-1 served as negative control. Since oligonucleotides may show unspecific effects, a non-specific siRNA (scrambled siRNA) was used to see if inhibitory effects on the TNF-α release might occur due to presence of the siRNA. The model used was a scrambled siRNA which, like the original siRNA against TNF-α, has 21 bp and a double-stranded structure. In addition, both siRNAs were incubated with the cell line without a carrier system but in the same concentration as in the formulation in order to show that pure siRNA cannot induce a significant biological response. At last, the biological activity after incubation with unloaded rods was analysed. After incubation, the cell line was stimulated once with LPS to see that the unloaded formulation does not cause cytokine reduction and

once not stimulated to show that the unloaded rods would not induce cytokine release. Figure 23 lists all these test groups.
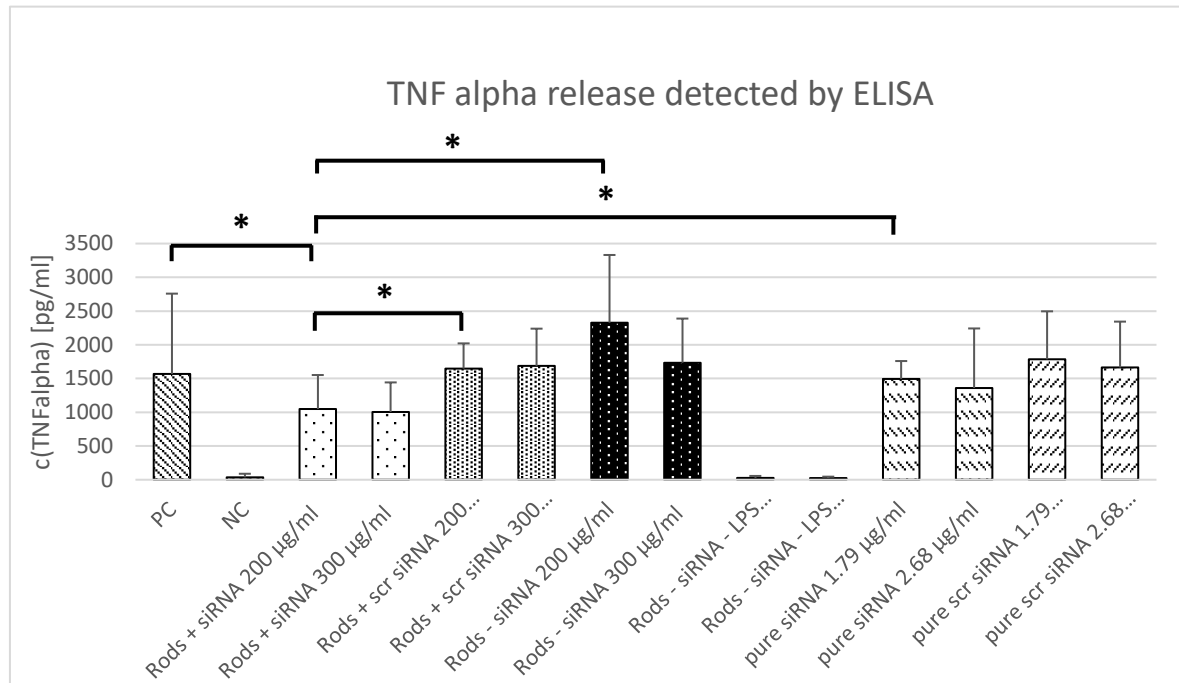

Figure 23: This graph shows the TNF-α release after incubation with different formulations over 2 d. In addition to the developed formulation, unloaded rods (Rods – siRNA) as well as rods with a non-specific RNA (Rods + scr siRNA) were used as controls. Furthermore, the siRNA against TNF-α as well as the non-specific RNA were incubated without carrier system (pure siRNA; pure scr siRNA) in order to detect possible changes in cytokine release. In all these samples, the cells were stimulated after incubation with LPS to activate cytokine production. To see if the unloaded rods induced an inflammation reaction, they were incubated with dTHP-1 without LPS stimulation. The results show, that the developed formulation significantly lowers the TNF-α level compared to the controls. Furthermore, the formulation alone does not show any inflammatory reaction. Thus it could be demonstrated that the microrods can successfully deliver siRNA against TNF-α and reduce the cytokine production. Unspecific effects do not play a role. 3 indepentent experiments were performed with each 3 different wells per measurement. Significances were calculated by Student's-t-test. * $p < 0.05$.

It becomes clear that a significant reduction of the TNF-α level with the formulation with siRNA against TNF-α occurs compared to the references used. Both the non-specific siRNA and the pure oligonucleotides without carrier system showed no reduction in cytokine release compared to the positive control. Furthermore, the unloaded formulation shows no biological response, both with and without LPS stimulation. In conclusion, it can be assumed that the shape and dimension of the delivery system is suitable to transport the siRNA into the macrophage and release it allowing to reach the site of action and thereby reducing cytokine release. However, the reduction of the TNF-α level needs to be improved as the levels reached are clearly above those of the control. This might be due to potential

degradation of the siRNA in the phagolysosome or might be due to the slow release. To improve the release other stabilization mechanism for the particles need to be evaluated in the future.

5.6   Conclusion

The performed experiments and the results obtained show that siRNA could be successfully incorporated in a rod-shaped nanostructured microparticle. The layer-by-layer approach allowed stabilization of the rods by using 3 double layers. Exchanging the outermost layer with siRNA did not alter the stability and the particles could be released from the template membrane without loss of integrity. The obtained stability of the rods was also sufficient to aerosolize the particles. The aerodynamic properties turned out to be well in the target region of 1–5 μm, were even below the width of the rods. This might be an indication for the potential the nanostructure with respect to tuning the aerodynamic properties. Due to its flight properties with an aerodynamic diameter of 2.51 μm, the formulation is capable to deposit in the deep lung reaching the macrophages. The efficient uptake is demonstrated as 90% of the THP-1 cells had taken up cylindrical particles after 48 h without acute toxic effects. This underlines the strong interaction of the aspheric particles with the macrophages. Furthermore, the results indicate, that cylindrical microparticles can be loaded with siRNA without degrading the oligonucleotide which would affect the activity. In addition, the exact content of the drug with a value of 0.371% [w/w] could be determined and the release kinetics of the oligonucleotide in the phagolysosome could be calculated using a developed release experiment. The absence of any burst release stresses the fact that the siRNA is fully adsorbed onto the particles being continuously released over several days. When observing the TNF-α values after incubation with the unloaded carrier system, no release of the cytokine is detected. This implies that the formulation itself does not induce an inflammatory reaction and TNF-α secretion. After loading with siRNA, the formulation reduced cytokine secretion compared to LPS stimulated cells. A significant difference was also detected between the scrambled siRNA and the free oligonucleotide without carrier. In future experiments, the disintegration of the nanostructured microparticles and the targeted addressing of immunologically

active epithelial cells would be of interest. This would allow two different cell populations to be addressed with the same carrier system, which could open new possibilities in RNA transport.
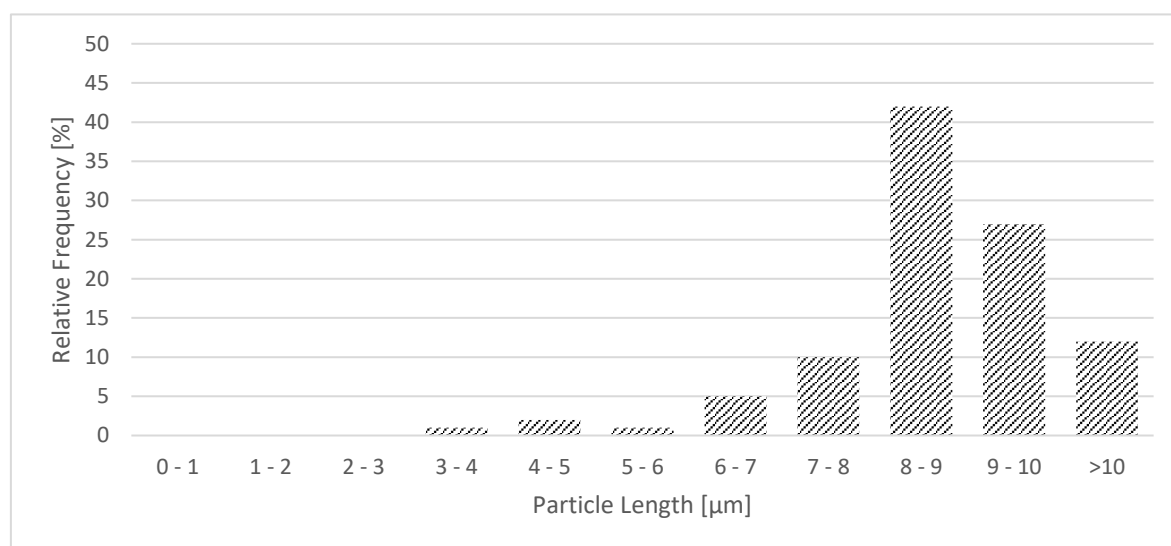
5.7   Supporting information

Figure 24: Statistical size distribution of aspherical, cylindrical microparticles with a length of 10 µm and a width of 3 µm. It is evident that the majority of the particles have a length between 8 and 10 µm. Particles < 8 µm may occur if not fully stabilized by the layer-by-layer technique, causing the particles to disintegrate during the purification step. However, this fraction is small. Particles > 10 µm are formed when the pores are not straight through the membrane but tilted. As a result, the pore is longer than the thickness of the membrane, resulting in values greater than 10 µm. For this statistic, 181 microparticles from three different batches were evaluated.

To generate the statistics in Figure 24, three different batches of the formulation with L=10 µm were prepared and recorded using CLSM. These images were then analysed with the ImageJ software to determine the length of the particles.

The results obtained show that the main part of the formulation has a length between 8 and 10 µm. Particle lengths below 8 µm occur if the particles are not completely stabilized by the layer-by-layer technique resulting in disintegration during the purification of the sample. Particles larger than 10 µm are formed when the pores of the template membrane are inclined in the membrane. This is the reason for particles exceeding the thickness of the membrane.

These statistics show that the method used to produce the microrods is suitable for producing the formulation in the postulated dimensions. Also, the distribution of the rods is small compared to other inhalable particles such as spray-dried particles [177].
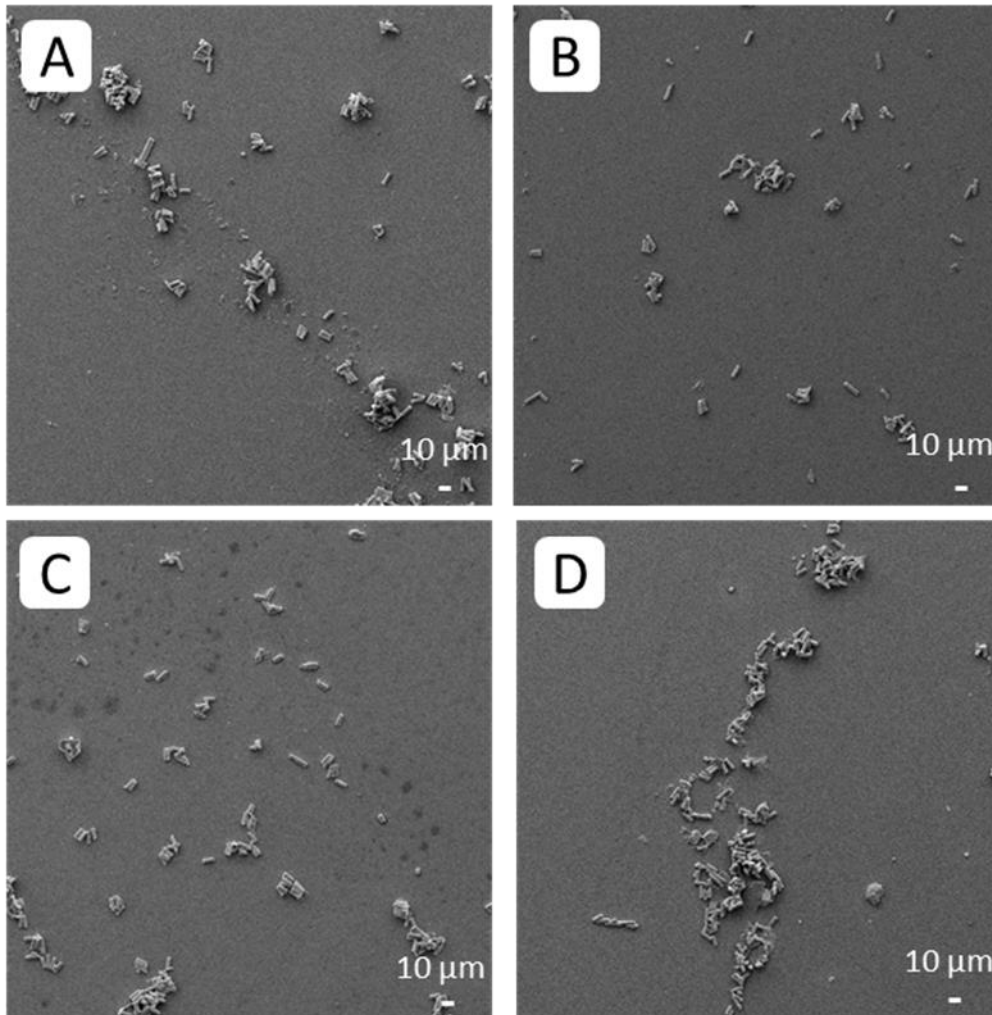
Figure 25: SEM images of collecting plates 1 to 4, numbered (A) to (D), to analyse the individual populations of the formulation after the NGI run. In these stages, the particles got a D_{50} value at a flow rate of 60 L/min from 8.06 µm (stage 1 (A)) to 1.66 µm (stage 4 (D)) [9]. Most of the formulation is transported to this area of the NGI. The pictures also show that the rods do not break during the experiment. In Stage 1 there are double rods as well as rods with a length of > 10 µm present, which is due to the Track-Etched membrane used.

The illustrated collecting plates 1 to 4 from Figure 25 show that a major part of the formulation lands in this section during NGI run. With the used flow rate of 60 L/min, particles with a D_{50} value of 8.06 µm (stage 1 (A)) over 4.46 µm (stage 2 (B)) and 2.82 µm (stage 3 (C)) to 1.66 µm (stage 4 (D)) [9] remain in these collecting plates after the experiment. In Stage 1 there are mainly double or multiple rods, which can be formed during the manufacturing process with the Track-Etched membranes used. In addition, rods > 10 µm can also be generated, as some pores are tilted and therefore do not go straight through the membrane, which results in an elongation

of the rods. However, when looking at Stages 1 to 4, it shows that the majority of the rods is not damaged by the conditions of the experimental set-up.
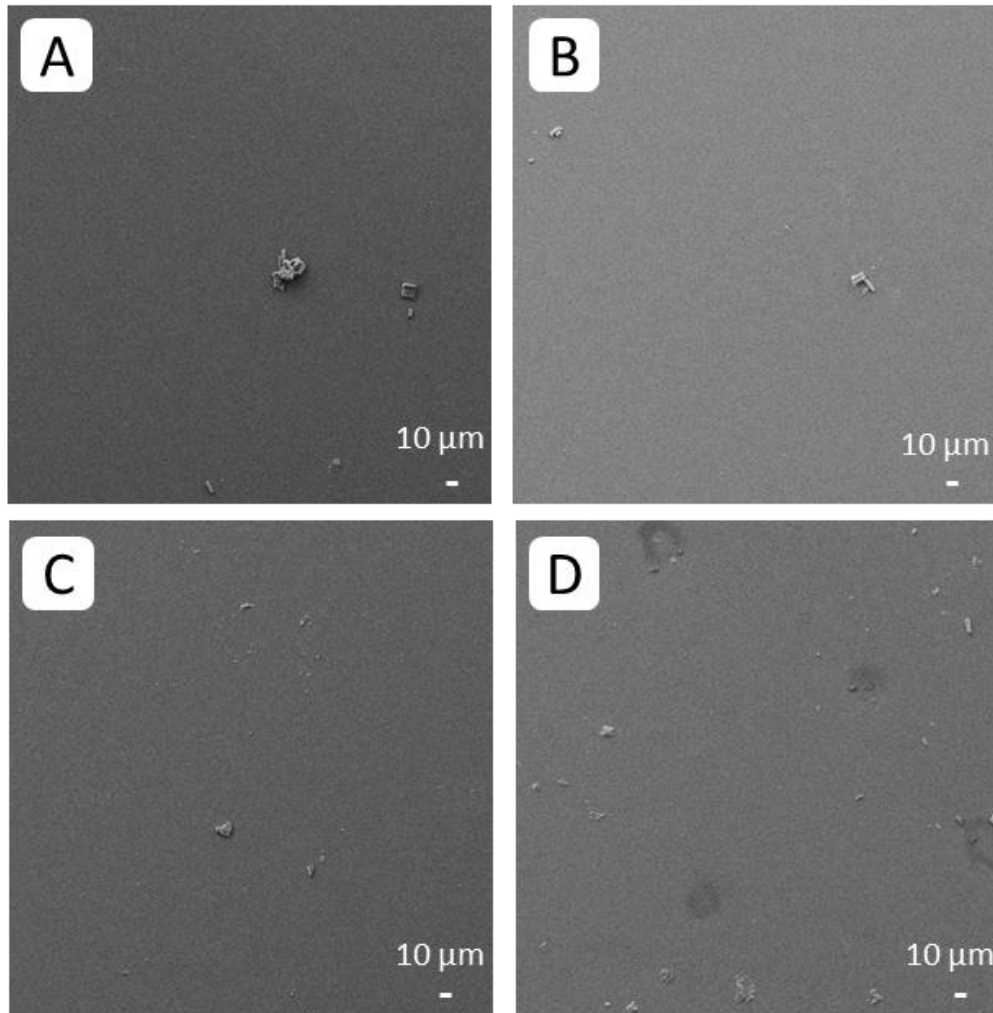
Figure 26: Illustrations of the SEM images of stages 5 (A) to 8 (D), which represent an aerodynamic diameter of ≤ 0.94 µm [9]. In comparison to Figure 25, less particles in the range of the small D_{50} values are present, which is consistent with the results of the NGI experiment. The particles that get into these stages are partly damaged rods, which have been generated during the NGI experiment or already during the manufacturing process. However, as can be seen in the pictures, this fraction is small.

The overview images in Figure 26 show the stages 5 to 8 of the NGI experiment and represent a D_{50} value of ≤ 0.94 µm [9]. These show that, compared to Stages 1 to 4 (Figure 25), only a small fraction of the formulation is damaged by the conditions of the experimental set-up, which has led to the low aerodynamic diameter collection plates.
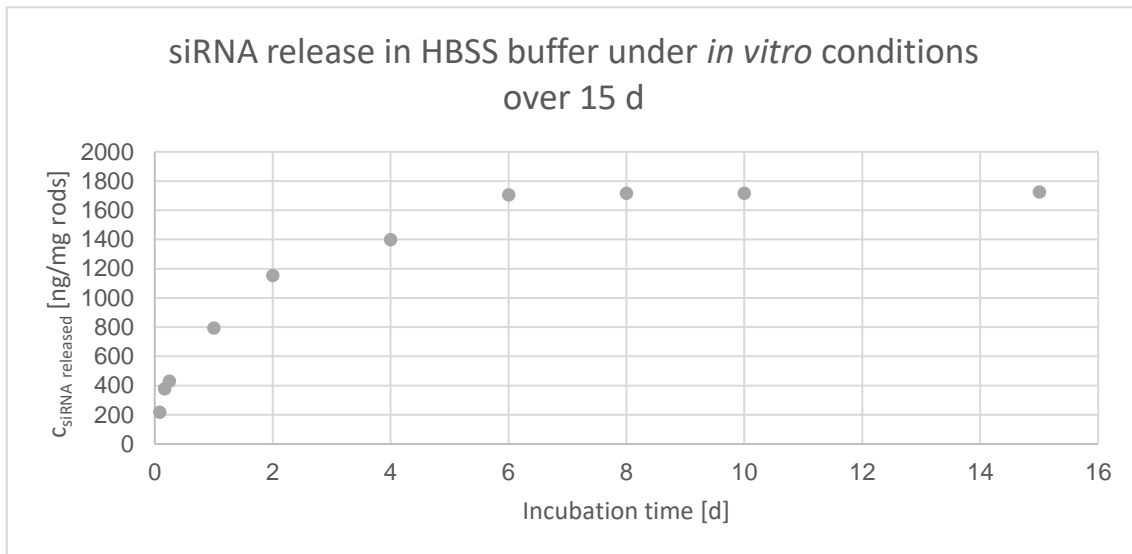
Figure 27: To check the siRNA release at different pH values, the release experiment was also performed in HBSS buffer. Compared to Figure 22, the release is much faster than in PSF. Here a plateau is reached already after 6 days.

When comparing the release of the oligonucleotide in PSF (pH 4.5) and HBSS (pH 7.4), the release occurs much faster at the higher pH value. This is due to the fact that the electrostatic interactions between the polyanionic siRNA and the polycationic bPEI are less pronounced at pH 7.4 than at pH 4.5, leading to an easier removal of the oligonucleotide layer [230].

6.   Silica nanoparticles of microrods enter lung epithelial cells

This section refers to the following publication:

Silica nanoparticles of microrods enter lung epithelial cells

Thomas Tschernig[1]*, **Thorben Fischer[2]*** Alexander Grissmer[1], Anja Beckmann[1], Carola Meier[1], Peter Lipp[1,3], Marc Schneider[2]

Affiliations
[1]Institute of Anatomy and Cell Biology, Saarland University, D-66421 Homburg/Saar
[2]Department of Pharmacy, Biopharmaceutics and Pharmaceutical Technology, Saarland University, D-66123 Saarbrücken
[3]Center for Molecular Signalling (PZMS), Saarland University, D-66421 Homburg/Saar, Germany

*Contributed equally

6.1   Abstract

A novel type of microparticle has recently been engineered. It consists of amorphous silica nanoparticles and has a corncob-like shape. It has already been demonstrated *in vivo* that alveolar macrophages in the lung are able to engulf this particulate carrier and that it also functions successfully as a gene delivery system. This subsequently raises the question as to whether epithelial cells may also be possible targets for these microrods. For this purpose, the alveolar epithelial cell line A549 was used presently. The epithelial character of these confluent cells was documented by the presence of tight junctions using a freeze-fracture technique and transmission electron microscopy. A toxic effect of the particles incubated with these cells was largely excluded. The interaction of the microparticles with the epithelial cells was observed using confocal microscopy and live cell imaging. Interestingly, the particles entered the epithelial cells within hours. After 1 day, the intracellular particles began to disaggregate and release the silica nanoparticles. Thus, even epithelial cells may serve as targets for this novel carrier and gene delivery system. This is particularly important since safe and effective gene delivery remains an unsolved problem. In addition, delivery of anti-cancer and anti-infective drugs may be an application of this novel particulate carrier.
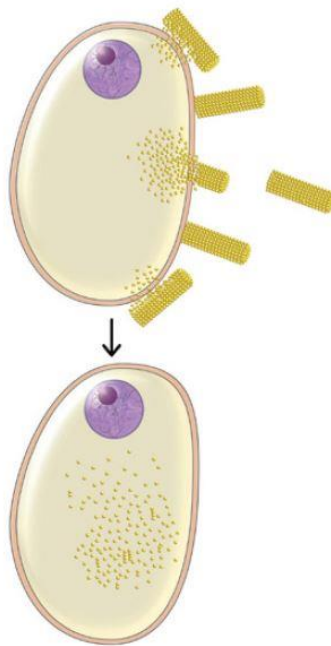

Figure 28: Graphical abstract. A schematic drawing illustrating the entry of microrods into an epithelial cell and their subsequent disaggregation within the cell.

6.2 Introduction

Genetic therapy is a prospective strategy for many genetic disorders and diseases. For instance, cystic fibrosis is an important inherited disease in which a specific membrane molecule, the cystic fibrosis transmembrane conductance regulator (CFTR), is absent or not functional [231]. The CFTR is a chloride channel and responsible for the chloride concentration and viscosity of secretions [231]. However, there remains to be a need for safe and efficient gene therapy carrier systems for different cell types. Recently, a novel carrier system was developed [96] and implemented for the delivery of drugs or plasmids to human macrophages [81]. A corncob-like microparticle composed of amorphous silica nanoparticles was created and loaded with a gene construct for luciferase. Those particles could serve as a gene delivery system to phagocytosing cells *in vitro* and *in vivo*; notably, it was demonstrated that the particles were engulfed by professional phagocytes, alveolar macrophages. Days after engulfment of the microparticles, the alveolar macrophages were confirmed to be transfected with luciferase [96]. Thus macrophages, as the primary phagocytes, may even engulf these relatively large microparticles of 10 µm in length and 3 µm in width. However, a prevailing issue was whether non-phagocytotic cells could also exhibit carrier uptake. It was therefore investigated in the current study whether the carrier system could be engulfed by epithelial cells. For the current study the human epithelial cell line A549 was selected. This cell line was derived from a lung tumour and reflects properties of the alveolar epithelial type II cells, meaning that the cells grow to a confluent layer *in vitro* [232]. In the present study, to confirm the epithelial phenotype of A549 cells, a freeze-fracture electron microscopy technique was employed. Overall the aim of the present study was to clarify whether these non-phagocytic A549 cells could engulf relatively large microrod carrier systems comprised of microparticles. Therefore, to observe the fate of the microrods within the alveolar epithelial cells, different imaging methods were applied: fluorescence microscopy and second confocal laser scanning microscopy. In addition, the viability of the A549 cells following microrod incubation for different times was investigated using the MTT assay.

6.3   Materials and methods

6.3.1 Cells and materials

The human epithelial cell line A549 was obtained from Merck KGaA, Darmstadt, Germany. Cells were cultivated at 37 °C in a humidified atmosphere with 5% CO2 in RPMI-1640 medium with 10% fetal bovine serum (Merck KGaA), 100 units ml^{-1} penicillin and 100 µg ml^{-1} streptomycin. The microparticles were produced from amorphous silica nanoparticles (Polysciences GmbH, Eppelheim, Germany) as described previously [96] and had a length of 10 µm and diameter of 3 µm. The microparticles were suspended in aqua dest distilled water, and the number of particles per µl were determined by the use of a Neubauer counting chamber. A total of $2x10^6$ particles were incubated with $1x10^5$ cells to establish a ratio of 20:1. The incubation times with the microparticles were 3, 6, 8, 24 and 48 h.

6.3.2 Fluorescence and confocal laser scanning microscopy

The living cells incubated with microrods were analysed by fluorescence microscopy (Carl Zeiss AG, Oberkochen, Germany) and confocal laser scanning microscopy (VTinfinity, VisiTech, UK), as previously described for mouse cardiac ventricular myocytes [233]. Cell borders were labelled using the membrane dye CellMask Deep Red according to the instructions of the supplier (Thermo Fisher Scientific, Inc., Waltham, MA, USA). All microscopy examinations were performed at room temperature (20-22 °C).

6.3.3 Cell viability

For an MTT assay, A549 cells were cultured in 96-well plates with 200 µl RPMI-1640 medium per well. Each well contained $1x10^4$ cells and 0 (control), $1x10^4$ or $1x10^5$ microrods. Following incubation for 1, 3, 6 and 24 h the cells were washed once with sterile phosphate-buffered saline (PBS). The cells were then incubated in a humidified atmosphere of 5% CO_2, 95% air at 37 °C with 5 mg/ml MTT (Merck KGaA) dissolved in PBS buffer at 1:10 ratio under gentle shaking for 4 h. Removal of the MTT reagent was followed by the addition of 100 µl dimethyl sulphoxide and

incubation for 20 min in the humidified atmosphere of 5% CO_2, 95% air at 37 °C to dissolve the formazan crystals. To determine cell viability, the absorbance at 550 nm was measured using a microplate spectrophotometer. For each concentration and time point, triplets were used.

6.3.4 Freeze-facture and electron microscopy

For freeze-fracture analysis, A549 cells were cultured on poly-L-lysine coated glass coverslips. The confluent layer was fixed with 2% paraformaldehyde at room temperature for 5 min. Incubation in 30% glycerol in Soerensen's phosphate buffer (0.15 M, pH 7.4) as pre-vitrificational cryoprotection was performed at 4 °C for 30 min. Small pieces of the glass coverslips were mounted headfirst onto the flat top of copper specimen carriers (Baltic-preparation, Niesgrau, Germany) and subsequently plunge-frozen in nitrogen-cooled liquid ethane using a cryopreparation chamber (Leica Microsystems GmbH, Wetzlar, Germany). Frozen samples were mounted onto a nitrogen-cooled double replica table and inserted into a BAF060 freeze-fracture device (Leica Microsystems GmbH). Freeze-fracturing was performed by cracking the double carrier open at -162 °C and $1x10^{-7}$ mbar pressure. Fractured samples were coated with a 1-nm pre-carbon coat applied at a shadowing angle of 90 °, a 1-nm platinum-carbon coat applied at 60 ° and a second carbon coat of 20 nm applied at 90 ° (carbon coat: carbon rods 3x50 mm, carbon/platinum coat: carbon rods 2x20 mm, platinum inlets 1.5x2 mm; Leica Microsystems GmbH). The frozen replicas were stabilized on a gold index grid (Plano GmbH, Wetzlar, Germany) using a drop of 0.5% Lexan polycarbonate plastic dissolved in dichloroethane (DCE; Acros Organics; Thermo Fisher Scientific, Inc.) [234]. To evaporate the DCE and consolidate the Lexan, the assembly of carrier-sample-replica-Lexan-grid was incubated at -20 °C for 16 h. Subsequently, the samples were thawed at room temperature and the carriers were removed. Digestion of the cell samples was performed under agitation in SDS-digestion buffer (2.5% SDS, 10 mM Tris-HCl, pH 8.9) at 60 °C for 27 h. Prior to electron microscopy analysis, the Lexan film was resolved and removed by dipping the replica in DCE. Analysis was performed in a FEI Technai G2 transmission electron microscope (Thermo Fisher Scientific, Inc.) at 100 kV. Pictures were taken with an 8-bit camera

at an image size of 1.42 megapixels (Olympus MegaView III; Olympus Soft Imaging Solutions GmbH, Münster, Germany).

6.4 Results

6.4.1 Confirmation of epithelial cell character

It was uncertain whether the microrods are able to enter epithelial cells. The A549 cell line used is established as an epithelial cell line, which was supported by the freeze-fracture analysis (Figure 29). In this representative image, distinct tight junctions are apparent.
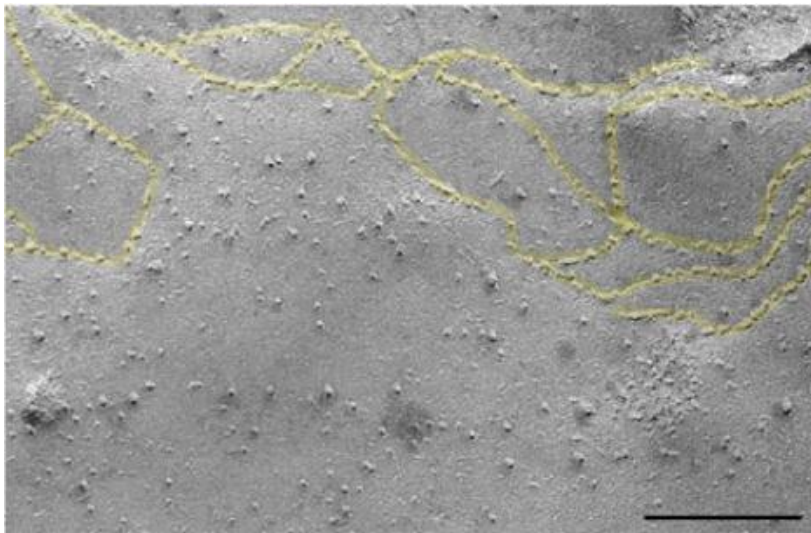
Figure 29: Tight junctions in A549 cell membranes. Freeze-fracture replica of the cell membrane, showing the protoplasmic leaflet (P-face). The formation of tight junction strands is characteristic of epithelial cells and was visible in the form of meandering arrangements of pits and particles (yellow overlay). Magnification, x120,000; scale bar, 100 nm.

6.4.2 Effects on viability

From the MTT assay, cell viability at a 1:1 ratio of cells to microparticles was 101.9±0.9% after 1 h, 99.9±3.7% after 3 h, 103.6±1.5% after 6 h, 95.9±5.6% after 24 h, and at a 10:1 ratio was 103.7±5.1% after 1 h, 94.0±3.2% after 3 h, 90.3±2.5% after 6 h and 83.6±2.1% after 24 h (data not shown).

6.4.3 Imaging

The fluorescence microscopy provided visualisation of the epithelial cells following co-incubation with the microrods at different time points (Figure 30).
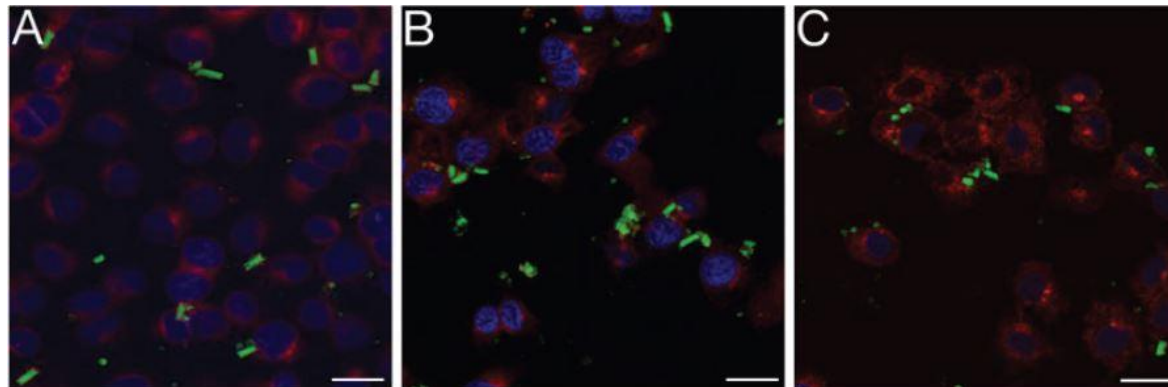
Figure 30: A549 cells and green fluorescent microrods detected by immunofluorescence after (A) 8, (B) 24 and (C) 48 h of incubation. The geometry of the microrods and its relation to the epithelial cells can be visualized. Magnification, x400; scale bars, 40 µm.

After 8 h, microparticles remained extracellular (Figure 30A). After 24 h, the majority of the rods had started to disaggregate (Figure 30B). After 48 h, nearly all of the rods appeared to have disaggregated, and nanoparticles or conglomerates of nanoparticles appeared to be intracellular (Figure 30C). Through confocal analysis, this process could be observed in greater detail and higher resolution (Figure 31). After 1 h, attachments of the rods to the cells were observed (Figure 31A and B). After 3 and 6 h (Figure 31C and D), disaggregated nanoparticles were observed within the cells. After 48 h (Figure 31E and F), many epithelial cells contained nanoparticles.

Figure 31: A549 cells (stained with 5 µg/ml CellMask Deep Red plasma membrane stain 15 min prior to imaging; red channel) at (A and B) 1 h after the addition of microrods in a ratio of 1:20 (green channel). The microrods appear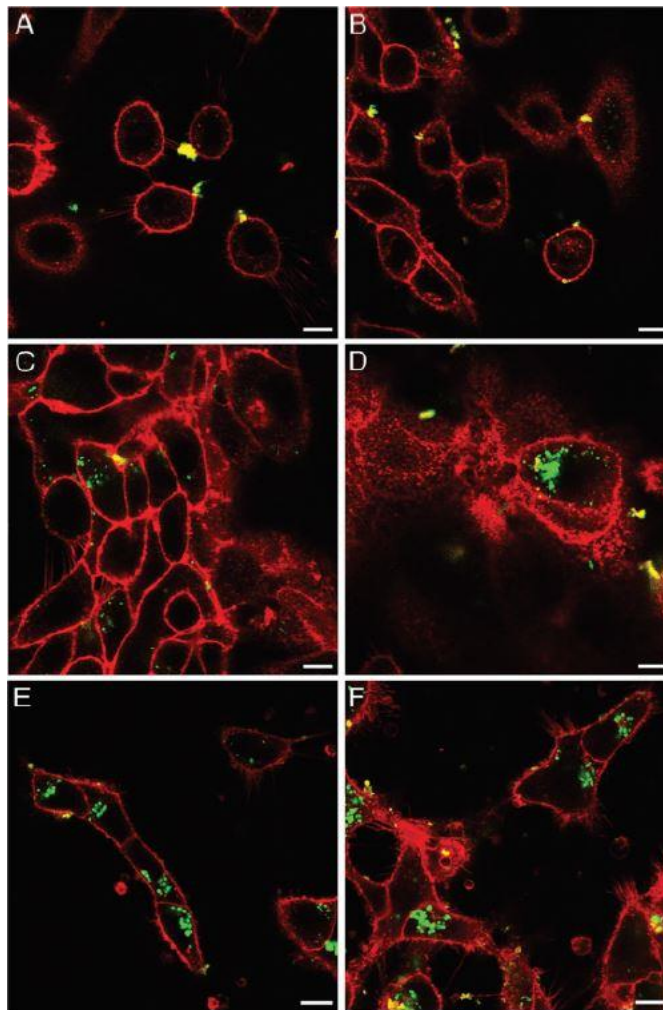ed attached to the plasma membrane. At (C) 3 and (D) 6 h into the experiment, the microrods were attached to the A549 cells and there was some disassembly to nanoparticle components. Nanoparticles and aggregates of nanoparticles were also observed within the cells. At (E and F) 48 h into the experiment, almost all microrods had disassembled and many nanoparticles were identified within the A549 cells. The nanoparticles appeared to accumulate around the golgi apparatus inside the cells. Magnification, x600; scale bars, 10 µm.

6.5   Discussion

The intention of this short report was to highlight that this novel drug delivery system may not only reach macrophages but also enter epithelial cells. The corncob-like microrods have previously been reported to be engulfed by macrophages and to successfully transfect macrophages [96]; however, due to their dimensions, they were considered incapable of entering epithelial cells. The epithelial cells used were A549 cells. These cells were originally derived from a lung carcinoma and share

many features with type II alveolar epithelial cells [81]. In particular, the cells are characterised by fast replication and confluential growth [232]. To confirm the epithelial character of these cells, a freeze-fracture technique was employed presently, in order to visualize tight junctions, the presence of which is characteristic for epithelial cells and tissues. The toxic effects of the microrods were generally excluded by determining the viability of the cells. However, a notable reduction of viability (<90%) was observed after 1 day of incubation at a particle-to-cell ratio of 10:1. Conventional fluorescence and confocal laser scanning microscopy were used to describe the transitional process undertaken by the microrods and provided spatial and temporal resolution. Following their initial adhesion to the A549 cells, the rods disaggregated to silica nanoparticles and these appeared to penetrate the cell membranes and enter the cytoplasm. The A549 cells are a useful cell line since they possess some remnants of alveolar type II cells, including the capacity for the synthesis of lamellar bodies [232]. These cells may possibly also have certain endocytotic properties. Admittedly, inhibitors of specific endocytosis pathways that could have detected phagocytotic mechanisms [235] were not tested.

A potential application of this microrod-based approach is the targeting of human bronchial and intestinal cells. In this regard the rods could be used to carry transcripts for a range of genetic disorders. One example would be the CFTR to rescue hereditary mutation in this molecule. This may be a viable option to treat patients with cystic fibrosis, as a common hereditary disease. A long-term aim is to reach epithelial basal cells or stem cells, in order to further target and potentially cure genetic disorders including cystic fibrosis.

7. Cylindrical microparticles composed of mesoporous silica nanoparticles for the targeted delivery of a small molecule and a macromolecular drug to the lungs: exemplified with curcumin and siRNA

This section refers to the following publication:

Cylindrical microparticles composed of mesoporous silica nanoparticles for the targeted delivery of a small molecule and a macromolecular drug to the lungs: exemplified with curcumin and siRNA

Thorben Fischer[1], Inga Winter[1], Robert Drumm[2], Marc Schneider[1*]

Affiliations

[1]Department of Pharmacy, Biopharmaceutics and Pharmaceutical Technology, Saarland University, Campus C4 1, 66123 Saarbrücken, Germany

[2]INM-Leibniz Institute for New Materials, Saarland University Campus D2 2, 66123 Saarbrücken, Germany

(submitted)

Cylindrical microparticles composed of mesoporous silica nanoparticles for the targeted delivery of a small molecule and a macromolecular drug to the lungs: exemplified with curcumin and siRNA

7.1 Abstract

The transport of macromolecular drugs such as oligonucleotides into the lung has become increasingly relevant in recent years due to their high potency. However, the chemical structure of this group of drugs poses a hurdle to their delivery, caused by the negative charge, membrane impermeability and instability. For example, siRNA to reduce tumour necrosis factor alpha (TNF-α) secretion to reduce inflammatory signals has been successfully delivered by inhalation. In order to increase the effect of the treatment, a co-transport of another anti-inflammatory ingredient can be applied. Combining curcumin-loaded mesoporous silica nanoparticles in nanostructured cylindrical microparticles stabilized using the layer-by-layer technique using polyanionic siRNA against TNF-α was used for demonstration. This system showed aerodynamic properties suited for lung deposition (mass median aerodynamic diameter of 2.85 ± 0.44 µm). Furthermore, these inhalable carriers showed no acute *in vitro* toxicity tested in both alveolar epithelial cells and macrophages up to 48 h incubation. Ultimately, TNF-α release was significantly reduced by the particles, showing an improved activity co-delivering both drugs using such a drug-delivery system for specific inhibition of TNF-α in the lungs.

7.2 Introduction

According to the World Health Organization (WHO), chronic respiratory diseases are among the most widespread diseases worldwide with a high mortality rate, which is expected to increase further in the future [115]. With several million cases, cystic fibrosis, idiopathic pulmonary fibrosis, tuberculosis, chronic obstructive pulmonary disease (COPD) and asthma represent the most common diseases for this clinical pattern [117], leading to a permanent inflammation [236-239] and thus affect the lung function over time [116, 239]. This proinflammatory status is caused by dysregulation of gene expressions, resulting in an imbalance of produced transcription factors [240], which translates into increased release of proinflammatory mediators such as cytokines [241]. The cell populations such as macrophages and immunologically active epithelial cells, which are mainly responsible for the production and release of these messenger substances, are located in the alveolar region of the lung [242].

To reach the deep lung, several inhalation systems have been developed to generate the highest possible efficiency. Most commonly used for pulmonary delivery are dry powder inhalers (DPIs) metered dose inhalers (MDIs), soft mist inhalers (SMIs), and nebulizers [63]. Having a closer look to DPIs, usually powder mixtures of the micronized drug particles are mixed with inert substances such as lactose, mannitol, trehalose, etc. in order to deliver the drug as efficient as possible to its target [243]. Spray-drying is often applied providing suitable particles for inhalation although many commercial formulation are reported to have a lung deposition as low as 14% [55].

A relatively new drug carrier for lung application are mesoporous silica particles. These are already commercially offered as transport system into the lungs, providing various positive characteristics [244]. Especially, mesoporous silica nanoparticles (mSNP) are better biocompatible due to their structure, which results in faster degradation and thus a lower toxic potential in comparison to amorphous silica nanoparticles [245]. In addition, the mSNP can be loaded in high quantities [246] with labile molecules like for example curcumin, as the pores create a protective environment [247].

The filled pores have only a small area where the outer medium comes into contact with the drug, leading to a slower release [248]. In addition, to further modify the release and better protect labile drugs in the pores, the surface of the mSNPs can be coated with polymers. Here, the strong negative surface charge of the silica particles can be exploited [247]. An established method for this represents the layer-by-layer technique [249]. This allows not only the surface to be loaded with drugs, but also polymers to be used as stabilizers for the formation of larger particle constructs [96, 159]. This property can be used to manufacture drug delivery systems for pulmonary application, where an aerodynamic diameter of 1-5 μm must be achieved to reach the deep lung [66].

To generate a stronger cell response and inhibit the release of proinflammatory cytokines, mSNPs can be loaded in the pores with multiple anti-inflammatory agents such as the natural compound curcumin and also a negatively charged oligonucleotide such as a specific siRNA on the surface to generate an improved effect [250]. However, since these two drugs have low stability and critical pharmacokinetic properties [251-253], targeted transport into immunologically active cells is of particular importance to prevent disintegration and also reduce side effects [205]. The use of aspheric particles for pulmonary delivery represents a possible mode of delivery for this purpose since the change in shape affects the interaction with immunological cells such as macrophages [206]. Here, a cylindrical shape has been established, since a change in length-width ratio, also called aspect ratio, leads to a modified cell uptake into macrophages [174]. In addition, the specific surface area of cylindrical microparticles is significantly larger than the surface area of their spherical counterparts, which allows higher loading quantities. This drug delivery system has already shown that loading with a specific siRNA sequence against TNF-α is possible and a significant reduction of this cytokine release from macrophages could be achieved, but still showed the need for improvement [159].

All the above-mentioned advantages of mSNPs and aspherical particles for siRNA delivery to the lung are combined in the drug delivery system described in this manuscript. The aim was to develop a nanostructured, cylindrical drug carrier system made of mSNPs to ensure the directed transport of siRNA in macrophages. Supplemental, curcumin as an additional anti-inflammatory agent was used to achieve a synergistic effect and further reduce the release of cytokines. In this work

we focused on the inhibition of tumour necrosis factor alpha (TNF-α) as one of the most prominent and active cytokines in the inflammation cascade [254]. Such a system should allow to enhance the effect combining the two drug types and may underline the potential of such a carrier system for future application.

7.3   Materials and methods

7.3.1 Materials

Mesoporous silica nanoparticles with a pore size of 4 nm and a diameter of 200 nm as well as curcumin, branched polyethyleneimine (bPEI) 25 kDa, L-leucine and 3-aminopropyltrimethoxy silane (APTS) were purchased from Sigma Aldrich (Steinheim, Germany). Dextran sulphate 10 HS was purchased from TdB Labs (Uppsala, Sweden). Nuclepore® Track-Etched Membranes with a pore size from 0.1 μm and 3 μm in diameter were purchased from Whatman plc (Kent, UK). RPMI-1640 cell culture medium, Hanks' Balanced Salt solution (HBSS), dimethyl sulphoxide (DMSO), phorbol 12-myristate 13-acetate (PMA), lipopolysaccharides from *Escherichia coli* (LPS), 3-(4,5-dimethylthiazol-2-yl)-2,5-diphenyltetrazolium bromide (MTT) and ethidium bromide solution were obtained from Sigma Aldrich Life Science GmbH (Seelze, Germany). Foetal calve serum (FCS) was purchased from Lonza (Basel, Switzerland). Nuclease-Free Water, TNF alpha Human ELISA Kit and tetrahydrofuran were obtained from Thermo Fisher Scientific Inc. (Darmstadt, Germany). Silencer® Pre-designed siRNA (Sequences: Sense (5´-GGACGAACAUCCAACCUUCtt-3´)   Antisense   (5´-GAAGGUUGGAUGUUCGUCCtc-3´)) was purchased from Ambion Inc (Austin, US). Silencer™ Select Negative Control No. 1 siRNA (Sequences: Sense (5´-UAACGACGCGACGACGUAAtt-3´)   Antisense   (5´-UUACGUCGUCGCGUCGUUAtt-3´)) used as negative control for siRNA (scrambled siRNA) was purchased from Invitrogen™ (Carlsbad, US).

7.3.2 Rhodamine B functionalization of mSNP for visualization

In order to improve detection and quantification of the colourless nanoparticles in various experiments, a fluorescent dye was added. Therefore 3-aminopropyltrimethoxy silane (APTS) was covalently bound to the hydroxy groups on the surface of the silica particles [255]. Previously, the primary amine group of APTS was bound with the carboxy group of rhodamine B to form an amide. This amide was then intended to functionalize the surface of the nanoparticles by covalently attaching the rhodamine B silane to the surface via the methoxy silanes.

For this, a 3 % rhodamine B solution in chloroform was prepared and mixed with APTS. This mixture was heated for 30 min to 60 °C under stirring. The remaining chloroform was then evaporated, the residue dissolved in ethanol and adjusted to pH 3.5 using 0.5 N hydrochloric acid. The resulting solution was then allowed to react for 1 h while stirring. Subsequently, mSNPs were mixed in a ratio of 1:10 with the prepared solution and incubated for 6 h while shaking in a thermal mixer at 60 °C. The suspension was then washed twice with ethanol, till no unreacted fraction of rhodamine B was present [256]. The result was fluorescent, violet-stained nanoparticles with an excitation wavelength of 545 nm and an emission wavelength of 567 nm.

7.3.3 BET measurement to evaluate pore volume and loading with curcumin

The measurement of the adsorption isotherm after Brunauer, Emmett and Teller (BET) determines the monolayer concentration of an adsorbed gas on the sample surface. From this value the specific surface of the sample can be determined. The physical adsorption observed is based on Van-der-Waals interactions between the adsorbed gas molecules and the adsorbing sample surface. Usually, nitrogen is used as adsorption gas in this method, as far as the temperatures and the sample allow it. The specific surface area determined in a BET measurement also includes the surface area of pores in porous materials and is therefore in relation to the relative surface area. Gas adsorption thus enables the determination of the size and volume distribution of micropores. In addition, comparative measurements can be used to directly check loading tests and to determine the loading quantities. For sample preparation, the powder was first dried in vacuum at elevated temperature followed by the measurement at the boiling point of nitrogen. After recording at least three data points, the BET value can be determined using the BET adsorption isothermal equation (equation 5). The amount of adsorbed gas is correlated with the total surface area of the particles, including pores in the outer surface [257].

$$\frac{p}{V_a \cdot (p_0 - p)} = \frac{1}{V_m \cdot C} + \frac{C-1}{V_m \cdot C} \cdot \frac{P}{P_0} \qquad \text{(equation 5)}$$

p = Partial vapor pressure of the adsorbed gas in equilibrium with the surface at 77.4 K (boiling point of liquid nitrogen) [Pa].

p_0 = Saturation pressure of the adsorbed gas [Pa]

V_a = Volume of adsorbed gas under standard conditions (273.15 K and 1.013×10^5 Pa) [ml].

V_m = Volume of the adsorbed gas, to enable monolayer formation on the sample surface [ml]

C = Dimensionless constant related to the adsorption enthalpy of the adsorbing gas on the powder sample

7.3.4 mSNP pore loading with curcumin

To load the pores of the mSNPs, curcumin was dissolved in acetonitrile and subsequently nanoparticles were added to the solution. This suspension was first homogenized in an ultrasonic bath and then heated for 1 h at 90 °C and 500 rpm to evaporate the solvent. By reducing the volume of the solvent, the hydrophobic drug is forced into the pores of the nanoparticles, due to the increasing curcumin concentration by solvent evaporation. Only a small amount of the curcumin attaches to the hydrophilic surface of the nanoparticles and was removed by washing with water for three times. To confirm this hypothesis, this loading method was first performed with non-porous, non-fluorescently labelled silica particles. These were also subsequently washed three times with water yielding particles with no detectable fluorescence thereafter.

7.3.5 Determination of colloidal properties

Zetasizer Nano ZS (Malvern Panalytical, Malvern, UK) was used to determine hydrodynamic diameter via dynamic light scattering. Here, the polydispersity index (PDI) was also determined describing the size distribution of the nanoparticles. The same device was used to determine the zeta potential according to the principle of laser doppler micro electrophoresis. For sample preparation, a stock solution of 1 mg/ml was diluted 1:20 with MiliQ® water and measured three times with each of the three measurements including 12 runs.

7.3.6 Preparation of cylindrical microparticles composed of mSNP

To produce the nanostructured, cylindrical microparticles (microrods), the mSNP must first be assembled in a cylindrical shape. Therefore, a template-assisted approach was used [81, 96] to transfer the nanoparticles into a template membrane with a defined length and width of 10 µm and 3 µm. This shaping membrane was stretched into a filter holder system, which was sealed with a silicon ring and provided with a blocking membrane underneath the template membrane so that the mSNPs could remain in the defined pores of the template membrane, allowing only the water of the suspension to pass through the small pores (d = 0.5 µm) of the blocking membrane. A syringe containing 500 µl of a 1.5 mg/ml mSNP suspension was subsequently put on the top of the filter holder and then continuously injected with a flowrate of 100 µl/min into the pores of the template membrane by a syringe pump (Legato 210; KD Scientific, US). This process was repeated three times to achieve uniform filling. Afterwards, the template membrane was washed with a lint-free tissue, to remove the particles on the top and bottom of the membrane.

Since the particles are only loosely assembled and not connected strongly to each other in the pores, the layer-by-layer technique was used to increase the ionic interactions and thus stabilize the microrods [160, 258]. As polycationic substances branched polyethyleneimine (bPEI) was used and dextran sulphate was applied due to its negative charge. These substances were used because they offer relevant properties. Dextran sulphate is highly branched and thus yields many anionic groups due to the high number of sulphate groups per glycosyl unit (approximately 2.3) [259] and its biocompatible [260]. bPEI was used because this polymer has a strong

buffering capacity, which is described to promote osmotic swelling of the lysosome and thus destabilizes the membrane of the vesicle. Through this so-called "'proton sponge effect" the diffusion of the active ingredients into the cytosol shall be facilitated [162] allowing reaching the target in the cytosol [254]. In a first step, the template membrane with the infiltrated mSNP was added to 2% bPEI solution for 12 min to allow the cationic polymer to adhere to the negatively charged surface of the nanoparticles. After a subsequent washing step with water, the membrane was placed in a 2% dextran sulphate solution for 12 min. After a second washing step this cycle of layering was repeated. A total of three double layers (PEI and dextran sulphate form one double layer) of the polymers was necessary to generate a stable formulation. To load the particles with siRNA, the dextran sulphate solution was replaced by an 0.05% siRNA solution in the last layering step. To release the stabilized formulation from the polycarbonate template membrane, it was dissolved in tetrahydrofuran (THF). The THF insoluble microrods were then centrifuged at 6,500 g for 7 min and the supernatant containing dissolved polycarbonate was discarded. Washing with THF was performed five times in total and after the last step the inorganic solvent was evaporated, resulting in a dry powder. Since the oligonucleotide used is sensitive to nucleases, the entire production process was performed under aseptic conditions.

7.3.7 Aerodynamic characteristics analysed by Next Generation Impactor

Since the developed formulation was intended for inhalation into the lungs, the aerodynamic properties were determined. Therefore, a Next Generation Impactor (NGI) (Copley Scientific, Nottingham, UK) with standardized settings was used [9]. An M1A flowmeter (Copley Scientific, Nottingham, UK) was used to adjust a continuous airflow of 60 l/min ensuring aerosolization of the microparticles [178, 179]. These were coated with L-leucine at the surface [261] before application to reduce hygroscopicity [176] and increase surface roughness to improve flight characteristics [262, 263]. Approximately 3 mg of the coated formulation was then filled into a capsule, placed in a HandiHaler® (Boehringer Ingelheim, Ingelheim, Germany) and punctured. An air flow of 60 l/min was then generated for 4 s by a vacuum pump (Erweka, Langen, Germany) to aerosolize the formulation into the

NGI. The particle concentrations in each stage were then analysed using a microplate spectrophotometer (TecanReader® infinite M200, Tecan, Männedorf; Switzerland) to determine the Mass Median Aerodynamic Diameter (MMAD), Fine Particle Fraction (FPF) and Geometric Standard Deviation (GSD). The calculation of these values was done analogous to Abdelrahim *et. al.* [180] as already described in different publications [28, 181].

7.3.8 Differentiation of human monocytes (THP-1) into macrophage like cells

To determine the interaction between the developed formulation and immunologically active cells, the human monocytic cell line THP-1 was used. In a first step, this cell line must be differentiated into M0 macrophage-like cells. Therefore, the cells were incubated with a mixture of RPMI 1640 medium with an addition of 10% fetal calf serum (FCS) and 50 ng/ml phorbol 12-myristate 13-acetate (PMA) for three days in a humidified atmosphere of 5% carbon dioxide at 37 °C. Afterwards the cells were washed twice with HBSS and supplemented with medium without PMA. The cells resulting from the differentiation process represent a M0 macrophage-like cell line (dTHP-1) [220]. As the method is well established, the successful differentiation was only monitored by light microscopy evaluation of the form of the cells and the fact that they turn into adhesive cells growing on the support.

7.3.9 Human alveolar basal epithelial cell line A549

Since not only immunologically active cell types interact with the formulation during pulmonary application of drug delivery systems, the A549 cell line was used as model for type II pulmonary epithelial cells to analyse possible reactions [264]. To cultivate the cells, they were incubated with RPMI 1640 medium with an addition of 10% FCS in a humidified atmosphere of 5% carbon dioxide at 37 °C.

7.3.10 Determination of cell viability by MTT assay

To get a first impression of how the cells interact with the developed formulation, a cytotoxicity test was performed. For this study, the 3-(4,5-Dimethylthiazol-2-yl)-2,5-diphenyltetrazoliumbromid (MTT)–Assay was applied to determine colourimetrically the metabolic activity of the cells after incubation with the drug delivery system [265]. For this, the cell lines A549 and dTHP-1 described above were cultivated in 96-well plates with a concentration of $2*10^4$ cells per well. Subsequently, the cells were incubated for 4, 24 and 48 h with a particle concentration of 10, 50 and 100 µg/ml. To obtain these concentrations the formulation was redispersed and diluted in RPMI 1640 + 10% FCS. After different periods of time the supernatant was removed and replaced by MTT reagent incubating for 4 hours. In a final step, the supernatant was removed and replaced with DMSO to dissolve the resulting formazan crystals. Cell viability was then determined by measuring the absorbance at 550 nm after 20 min using microplate spectrophotometer. Untreated cells grown in medium and Triton-X treated cells were used a negative and positive control.

7.3.11 *In vitro* release of siRNA and curcumin under phagolysosomal conditions

When incubating cells with particles, usually not 100% of the active ingredient is released in time [266]. Therefore, it is unclear what amount is available for drug action. Consequently, a release study in phagolysosomal simulant fluid (PSF) [221] was performed to determine the amount of released drug in a phagolysosomal-like milieu for correlating the results with the later performed Enzyme Linked Immunosorbent Assay (ELISA) for cytokine determination. For the procedure, the formulation was placed in different micro reaction tubes under sink conditions and incubated at 37 °C with gentle shaking for 1; 2; 3; 4; 6; 24 and 48 hours. To analyse the released amount, the tubes were centrifuged at 24,000 g for 30 min. The resulting supernatant was then analysed using a microplate spectrophotometer. To determine the curcumin content, the supernatant was mixed 1:1 with ethanol to facilitate dissolution of the compound and measured at $\lambda_{ex}= 430\,nm$ and $\lambda_{em}= 535\,nm$. For quantification of the released oligonucleotides, the supernatant

was mixed with ethidium bromide followed by fluorescence measurement at λ_{ex}= 526 nm and λ_{em}= 605 nm [267]. Each value was determined as independent triplicate.

7.3.12 Quantification of TNF-α release by Enzyme Linked Immunosorbent Assay (ELISA)

To detect the influence of the developed formulations on the cytokine release (TNF- a) of the macrophage-like dTHP-1 cells after induced inflammation by lipopolysaccharide (LPS), an ELISA was performed [268]. 200,000 THP-1 cells were seeded per well in a 24-well plate and differentiated with PMA to M0 macrophages as described in the section above. Subsequently, the cells were incubated with 500 µl of the different microrod formulations and a concentration of 40, 200 and 400 µg/ml for 2 days at 37 °C in a humidified atmosphere of 5% carbon dioxide. These concentrations represent the same concentrations per cell as used in the cytotoxicity assay. After incubation, the supernatant was discarded and replaced by 500 µl of 200 µg/ml LPS from Salmonella typhimurium for 6 h to induce inflammation of the macrophages leading to an increased release of proinflammatory cytokines like TNF-α [269]. The resulting supernatants were then centrifuged at 200 g for 10 min to remove cell residues and finally analysed by ELISA for the cytokines. As positive control (PC) dTHP-1 stimulated with LPS for 6 h without treatment where used. Untreated cells served as negative control (NC). Further controls included the plain drugs curcumin and siRNA without carrier system, as well as scrambled siRNA with and without carrier were used to exclude possible unspecific reactions with oligonucleotides.

7.3.13 Scanning electron microscopy for analysis of rod morphology

Morphology of the nanostructured microrods was determined by scanning electron microscopy (SEM). For visualization, a Zeiss Evo HD 15 Electron Microscope (Carl Zeiss AG, Jena, Germany) was used, equipped with a Lanthanum hexaboride (LaB$_6$) cathode. To prepare the samples for the measurement, the microrods were redispersed in water and a few drops of the suspension were placed on a silica

wafer and left to dry. These samples were then sputtered with an approximately 10 nm thick gold layer using a Quorum Q150R ES sputter coater (Quorum Technologies Ltd., East Grinstead, UK) to minimize surface artifacts and allow high magnifications [270]. The images were taken at a voltage of 5 kV and a magnification of 15 kX.

7.3.14 Confocal laser scanning microscopy for particle visualization

In addition to SEM visualization, confocal laser scanning microscopy (CLSM) (LSM710, Carl Zeiss AG, Jena, Germany) was used to characterize the morphology of the microrods. Therefore, the formulation was redispersed in water and dropped onto a glass slide and covered with a cover glass. To visualize the Rhodamine B-labelled microrods λ_{ex}= 545 nm and λ_{em}= 567 nm were used, for curcumin λ_{ex}= 440 nm and λ_{em}= 542 nm and for the siRNA stained with ethidium bromide λ_{ex}= 526 nm and λ_{em}= 605 nm. For the measurement, a water corrected objective M27 was used with a magnification objective of 40x and a numerical aperture of 1.2.

7.3.15 Statistical evaluation

Two-sided Student´s t-test from Excel 365 software was used to check for significance between two measurements. A significant change was adopted for $p < 0.05$.

7.4   Results

7.4.1   Particle characterization

In a first step, the manufactured formulation of nanostructured, cylindrical microparticles (microrods) consisting of 260 nm mesoporous silica nanoparticles (mSNPs) were characterized by observing the morphology using SEM and CLSM. Therefore, unlabelled nanoparticles were stained with rhodamine B to generate a fluorescence signal for CLSM imaging on the one hand and to be able to perform quantification by fluorometry in the NGI experiments on the other hand. Due to the large number of hydroxy groups on the surface of the mSNPs and the resulting strongly negative zeta potential of - 40.03 ± 0.80 mV (Table 4). These groups are well suited for chemical modification of the surface [271]. Commonly 3-aminopropyltrimethoxy silane (APTS) is used as a coupling agent preparing the surface of silica nanoparticle to be stained with dyes [255]. As demonstrated in table 4, surface modification with APTS led to a change in zeta potential to 36.07 ± 0.57 mV, which turns less positively charged after coupling rhodamine B to the amino groups (22.70 ± 1.06 mV), but is still sufficient to be coated during the layer-by-layer procedure. The size of the particles remains constant due to the modification of the surface, with a small decrease after covalent binding of rhodamine B. This phenomenon can be explained by the fact that rhodamine B reduces the polarity of the particles, which results in reduced water association at the surface of the particles and therefore to a decrease in the hydrodynamic diameter [272].

Table 4: Hydrodynamic diameter, PDI and zeta potential of the unmodified mSNPs, covalently bound APTS and with rhodamine B and APTS modified mSNPs. The numbers presented show, that APTS modification leads to a change of zeta potential from negative to positive values without influencing the hydrodynamic diameter.

	unmodified mSNPs	APTS modified mSNPs	rhodamine B + APTS modified mSNPs
hydr. diameter [nm]	262.13 ± 3.98	263.23 ± 1.33	245.8 ± 2.97
PDI	0.102 ± 0.013	0.045 ± 0.022	0.084 ± 0.068
zeta potential [mV]	-40.03 ± 0.80	36.07 ± 0.57	22.7 ± 1.06

After staining, the mSNPs were used as building blocks for the microrods. In the beginning, an unloaded batch was produced to verify the process of staining and

subsequent stabilization by the layer-by-layer technique to the microrods. As illustrated in Figure 32, the formation of such nanostructured cylinders could be successfully achieved as demonstrated by SEM (Figure 32A and B). The successful modification with the fluorescent probe is clearly visible by CLSM showing the respective cylindrical form of the particles (Figure 32C). Both images depict cylinders in the expected size rage. The template-assisted approach allowed to produce the microrods with a defined length of 10 μm and width of 3 μm. The microparticles seem to assemble in larger arrangements and piles as obvious from the SEM micrographs due to drying. Looking at redispersed conditions in aqueous environment, it can be clearly seen that the particles are not agglomerated but well separated from each other. Neubauer counting chamber was used to determine the number of particles per membrane, resulting in 6 x 10^6 rods per membrane. The length-width ratio (aspect ratio) chosen here is 3.3, which is assumed to delay uptake of the particles into macrophages compared to spherical particles [102]. This prolongation of internalization favours longer retention in the lungs and slower degradation of the active ingredients, thus increasing effectiveness [95].
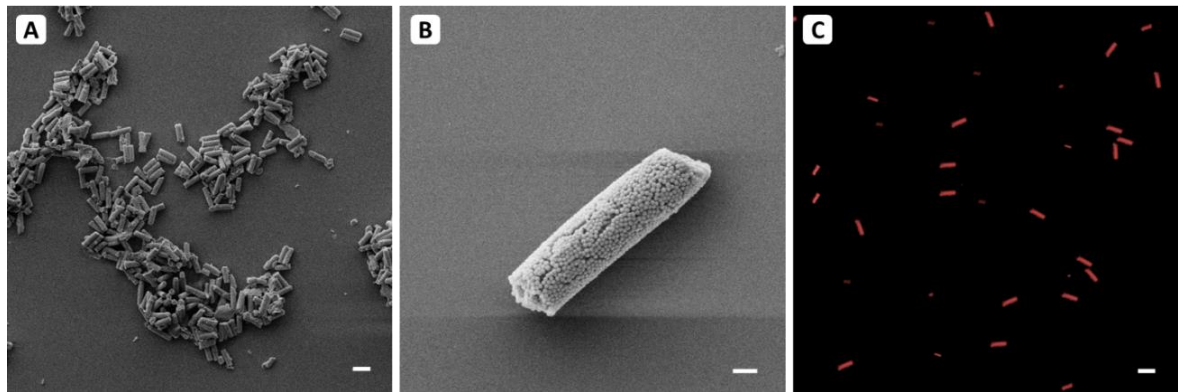
Figure 32: The microparticle formulation composed of mSNP functionalized with rhodamine B visualized (A) and (B) by SEM and (C) by CLSM. In all three images, the cylindrical shape can be seen. In (A), the particles are not well dispersed due to drying effects. With an higher magnification used in (B), the nanostructure of the formulation is visible. (C) The formulation was visualised by CLSM with λ_{ex}= 545 nm, λ_{em}= 567 nm, dispersed in water. The homogeneous particle dispersion is clearly visible, and the fluorescent signal indicates that the functionalization with rhodamine B was successful. Representative sections were used for all images. Scale represents 10 μm for (A) and (C) and 1 μm for (B). The brightness of the CLSM image (C) has been increased for better visibility.

7.4.2 Evaluation of aerodynamic properties by Next Generation Impactor

After verifying the morphology of the fluorescently labelled microrods, the flight characteristics were determined by NGI. The determination of these parameters is of interest to get an estimation if the formulation may be able to reach the deep lung. To enable deposition in the deep lung, an aerodynamic diameter of 1-5 µm need to be realized [183]. For the microrod formulation an MMAD of 2.85 ± 0.44 µm was determined, which favours deposition in the deep lungs [223]. The percentage of mass for particles < 5 µm, represented by the FPF [12], is with a value of 32.86 ± 2.93% in an acceptable range compared to many commercially applied DPIs [16]. This value is mainly promoted by coating with L-leucine, which reduces hygroscopicity and increases surface roughness, resulting in a powder with less agglomeration and better flow properties [176, 262, 263].

Having a closer look to the MMAD of the microrods it is evident, that the value of 2.85 µm is lower than both length and width of the particles. This is in accordance with the equation below, correlating the aerodynamic diameter with the volume equivalent sphere [88, 89].

$$d_a = d_{ve} \sqrt{\frac{1}{\chi} \frac{\rho_p}{\rho_0} \frac{C_c(d_{ve})}{C_C(d_a)}}.$$

d_a = aerodynamic diameter

d_{ve} = volume equivalent diameter

χ = dynamic shape factor

ρ_p = particle density

ρ_0 = standard density

$C_c(d_{ve})$ = Cunningham slip correction factor of the volume equivalent diameter

$C_c(d_a)$ = Cunningham slip correction factor of the aerodynamic diameter

The important parameter in this equation for aspherical particles is the dynamic shape factor χ. Calculating this factor according to Sturm [6] results in a value of 1.47 for an aspect ratio of 3.3. This means, that in comparison to spherical particles, where χ is equal to one [88], while keeping the other parameters of the equation constant, the value under the root decreases leading to a lower aerodynamic

diameter (d_a) for the same volume equivalent diameter (d_{ve}). This value underlines the advantageous properties of the nanostructured cylinders for aerosol application. Looking at the aerodynamic parameters with an MMAD of 2.85 ± 0.44 µm and an FPF of > 30%, they are found in the relevant range for deep lung deposition and thus enabling lung application [182-184].

7.4.3 Drug loading and release kinetics

The microrods were loaded with two different drugs exerting anti-inflammatory effects to generate a combined and enhanced biological effect in comparison to one drug alone and thus the inhibition of TNF-α release after inflammation was stronger. Therefore, curcumin was loaded into the pores of the mSNPs, as they create a protective environment [247] which leads to a slower degradation of this instable drug [273]. To determine the highest possible loading of the pores, a BET measurement was performed. A pore volume of 0.1675 ± 0.0089 cm^3/g was found leading to a possible loading of approx. 22% loaded mass of curcumin with respect to the particles weight. For the preparation, the amounts were chosen in such a way, that a load of 20% [m/m] would be theoretically achievable.

The siRNA was adsorbed to the surface of the microrods during the stabilization step using the layer-by-layer technique. In a first step, the loaded formulation was visualized with both SEM and CLSM, as the curcumin is fluorescent, and the siRNA used was stained with ethidium bromide. As shown in Figure 33, curcumin (C) and siRNA against TNF-α (D) can be visualized fluorometrically. The signal obtained indicates that the entire formulation is homogeneously loaded with both substances. When looking at the morphology under the SEM (Figure 33A and B), the nanostructured, cylindrical shape of the microrods can be seen without affecting the stability.

Cylindrical microparticles composed of mesoporous silica nanoparticles for the targeted delivery of a small molecule and a macromolecular drug to the lungs: exemplified with curcumin and siRNA
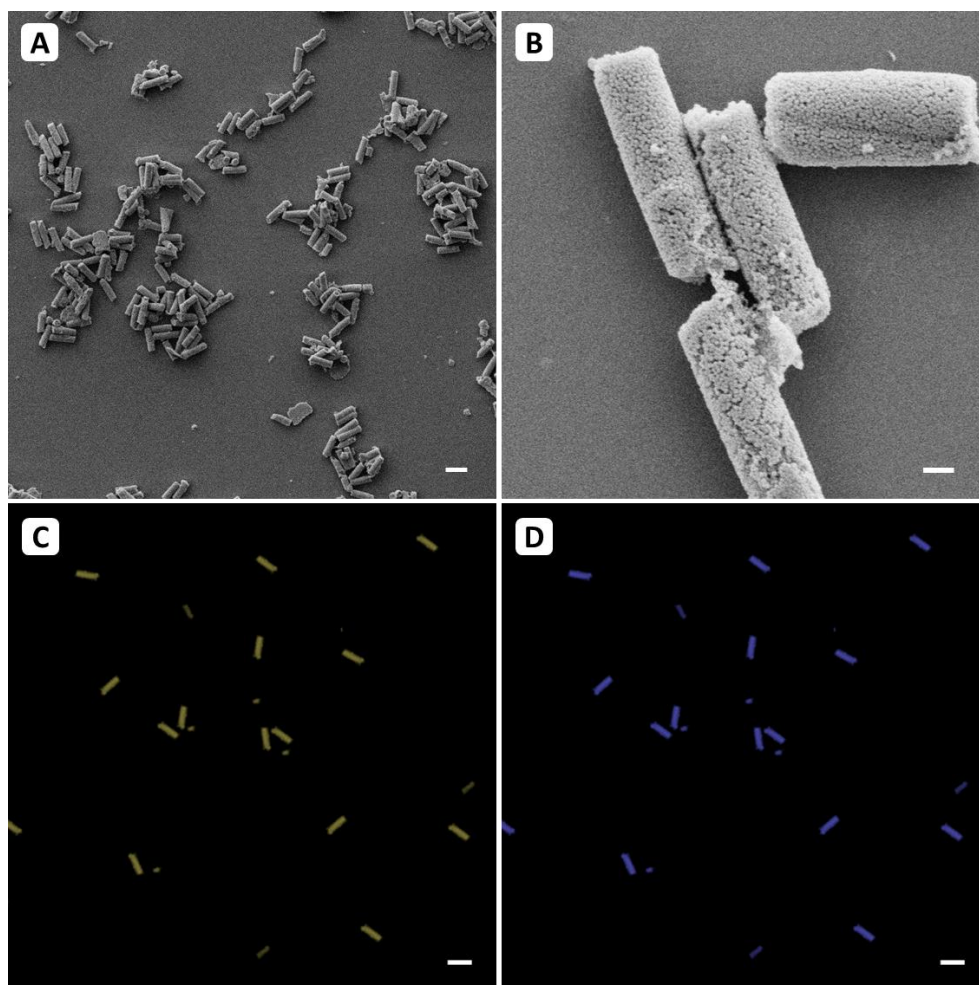

Figure 33: The curcumin and siRNA loaded formulation under the SEM (A) and (B) and CLSM (C) and (D). (A) The SEM image shows that neither the stability nor the morphology of the microrods are affected by drug loading. (B) Here, the nanostructure as well as the cylindrical shape is visible. (C) Visualization of curcumin fluorescence of λ_{em}= 542 nm was realized after excitation at λ_{ex}= 440 nm. Here the homogeneous loading of the mSNPs can be seen (D) To visualize the double-stranded siRNA used for CLSM measurement, the formulation was treated with ethidium bromide to generate an intercalation, which allowed the detection of a signal at λ_{ex}= 526 nm, λ_{em}= 605 nm. The fluorescence is homogeneously distributed over the whole microparticle surface indicating a homogeneous loading along the particle. Representative sections were used for all images. Scale represents 10 µm for (A), (C) and (D) and 1 µm for (B).

After successful loading, the release kinetics of the drugs were investigated. Therefore, an artificial phagolysosomal fluid (PSF) was prepared [221]. This medium was chosen for the *in vitro* release as the microrods are phagocytized by macrophages due to their size [274] after reaching the lungs. Looking at the release kinetics in Figure 34, the siRNA shows a sustained release whereas the curcumin exhibits a delayed release. These release profiles correspond to the expected results, as the siRNA is directly available due to its localization on the surface of the microrods and thus offers a large area to be detached, whereas the curcumin is

protected twice from release, once by the hydrophobic environment in the pores and secondly by the polymer layers covering the mSNPs. Therefore, the amount of curcumin released was below the detection limit during the first 24 h and after 48 h at 15 µg/mg microrods, which is about 8% of the total dose. For siRNA, approx. 540 ng/mg microrods were released, which is about 15% of the total amount. Thus, after 48 hours, the siRNA was released roughly twice as fast as curcumin. The release profile of siRNA, which is characterized by a step pattern consisting of a sharp increase in release leading to a plateau followed by a slower increase, is favoured by several factors. These are, on the one hand, the swelling of the polymer layers, as well as an ion exchange with the surrounding counterions and the detachment of the various layers. This influences the release of the different polymers and thus also of the siRNA, which results in the release pattern observed [275, 276].

The release time was only considered for 48 h, as this corresponds to the time of incubation of the dTHP-1 with microrods before the ELISA experiment. This allows estimating the amount of drug released during the experiment.
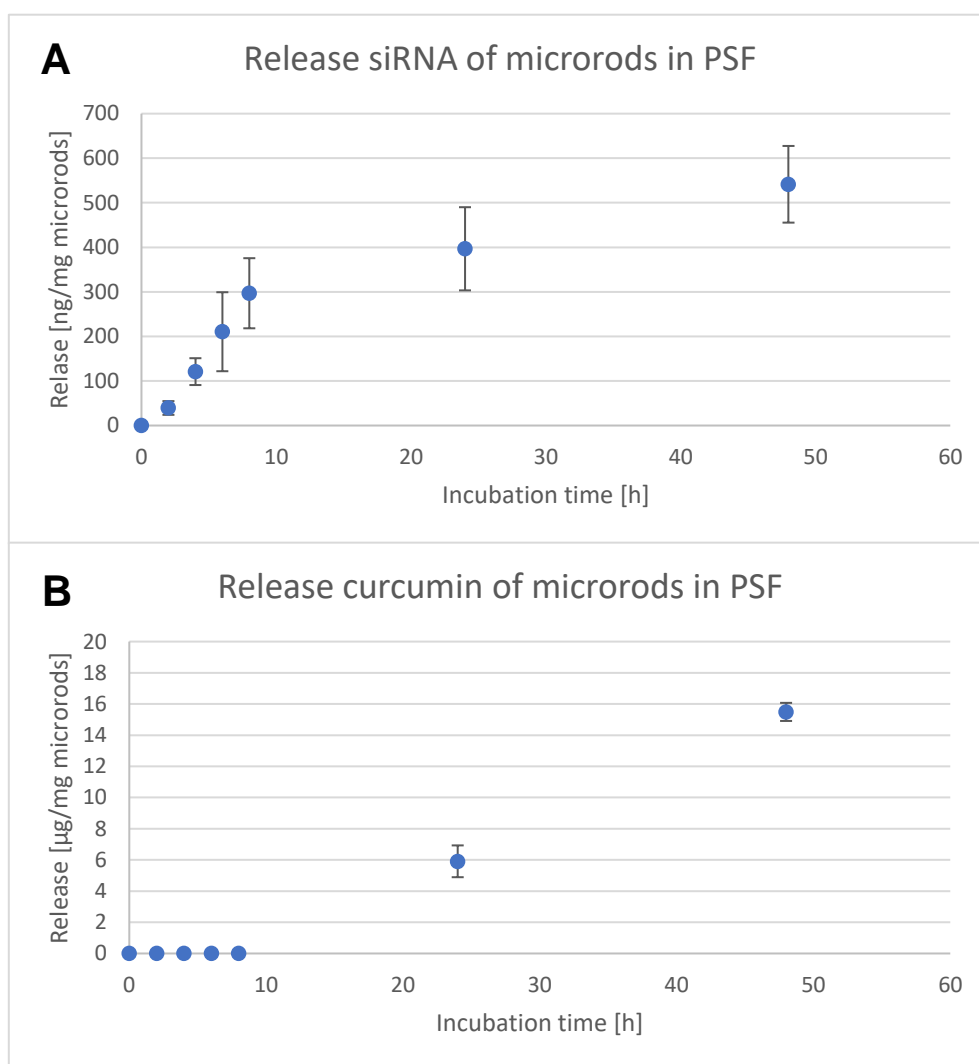
Figure 34: *In vitro* release kinetics of siRNA (A) and curcumin (B) in PSF for 48 h at 37 °C under gentle shaking. The release profiles show that the two drugs release with different kinetics. The curcumin, which was located in the pores of the mSNPs and covered by various polymers, was only detected at 24 h. After two days 15 µg per mg rods were released, which is about 8% of the total load. The siRNA found on the surface of the microrods was released continuously with a final amount of about 540 ng per mg microrods after 48 h, which is about 15% of the load. For each time point three individual tests were performed and the mean values, as well as standard deviation was determined (n=3).

7.4.4 Cell viability of alveolar basal epithelial cells and macrophages

After the formulation was successfully loaded with the selected anti-inflammatory drugs, acute cytotoxicity was evaluated. Since during pulmonary application immunologically active cells as well as epithelial cells encounter the applied formulation, a toxicity test was performed on both A549 cells as model for alveolar epithelial cells as well as on dTHP-1 cells as macrophages. As illustrated in Figure 35, the MTT assay showed no toxicity for 10 to 100 µg/ml up to an incubation time of 48 h. Here, the loaded microrods represents 20% curcumin loading with siRNA against TNF-α in the outer layer and the unloaded microrods are the formulation without any drug. The concentrations used per cell were chosen to provide the same conditions as in the ELISA performed subsequently. Since no toxicity was generated by the selected parameters, the formulation was used to determine the effect on the cytokine release.
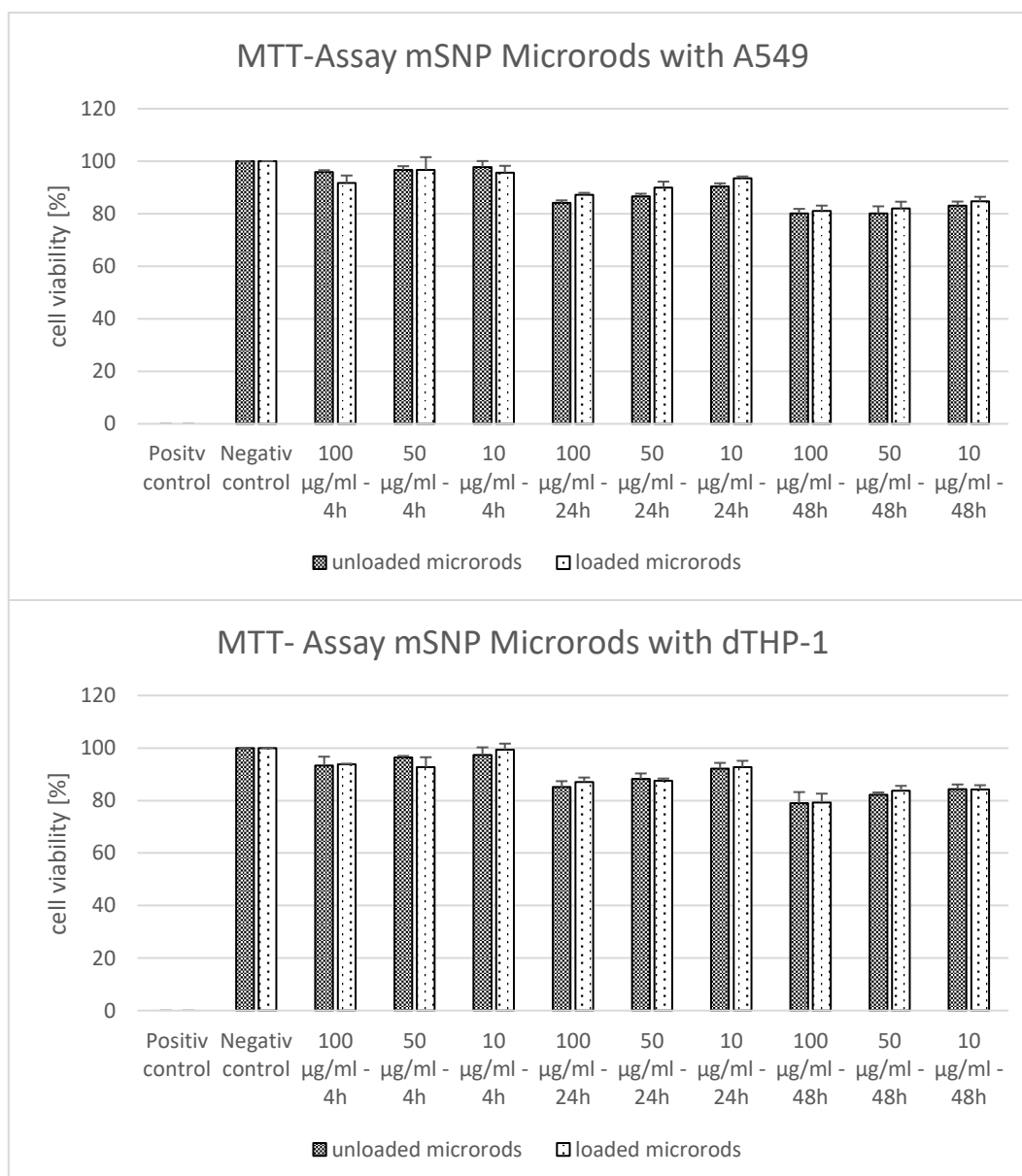
Figure 35: Determination of cell viability after incubation of the human alveolar epithelial cell line A549 (upper graph) and the human macrophage cell line dTHP-1 (lower graph) with unloaded and curcumin + siRNA loaded microrods. Incubation times of 4 to 48 h were chosen with a concentration of 10, 50 and 100 µg/ml. These parameters were adjusted to those of the ELISA performed later to see if the conditions are suitable for cytokine determination, as toxicity would cause high cytokine levels. Up to 48 h incubation time, no relevant toxicity can be observed.

7.4.5 TNF-α quantification *via* ELISA

The successfully prepared nanostructured microrods loaded with curcumin and siRNA showing no toxicity on relevant time scales allowed the investigation of the cytokine inhibition potential of the microrods. The dTHP-1 cells were grown in 24-well plates with $2*10^5$ cells per well and incubated with 500 µl of 400 to 40 µg/ml microrods suspension for 48 h to generate the same rod-to-cell ratio as in the previous MTT assay (no toxicity observed). Subsequently, the cells were incubated for 6 h with LPS to induce an inflammation and afterwards cytokine release was measured. In addition to the formulation loaded with curcumin and siRNA, further control groups were tested for TNF-α inhibition allowing to separate the effect of the different compounds. Therefore, microrods only loaded with curcumin as well as curcumin solution were tested: To exclude unspecific gene silencing by an oligonucleotide sequence, a scrambled siRNA with the same number of base pairs was used as control. Additionally, all drugs were used without carrier system, to check their behaviour with respect to cytokine inhibition. As positive control (PC) dTHP-1 were cultivated without LPS stimulation whereas for the negative control (NC), cells were only incubated with LPS for 6 h without any drug delivery system or drug applied. Comparing the results of the ELISA (Figure 36), the microrods loaded with both anti-inflammatory reagents were found to be most powerful and inhibit the TNF-α release significantly in comparison to the NC, as well as the loaded formulation with just one drug. Also, the unspecific siRNA and the pure drugs without carrier system had no influence in cytokine inhibition as expected. This demonstrates that loading the microrods with two drugs has a positive effect on TNF-α reduction and is significantly more effective than applying just one drug. Additionally, the results obtained show, that the developed nanostructured, cylindrical microparticles loaded with curcumin and siRNA is a drug delivery system with suitable properties to reduce inflammation reaction of macrophages in the lungs. The release kinetics only providing a small fraction of the loaded drug released after two days might be also a beneficial aspect for future *in vivo* studies, as inflammation will not just last 48 hours.
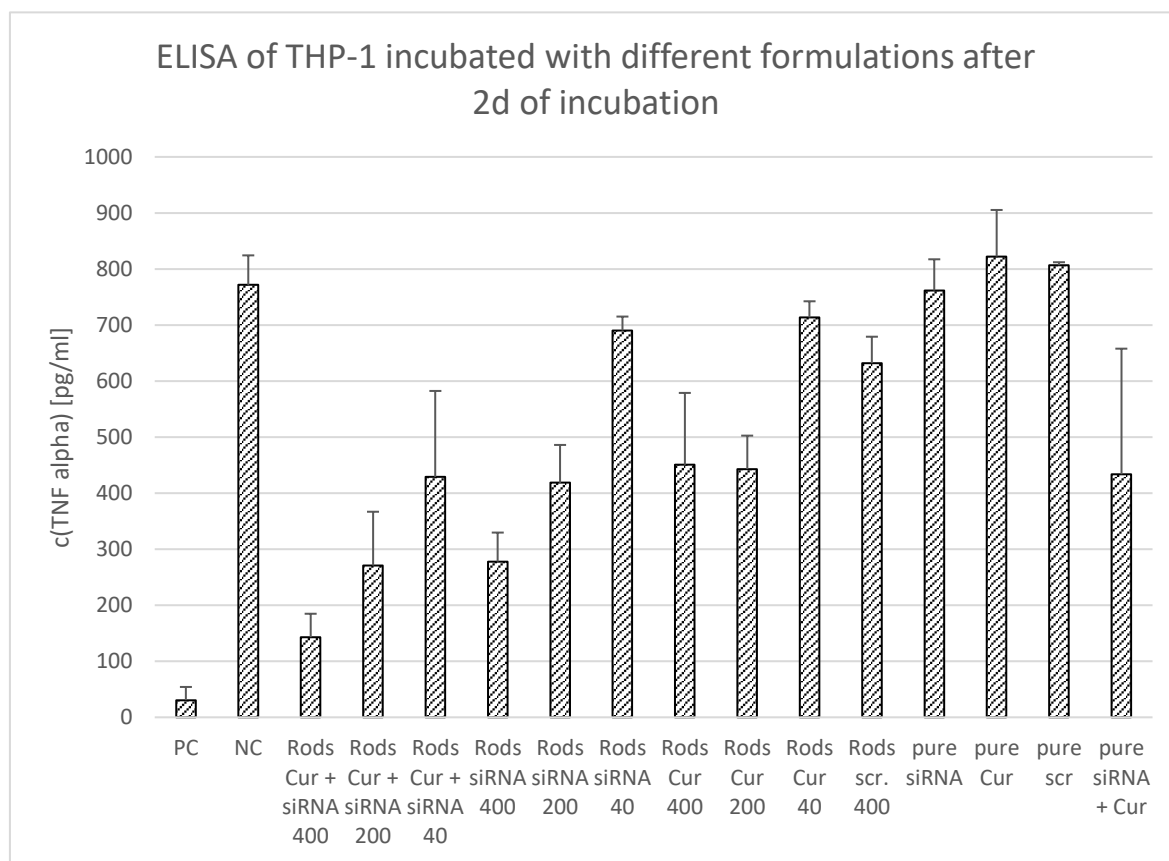
Figure 36: Determination of TNF-α release after incubation with different formulations for 48 h followed by LPS stimulation. As NC, cells were stimulated only with LPS without any carrier system, whereas the PC represents unstimulated cells. In order to compare the microrods loaded with both active ingredients (Rods Cur+siRNA) and the individually loaded microrods, a formulation containing only curcumin (Rods Cur) and only siRNA (Rods siRNA) were prepared and its influence on cytokine release determined. To exclude possible unspecific gene silencing by an oligonucleotide sequence, a scrambled siRNA with the same number of base pairs was used as an additional control. In addition, the drugs were applied to the cells without a carrier system to show the influence of the microrods as a means of transport. The results obtained show that the formulation with both active ingredients can significantly reduce the TNF release in contrast to the formulations with just one drug, or the active ingredients without carrier. Also, no unspecific inhibition by scrambled siRNA was observed. However, it can also be seen, that all microrod formulations can inhibit cytokine release, which also shows that the cylindrical microparticles can effectively transport the active ingredients into the macrophages. Significances were calculated by two-sided Student's-t-test. * $p < 0.05$.

7.5   Discussion

The manuscript described the stepwise production of a nanostructured, cylindrical microparticle system for pulmonary application, loading two anti-inflammatory drugs to reduce TNF-α release by human macrophage cell line THP-1. Mesoporous silica nanoparticles were used as building blocks of these microparticles as they have various positive properties in terms of drug delivery. Due to their large specific surface area and pore volume, high quantities of drug can be loaded into the pores and additionally this porous structure leads to an improved biocompatibility [277]. Another advantage of pore loading is the protection of unstable drugs such as curcumin due to the protective environment created in the pores [247]. This property was taken advantage of when loading curcumin, as this anti-inflammatory drug [278] is subject to rapid degradation [252] and thus should be transported as closely as possible to the target. After loading the mSNPs, they had to be moved to a next larger dimension, since the aerodynamic properties were not sufficient to reach the deep lungs [183]. To allow for formation of inhalable objects, the layer-by-layer technique was used to increase the adhesion forces of the nanoparticles to each other. Thus, a stable microparticulate formulation was generated. Various polyionic polymers can be used in this technique, but also biomolecules such as proteins, polypeptides and nucleic acids [279]. In the developed formulation, a specific siRNA against TNF-α was used as layering material to stabilize the formulation and to act at the same time as anti-inflammatory active ingredient. The delivery of siRNA faces many hurdles due to the chemical structure. The typically low stability, as well as the membrane impermeability caused by the polyanionic character are the biggest challenges [280]. As the target location of siRNA is the cytoplasm [281], branched polyethyleneimine was used as polycationic polymer for stabilisation, as this molecule has a strong buffering capacity, which promotes osmotic swelling of the lysosome and thus destabilizes the membrane of the vesicle, leading to a diffusion of the siRNA in the cytoplasm (proton sponge effect) [162]. A provision of siRNA and curcumin without the delivery system did not impact on the TNF-a secretion. However, the combination of both anti-inflammatory drugs with the developed drug delivery system showed a significant reduction in cytokine release, compared to the

individual agents. This suggests that the combination of such two drugs will allow to obtain stronger effects reducing the inflammatory status.

The use of different particle shapes for drug delivery has been of increasing interest in recent years [14]. For lung application, a cylindrical shape is of interest, since on the one hand the aerodynamic properties are suitable for inhalation (as described in the manuscript) and on the other hand the particle-cell interaction is different to spherical particles. By changing the aspect ratio of the microrods, particle uptake into macrophages can be prolonged [174] which allows a sustained residence time of the formulation and the active ingredient. This was also demonstrated *in vivo* for cylindrical microparticles using plasmid DNA [96]. In addition, the surface of the cylindrical nanostructured microparticles is significantly higher than their spherical counterparts due to the large internal surface. This allows a larger amount of drug to be loaded. Thus, larger quantities can be transported to the target cell population, which is particularly important for siRNA delivery [282]. Especially the effective transport of siRNA into the lungs is still a major hurdle at present [283]. However, the data discussed above in terms of pulmonary deposition (NGI data) and the inhibition of TNF-a release (ELISA data) depicts an intriguing direction with respect to co-application as well as with respect to novel formulation approaches.

7.6   Conclusion

The delivery of curcumin and siRNA is difficult due to chemical properties of the two compounds. Therefore, it is important to develop suitable drug carrier systems to enable effective transport. Due to the rapid decay of curcumin, protection of this substance is particularly important. This was provided by the pores of the mSNPs and the protective environment formed there, as well as the polymer layers above. The loading, as well as the transport of siRNA to macrophages could be successfully evaluated resulting in a significant reduction of TNF-α. The combination of both anti-inflammatory drugs proved to be the most efficient. Besides the positive biological results, the obtained aerodynamic characteristics with a MMAD of 2.85 µm and a FPF > 30% render a possible pulmonary application feasible using such systems.

In summary, the developed nanostructured, cylindrical particle formulation is suitable for the transport of labile drugs and due to its flight properties, can enable

transport into the lungs. In addition, the formulation is non-toxic to both alveolar epithelial cells and macrophages and can significantly inhibit TNF-α release after inflammation with LPS, making it a potential alternative to a drug delivery system for the lungs.

8.   Conclusion and perspectives

The development of new oligonucleotide therapeutics has increased significantly in recent years, which is also reflected in the rising number of approvals. This highly potent group of drugs not only offers a more effective treatment method for various diseases, but also an opportunity to treat currently incurable diseases [135]. For this reason, it is all the more important that effective drug delivery systems are developed to enable efficient transport and thereby improve therapy [142].

In this work, the development of a delivery system for pulmonary administration was in focus to enhance the effectivity of drug transport to the lungs leading to an increased biological response. Special attention was paid to overcome the hurdles of oligonucleotide transport in order to generate the highest possible drug concentration in the target tissue.

Therefore, at the beginning of the work, the focus was on the development of the carrier system. The existing template method was used to generate the specific cylindrical shape of the particles. In this process, the nanoparticles were interconnected with different polymers using the layer-by-layer technique to maintain the cylindrical shape after release from the template membrane. This stabilization method also had the advantage that the polyanionic oligonucleotide sequence could be loaded onto the surface of the rods without disintegration. However, this result was not self-evident, since an unmodified RNA sequence was used, which is characterized by high instability [31]. In addition, the polymer multilayers served as protection of the loaded drugs in the pores of mesoporous silica nanoparticles. Finally, to improve the flight properties of the microparticles, the prepared formulation was coated with L-leucine to reduce hygroscopicity and increase roughness to minimize interaction between particles.

To address the first research issue of the thesis, the flight characteristics of different microrods with variations in the AR were analysed using NGI and were then compared to the data obtained for their volume equivalent spherical counterparts. It was shown that a change in shape and the associated shape factor χ significantly influence the aerodynamic properties. The AR plays a decisive role, especially for

cylindrical particles, which influences χ particularly at high length ratios. Thus, NGI experiments showed that for volume equivalent particles, the cylindrical microparticles with an AR of 3.3 had a 2.8-fold lower aerodynamic diameter compared to their spherical counterpart. This offers the potential that cylindrical particles with a large volume equivalent diameter can be used to reach the deep lungs, allowing a higher amount of drug to be delivered directly to the target organ due to the larger surface area. In addition, the design of the drug delivery system offers the possibility of loading the individual nanoparticles that comprise the formulation to achieve a further increase in drug quantity, making transport more efficient than using a spherical particle with the same aerodynamic properties.

Based on these positive flight properties, the particle system could be characterized with respect to its biological properties. In this process, the loaded microrods were first characterized in terms of their morphology and loading. Here, the nanostructured surface could be imaged by SEM and the loading of oligonucleotides was visualized by CLSM. To ensure that the loading did not cause degradation of the chemical structure of the nucleotides, the sequence length was characterized by gel electrophoresis and Bioanalyzer® showing an intact structure after the production process. Based on this finding, quantification of phosphorus was performed by ICP-MS, which revealed an siRNA loading of 0.371% [%w/w]. Release kinetics were then performed in a phagolysosomal medium to estimate the amount of drug after different time points in the cell following uptake and whether nucleotide sequence detachment could generally be measured. Since a release was detectable, this demonstrated that the developed delivery system could be successfully loaded with an oligonucleotide without causing a degradation and, in addition, that a release occurs under biological conditions. These results were confirmed by subsequent determination of cytokine release from macrophages with and without the loaded drug carrier system after an inflammation was induced by LPS, where a significant reduction in pro-inflammatory TNF-α was obtained by the formulation *in vitro*.

Nevertheless, prolonged incubation of the microrods in biological media leads to disintegration into small fragments and nanoparticles. However, this can be used to

specifically target epithelial cells, which are not able to take up microparticles and yet play a role in some chronic pro-inflammatory lung diseases like asthma, COPD and CF. The advantage is firstly the manufacturing method, which allows the individual nanoparticles to be loaded and also causes rapid absorption by epithelial cells due to the small size. Thus, the developed delivery system can address both, macrophages as microparticles and epithelial cells after disintegration. Which cell population to target can be achieved by changing the polymer layers. Decreasing the amount of layers also reduces the intraparticle adhesion forces, which leads to faster disintegration and thus favours the uptake in epithelial cells [284]. Increasing the number of polymer layers and the associated stability induces an increased uptake by macrophages due to the more resistant micron size of the particles.

Since silica nanoparticles were used as a model in the first three sections to produce the microrods, the last part of the thesis consisted of using a more biocompatible building material to produce the cylindrical microparticles. Therefore, mesoporous silica nanoparticles were used because they combine different advantages as drug delivery system since they represent a special morphology and interesting chemical properties [246]. Due to the mesoporous structure, a higher loading can be achieved. Since the environment in the pores also changes due to the loaded drug, the drug is also protected from the external medium and the release kinetics are also altered [247]. This protection of the pore content can also be enhanced by coating the surface. Here, the high negative surface charge is helpful in adsorbing loaded polymers. Furthermore, a chemical modification of the hydroxy groups of the surface can be performed to change the characteristics of the particles as well as to stain them for visualization [285]. These properties of mesoporous particles were exploited in the last section to improve the previously developed delivery system. For this purpose, the system was loaded with two anti-inflammatory agents to promote a possible enhancement of the biological response. Here, the combination of the herbal immune modulating substance curcumin and a siRNA sequence against TNF-α proved to be very effective, eliciting a strong reduction of TNF-α release after induced inflammation in macrophages. Although the results obtained so far show a positive trend, further characterizations are still needed. In a next step, more cytokines (*e.g.,* IL 1, IL 6) should be considered after incubation with the

formulation to evaluate the potential of inhibition in more detail. Additionally, the biological response *in vivo* should be investigated to verify the current *in vitro* data. The potential of mesoporous silica nanoparticles in terms of morphological and chemical conditions still give many approaches for modifying the release kinetics of the loaded pores. Several methods like pH triggering, surface coating and functionalization, as well as capping the pores with gatekeepers, represent possible opportunities for an altered release [286, 287]. Not only drug release can be influenced by modifying the surface, but also targeting of cell populations and enhanced biocompatibility could be induced by using different ligands like poly (ethylene glycol), poly (2-hydroxyethyl methacrylate), folate or antibodies [288]. All these modification possibilities need to be considered in further optimization of the developed formulation to better understand the system and define the limits in both technological and biological implementation.

In the present thesis, an innovative drug delivery system for transporting oligonucleotides to the lungs was described. In this context, a possible addressing of the deep lungs based on the aerodynamic properties was demonstrated and the interaction with representative cell types was characterized. Since the developed carrier system was constructed from silica nanoparticles as a model substance, these had to be replaced with an alternative. Therefore, mesoporous silica particles were chosen, as they have similar chemical properties and also result in better biocompatibility. However, for future systems, a change to biodegradable and biocompatible polymers such as poly-l-lactic-co-glycolic acid or gelatine, as well as inorganic compounds like calcium phosphate should be sought to avoid toxic potential and side effects due to the chemical structure of silica. Another critical point is the low yield in the present production method. An *in vivo* application would require large amounts of the formulation, which would not be easy to realize due to cost and time constraints. This would have to be considered in future investigations. Nevertheless, the data obtained indicate that the developed innovative delivery system is a potential candidate for effective delivery of oligonucleotides, which may improve future therapies.

9. References

[1] S. Aras, M.R. Zaidi, TAMeless traitors: macrophages in cancer progression and metastasis, British journal of cancer, 117 (2017) 1583-1591.

[2] C.D. Klaassen, J.B. Watkins, Casarett & Doull's essentials of toxicology, McGraw Hill Professional, 2015.

[3] European Pharmacopoeia (Ph.Eur.) 10.0, 2.9.18. Preparations for inhalation: aerodynamic assessmentof fine particles, Council of Europe, Strasbourg, France., 2020.

[4] J.P. Mizgerd, Acute lower respiratory tract infection, New England Journal of Medicine, 358 (2008) 716-727.

[5] J.S. Patton, Mechanisms of macromolecule absorption by the lungs, Advanced drug delivery reviews, 19 (1996) 3-36.

[6] R. Sturm, Nanotubes in the human respiratory tract–deposition modeling, Zeitschrift für medizinische Physik, 25 (2015) 135-145.

[7] L. Müller, S. Di Benedetto, G. Pawelec, The immune system and its dysregulation with aging, in: Biochemistry and Cell Biology of Ageing: Part II Clinical Science, Springer, 2019, pp. 21-43.

[8] E.R. Weibel, Lung morphometry: the link between structure and function, Cell and tissue research, 367 (2017) 413-426.

[9] V.A. Marple, D.L. Roberts, F.J. Romay, N.C. Miller, K.G. Truman, M. Van Oort, B. Olsson, M.J. Holroyd, J.P. Mitchell, D. Hochrainer, Next generation pharmaceutical impactor (a new impactor for pharmaceutical inhaler testing). Part I: Design, Journal of aerosol medicine, 16 (2003) 283-299.

[10] D. Bumcrot, M. Manoharan, V. Koteliansky, D.W. Sah, RNAi therapeutics: a potential new class of pharmaceutical drugs, Nature chemical biology, 2 (2006) 711-719.

[11] W. Hofmann, Modelling inhaled particle deposition in the human lung—A review, Journal of Aerosol Science, 42 (2011) 693-724.

[12] C. Van Holsbeke, J. Marshall, J. De Backer, W. Vos, Median mass aerodynamic diameter (MMAD) and fine particle fraction (FPF): Influence on lung deposition?, European Respiratory Journal, 44 (2014) P912.

[13] B. Yu, H. Cong, Q. Peng, C. Gu, Q. Tang, X. Xu, C. Tian, F. Zhai, Current status and future developments in preparation and application of nonspherical polymer particles, Advances in colloid and interface science, 256 (2018) 126-151.

[14] J.A. Champion, Y.K. Katare, S. Mitragotri, Particle shape: a new design parameter for micro-and nanoscale drug delivery carriers, Journal of controlled release, 121 (2007) 3-9.

[15] M. Ochs, J. Hegermann, E. Lopez-Rodriguez, S. Timm, G. Nouailles, J. Matuszak, S. Simmons, M. Witzenrath, W.M. Kuebler, On Top of the Alveolar Epithelium: Surfactant and the Glycocalyx, International Journal of Molecular Sciences, 21 (2020) 3075.

[16] A.H. de Boer, P. Hagedoorn, M. Hoppentocht, F. Buttini, F. Grasmeijer, H.W. Frijlink, Dry powder inhalation: past, present and future, Expert opinion on drug delivery, 14 (2017) 499-512.

[17] D.T. Pham, A. Chokamonsirikun, V. Phattaravorakarn, W. Tiyaboonchai, Polymeric micelles for pulmonary drug delivery: a comprehensive review, Journal of Materials Science, (2020) 1-21.

[18] J. Bousquet, R. Dahl, N. Khaltaev, Global alliance against chronic respiratory diseases, European Respiratory Journal, 29 (2007) 233-239.

[19] W. Wu, N. Kaminski, Chronic lung diseases, Wiley Interdisciplinary Reviews: Systems Biology and Medicine, 1 (2009) 298-308.

[20] P. Jones, G. Harding, P. Berry, I. Wiklund, W. Chen, N.K. Leidy, Development and first validation of the COPD Assessment Test, European Respiratory Journal, 34 (2009) 648-654.

[21] A. Oliver, R. Cantón, P. Campo, F. Baquero, J. Blázquez, High frequency of hypermutable Pseudomonas aeruginosa in cystic fibrosis lung infection, Science, 288 (2000) 1251-1253.

[22] B.R. Mash, A. Bheekie, P. Jones, Inhaled versus oral steroids for adults with chronic asthma, Cochrane Database of Systematic Reviews, (2001).

[23] J. Wright, D. Brocklebank, F. Ram, Inhaler devices for the treatment of asthma and chronic obstructive airways disease (COPD), Quality and Safety in Health Care, 11 (2002) 376-382.

[24] Y.S. López-Boado, B.K. Rubin, Macrolides as immunomodulatory medications for the therapy of chronic lung diseases, Current opinion in pharmacology, 8 (2008) 286-291.

[25] H. Magnussen, B. Disse, R. Rodriguez-Roisin, A. Kirsten, H. Watz, K. Tetzlaff, L. Towse, H. Finnigan, R. Dahl, M. Decramer, Withdrawal of inhaled glucocorticoids and exacerbations of COPD, N Engl J Med, 371 (2014) 1285-1294.

[26] M. Cazzola, F. Cavalli, O.S. Usmani, P. Rogliani, Advances in pulmonary drug delivery devices for the treatment of chronic obstructive pulmonary disease, Expert Opinion on Drug Delivery, 17 (2020) 635-646.

[27] J.F. Pontes, A. Grenha, Multifunctional nanocarriers for lung drug delivery, Nanomaterials, 10 (2020) 183.

[28] N. Lababidi, E.O. Kissi, W.A. Elgaher, V. Sigal, J. Haupenthal, B.C. Schwarz, A.K. Hirsch, T. Rades, M. Schneider, Spray-drying of inhalable, multifunctional formulations for the treatment of biofilms formed in cystic fibrosis, Journal of Controlled Release, 314 (2019) 62-71.

[29] M. Joshi, M. Nagarsenkar, B. Prabhakar, Albumin nanocarriers for pulmonary drug delivery: An attractive approach, Journal of Drug Delivery Science and Technology, 56 (2020) 101529.

[30] A. Garcia, P. Mack, S. Williams, C. Fromen, T. Shen, J. Tully, J. Pillai, P. Kuehl, M. Napier, J.M. DeSimone, Microfabricated engineered particle systems for respiratory drug delivery and other pharmaceutical applications, Journal of drug delivery, 2012 (2012).

[31] Y. Sun, Y. Zhao, X. Zhao, R.J. Lee, L. Teng, C. Zhou, Enhancing the therapeutic delivery of oligonucleotides by chemical modification and nanoparticle encapsulation, Molecules, 22 (2017) 1724.

[32] T.H. Schiebler, W. Schmidt, Lehrbuch der gesamten Anatomie des Menschen: Cytologie Histologie Entwicklungsgeschichte Makroskopische und Mikroskopische Anatomie, Springer, 1977.

[33] X. Murgia, C. de Souza Carvalho, C.-M. Lehr, Overcoming the pulmonary barrier: new insights to improve the efficiency of inhaled therapeutics, European Journal of Nanomedicine, 6 (2014) 157-169.

[34] S. Newman, P. Anderson, Respiratory drug delivery: Essential theory and practice, Respiratory Drug Delivery Online, 2009.

[35] A.R. Leff, P.T. Schumacker, Respiratory physiology: basics and applications, (1993).

[36] M. Bur, C.-M. Lehr, Pulmonary cell culture models to study the safety and efficacy of innovative aerosol medicines, Expert opinion on drug delivery, 5 (2008) 641-652.

[37] A. Steimer, E. Haltner, C.-M. Lehr, Cell culture models of the respiratory tract relevant to pulmonary drug delivery, Journal of aerosol medicine, 18 (2005) 137-182.

[38] L. Reid, B. Meyrick, V.B. Antony, L.-Y. Chang, J.D. Crapo, H.Y. Reynolds, The mysterious pulmonary brush cell: a cell in search of a function, American journal of respiratory and critical care medicine, 172 (2005) 136-139.

[39] Y. Inayama, G. Hook, A. Brody, G. Cameron, A. Jetten, L. Gilmore, T. Gray, P. Nettesheim, The differentiation potential of tracheal basal cells, Laboratory investigation; a journal of technical methods and pathology, 58 (1988) 706-717.

[40] J. Widdicombe, R. Pack, The Clara cell, European journal of respiratory diseases, 63 (1982) 202.

[41] M. Munkholm, J. Mortensen, Mucociliary clearance: pathophysiological aspects, Clinical physiology and functional imaging, 34 (2014) 171-177.

[42] N. Sanders, C. Rudolph, K. Braeckmans, S.C. De Smedt, J. Demeester, Extracellular barriers in respiratory gene therapy, Advanced drug delivery reviews, 61 (2009) 115-127.

[43] E. Houtmeyers, R. Gosselink, G. Gayan-Ramirez, M. Decramer, Regulation of mucociliary clearance in health and disease, European Respiratory Journal, 13 (1999) 1177-1188.

[44] L. Müller, M. Riediker, P. Wick, M. Mohr, P. Gehr, B. Rothen-Rutishauser, Oxidative stress and inflammation response after nanoparticle exposure: differences between human lung cell monocultures and an advanced three-dimensional model of the human epithelial airways, Journal of the Royal Society Interface, 7 (2010) S27-S40.

[45] J. Perez-Gil, T.E. Weaver, Pulmonary surfactant pathophysiology: current models and open questions, Physiology, 25 (2010) 132-141.

[46] E. Evren, E. Ringqvist, T. Willinger, Origin and ontogeny of lung macrophages: from mice to humans, Immunology, 160 (2020) 126-138.

[47] A.S. Neupane, M. Willson, A.K. Chojnacki, F.V.E.S. Castanheira, C. Morehouse, A. Carestia, A.E. Keller, M. Peiseler, A. DiGiandomenico, M.M. Kelly, Patrolling alveolar macrophages conceal bacteria from the immune system to maintain homeostasis, Cell, 183 (2020) 110-125. e111.

[48] N.S. Csaba, M.J. Alonso, D.E. Thurston, Nanostructured Biomaterials for Overcoming Biological Barriers, Royal Society of Chemistry, 2012.

[49] C.A. Ruge, J. Kirch, O. Cañadas, M. Schneider, J. Perez-Gil, U.F. Schaefer, C. Casals, C.-M. Lehr, Uptake of nanoparticles by alveolar macrophages is triggered by surfactant protein A, Nanomedicine: Nanotechnology, Biology and Medicine, 7 (2011) 690-693.

[50] R. Miyata, S.F. van Eeden, The innate and adaptive immune response induced by alveolar macrophages exposed to ambient particulate matter, Toxicology and applied pharmacology, 257 (2011) 209-226.

[51] A.J. Byrne, S.A. Mathie, L.G. Gregory, C.M. Lloyd, Pulmonary macrophages: key players in the innate defence of the airways, Thorax, 70 (2015) 1189-1196.

[52] W. Sepúlveda-Loyola, C. Osadnik, S. Phu, A.A. Morita, G. Duque, V.S. Probst, Diagnosis, prevalence, and clinical impact of sarcopenia in COPD: a systematic review and meta-analysis, Journal of cachexia, sarcopenia and muscle, 11 (2020) 1164-1176.

[53] P. Sangaphunchai, I. Todd, L.C. Fairclough, Extracellular vesicles and asthma: A review of the literature, Clinical & Experimental Allergy, 50 (2020) 291-307.

[54] J. Reiter, A. Gileles-Hillel, M. Cohen-Cymberknoh, D. Rosen, E. Kerem, D. Gozal, E. Forno, Sleep disorders in cystic fibrosis: A systematic review and meta-analysis, Sleep Medicine Reviews, (2020) 101279.

[55] A. Lechanteur, B. Evrard, Influence of Composition and Spray-Drying Process Parameters on Carrier-Free DPI Properties and Behaviors in the Lung: A review, Pharmaceutics, 12 (2020) 55.

[56] M. Sockrider, Nebulizer Breathing Treatments at Home, American journal of respiratory and critical care medicine, 202 (2020) P7-P8.

[57] A. Ari, Aerosol therapy in pulmonary critical care, Respiratory care, 60 (2015) 858-879.

[58] S.D. McCarthy, H.E. González, B.D. Higgins, Future Trends in Nebulized Therapies for Pulmonary Disease, Journal of Personalized Medicine, 10 (2020) 37.

[59] H.-L. Lin, C.-S. Chen, J.B. Fink, G.-H. Lee, C.-W. Huang, J.-C. Chen, Z.Y. Chiang, In Vitro Evaluation of a Vibrating-Mesh Nebulizer Repeatedly Use over 28 Days, Pharmaceutics, 12 (2020) 971.

[60] S.P. Newman, Principles of metered-dose inhaler design, Respiratory care, 50 (2005) 1177-1190.

[61] L. Payares-Salamanca, S. Contreras-Arrieta, V. Florez-García, A. Barrios-Sanjuanelo, I. Stand-Niño, C.E. Rodriguez-Martinez, Metered-dose inhalers versus nebulization for the delivery of albuterol for acute exacerbations of wheezing or asthma in children: A systematic review with meta-analysis, Pediatric Pulmonology, 55 (2020) 3268-3278.

[62] A.R. Clark, J.G. Weers, R. Dhand, The confusing world of dry powder inhalers: It is all about inspiratory pressures, not inspiratory flow rates, Journal of Aerosol Medicine and Pulmonary Drug Delivery, 33 (2020) 1-11.

[63] N. Shetty, D. Cipolla, H. Park, Q.T. Zhou, Physical stability of dry powder inhaler formulations, Expert Opinion on Drug Delivery, 17 (2020) 77-96.

[64] K.K. Jain, Drug delivery systems-an overview, in: Drug delivery systems, Springer, 2008, pp. 1-50.

[65] T.G. Capstick, I.J. Clifton, Lavorini, Crompton, Broeders, Horne, Horne, Menckeberg, Cochrane, Horne, Inhaler technique and training in people with chronic obstructive pulmonary disease and asthma, Expert review of respiratory medicine, 6 (2012) 91-103.

[66] T.C. Carvalho, J.I. Peters, R.O. Williams III, Influence of particle size on regional lung deposition–what evidence is there?, International journal of pharmaceutics, 406 (2011) 1-10.

[67] S.P. Newman, Can lung deposition data act as a surrogate for the clinical response to inhaled asthma drugs?, British journal of clinical pharmacology, 49 (2000) 529-537.

[68] A.A. Matthews, P.L.R. Ee, R. Ge, Developing inhaled protein therapeutics for lung diseases, Molecular Biomedicine, 1 (2020) 1-14.

[69] D. Muir, C. Davies, The Deposition of 0· 5 μ Diameter Aerosols in the Lungs of Man, Annals of Occupational Hygiene, 10 (1967) 161-174.

[70] H. Yu, H.-L. Yen, Y. Li, Deposition of bronchiole-originated droplets in the lower airways during exhalation, Journal of Aerosol Science, 142 (2020) 105524.

[71] I.M. El-Sherbiny, N.M. El-Baz, M.H. Yacoub, Inhaled nano-and microparticles for drug delivery, Global Cardiology Science and Practice, 2015 (2015) 2.

[72] X.M. Zeng, G.P. Martin, C. Marriott, Particulate Interactions in Dry Powder Formulation for Inhalation, CRC Press, 2000.

[73] B. Pharmacopoeia, Preparations for inhalation. Aerodynamic assessment of fine particles-fine particle dose and particle size distribution (Ph. Eur. method 2.9. 18), British Pharmacopoeia, 4 (2005) A277-290.

[74] M.E. Abdelrahim, Aerodynamic characteristics of nebulized terbutaline sulphate using the Andersen Cascade Impactor compared to the Next Generation Impactor, Pharmaceutical development and technology, 16 (2011) 137-145.

[75] M. Taki, C. Marriott, X.-M. Zeng, G.P. Martin, Aerodynamic deposition of combination dry powder inhaler formulations in vitro: a comparison of three impactors, International journal of pharmaceutics, 388 (2010) 40-51.

[76] S. Sacanna, D.J. Pine, Shape-anisotropic colloids: Building blocks for complex assemblies, Current opinion in colloid & interface science, 16 (2011) 96-105.

[77] M.A. Fernandez-Rodriguez, M.A. Rodriguez-Valverde, M.A. Cabrerizo-Vilchez, R. Hidalgo-Alvarez, Surface activity of Janus particles adsorbed at fluid–fluid interfaces: Theoretical and experimental aspects, Advances in Colloid and Interface Science, 233 (2016) 240-254.

[78] K.J. Lee, J. Yoon, J. Lahann, Recent advances with anisotropic particles, Current Opinion in Colloid & Interface Science, 16 (2011) 195-202.

[79] B.V. Parakhonskiy, A.M. Yashchenok, M. Konrad, A.G. Skirtach, Colloidal micro-and nano-particles as templates for polyelectrolyte multilayer capsules, Advances in colloid and interface science, 207 (2014) 253-264.

[80] K. Thorkelsson, P. Bai, T. Xu, Self-assembly and applications of anisotropic nanomaterials: A review, Nano Today, 10 (2015) 48-66.

[81] D. Kohler, M. Schneider, M. Krüger, C.M. Lehr, H. Möhwald, D. Wang, Template-Assisted Polyelectrolyte Encapsulation of Nanoparticles into Dispersible, Hierarchically Nanostructured Microfibers, Advanced Materials, 23 (2011) 1376-1379.

[82] L.-T.-C. Tran, S. Lesieur, V. Faivre, Janus nanoparticles: materials, preparation and recent advances in drug delivery, Expert opinion on drug delivery, 11 (2014) 1061-1074.

[83] A. Kumar, J.J. Higdon, Dynamics of the orientation behavior and its connection with rheology in sheared non-Brownian suspensions of anisotropic dicolloidal particles, Journal of Rheology, 55 (2011) 581-626.

[84] K. Shin, D. Kim, J.-C. Cho, H.-S. Lim, J.W. Kim, K.-D. Suh, Monodisperse conducting colloidal dipoles with symmetric dimer structure for enhancing electrorheology properties, Journal of colloid and interface science, 374 (2012) 18-24.

[85] S. Tseng, C.-H. Cho, Z.-S. Chen, J.-P. Hsu, Electrophoresis of an ellipsoid along the axis of a cylindrical pore: Effect of a charged boundary, Langmuir, 24 (2008) 2929-2937.

[86] K. Kempe, R.A. Wylie, M.D. Dimitriou, H. Tran, R. Hoogenboom, U.S. Schubert, C.J. Hawker, L.M. Campos, L.A. Connal, Preparation of non-spherical particles from amphiphilic block copolymers, Journal of Polymer Science Part A: Polymer Chemistry, 54 (2016) 750-757.

[87] T. Laemthong, H.H. Kim, K. Dunlap, C. Brocker, D. Barua, D. Forciniti, Y.-W. Huang, S. Barua, Bioresponsive polymer coated drug nanorods for breast cancer treatment, Nanotechnology, 28 (2016) 045601.

[88] P.F. DeCarlo, J.G. Slowik, D.R. Worsnop, P. Davidovits, J.L. Jimenez, Particle morphology and density characterization by combined mobility and aerodynamic diameter measurements. Part 1: Theory, Aerosol Science and Technology, 38 (2004) 1185-1205.

[89] W.C. Hinds, Aerosol technology: properties, behavior, and measurement of airborne particles, John Wiley & Sons, 1999.

[90] M. Allen, O. Raabe, Re-evaluation of Millikan's oil drop data for the motion of small particles in air, Journal of Aerosol Science, 13 (1982) 537-547.

[91] M.D. Allen, O.G. Raabe, Slip correction measurements of spherical solid aerosol particles in an improved Millikan apparatus, Aerosol Science and Technology, 4 (1985) 269-286.

[92] M. Lippmann, Effects of fiber characteristics on lung deposition, retention, and disease, Environmental health perspectives, 88 (1990) 311-317.

[93] R. Sturm, W. Hofmann, A theoretical approach to the deposition and clearance of fibers with variable size in the human respiratory tract, Journal of hazardous materials, 170 (2009) 210-218.

[94] W.-C. Su, Y.S. Cheng, Deposition of fiber in a human airway replica, Journal of aerosol science, 37 (2006) 1429-1441.

[95] J.A. Champion, S. Mitragotri, Role of target geometry in phagocytosis, Proceedings of the National Academy of Sciences, 103 (2006) 4930-4934.

[96] M. Möhwald, S.R. Pinnapireddy, B. Wonnenberg, M. Pourasghar, M. Jurisic, A. Jung, C. Fink-Straube, T. Tschernig, U. Bakowsky, M. Schneider, Aspherical, nanostructured microparticles for targeted gene delivery to alveolar macrophages, Advanced healthcare materials, 6 (2017) 1700478.

[97] W.-C. Su, Y.S. Cheng, Deposition of man-made fibers in human respiratory airway casts, Journal of aerosol science, 40 (2009) 270-284.

[98] W.-C. Su, Y.S. Cheng, Estimation of carbon nanotubes deposition in a human respiratory tract replica, Journal of Aerosol Science, 79 (2015) 72-85.

[99] M. Lippmann, Asbestos exposure indices, Environmental research, 46 (1988) 86-106.

[100] J.L. Perry, S. Tian, N. Sengottuvel, E.B. Harrison, B.K. Gorentla, C.H. Kapadia, N. Cheng, J.C. Luft, J.P.-Y. Ting, J.M. DeSimone, Pulmonary Delivery of Nanoparticle-Bound Toll-Like Receptor 9 Agonist for the Treatment of Metastatic Lung Cancer, ACS Nano, (2020).

[101] T. Fischer, T. Tschernig, F. Drews, K. Brix, C. Meier, M. Simon, R. Kautenburger, M. Schneider, siRNA delivery to macrophages using aspherical, nanostructured microparticles as delivery system for pulmonary administration, European Journal of Pharmaceutics and Biopharmaceutics, 158 (2021) 284-293.

[102] J. Möller, T. Luehmann, H. Hall, V. Vogel, The race to the pole: how high-aspect ratio shape and heterogeneous environments limit phagocytosis of filamentous Escherichia coli bacteria by macrophages, Nano letters, 12 (2012) 2901-2905.

[103] K. Hoebe, E. Janssen, B. Beutler, The interface between innate and adaptive immunity, Nature immunology, 5 (2004) 971-974.

[104] M.M. Melssen, K.E. Pollack, M.O. Meneveau, M.E. Smolkin, J. Pinczewski, A.F. Koeppel, S.D. Turner, K. Sol-Church, A. Hickman, D.H. Deacon, Characterization and comparison of innate and adaptive immune responses at vaccine sites in melanoma vaccine clinical trials, Cancer Immunology, Immunotherapy, (2021) 1-14.

[105] P.F. Duffney, M.L. Falsetta, A.R. Rackow, T.H. Thatcher, R.P. Phipps, P.J. Sime, Key roles for lipid mediators in the adaptive immune response, The Journal of clinical investigation, 128 (2018) 2724-2731.

[106] A. Vollmar, I. Zündorf, T. Dingermann, Immunologie: Grundlagen und Wirkstoffe; mit 216 Tabellen, Wiss. Verlag-Ges., 2013.

[107] O. Abdel-Razek, T. Liu, X. Chen, Q. Wang, G. Vanga, G. Wang, Role of Surfactant Protein D in Experimental Otitis Media, Journal of Innate Immunity, (2021) 1-14.

[108] Z. Liu, S. Chen, Y. Xu, X. Liu, P. Xiong, Y. Fu, Surfactant protein A expression and distribution in human lung samples from smokers with or without chronic obstructive pulmonary disease in China, Medicine, 99 (2020).

[109] E.M. Conway, L.A. Pikor, S.H. Kung, M.J. Hamilton, S. Lam, W.L. Lam, K.L. Bennewith, Macrophages, inflammation, and lung cancer, American journal of respiratory and critical care medicine, 193 (2016) 116-130.

[110] P.J. Murray, Macrophage polarization, Annual review of physiology, 79 (2017) 541-566.

[111] Y.-c. Huang, Z.-p. Feng, The good and bad of microglia/macrophages: new hope in stroke therapeutics, Acta Pharmacologica Sinica, 34 (2013) 6-7.

[112] D.J. Royer, D.N. Cook, Regulation of immune responses by nonhematopoietic cells in asthma, The Journal of Immunology, 206 (2021) 292-301.

[113] P.J. Murray, T.A. Wynn, Protective and pathogenic functions of macrophage subsets, Nature reviews immunology, 11 (2011) 723-737.

[114] J.B. Morjaria, M. Malerba, R. Polosa, Biologic and pharmacologic therapies in clinical development for the inflammatory response in COPD, Drug discovery today, 15 (2010) 396-405.

[115] N. Khaltaev, S. Axelrod, Chronic respiratory diseases global mortality trends, treatment guidelines, life style modifications, and air pollution: preliminary analysis, Journal of Thoracic Disease, 11 (2019) 2643.

[116] M. Mehta, D.S. Dhanjal, K.R. Paudel, B. Singh, G. Gupta, S. Rajeshkumar, L. Thangavelu, M.M. Tambuwala, H.A. Bakshi, D.K. Chellappan, Cellular signalling pathways mediating the pathogenesis of chronic inflammatory respiratory diseases: an update, Inflammopharmacology, (2020) 1-23.

[117] M. Mehta, S. Satija, K.R. Paudel, V. Malyla, V.K. Kannaujiya, D.K. Chellappan, M. Bebawy, P.M. Hansbro, P.R. Wich, K. Dua, Targeting respiratory diseases using miRNA inhibitor based nanotherapeutics: Current status and future perspectives, Nanomedicine: Nanotechnology, Biology and Medicine, 31 (2020) 102303.

[118] J.R. Murdoch, C.M. Lloyd, Chronic inflammation and asthma, Mutation Research/Fundamental and Molecular Mechanisms of Mutagenesis, 690 (2010) 24-39.

[119] A.S. Poltavets, P.A. Vishnyakova, A.V. Elchaninov, G.T. Sukhikh, T.K. Fatkhudinov, Macrophage modification strategies for efficient cell therapy, Cells, 9 (2020) 1535.

[120] J. Zhang, Y. Zhao, T. Hou, H. Zeng, D. Kalambhe, B. Wang, X. Shen, Y. Huang, Macrophage-based nanotherapeutic strategies in ulcerative colitis, Journal of Controlled Release, (2020).

[121] F. Jiang, J.A. Doudna, CRISPR–Cas9 structures and mechanisms, Annual review of biophysics, 46 (2017) 505-529.

[122] D. He, K. Müller, A. Krhac Levacic, P. Kos, U. Lächelt, E. Wagner, Combinatorial optimization of sequence-defined oligo (ethanamino) amides for folate receptor-targeted pDNA and siRNA delivery, Bioconjugate Chemistry, 27 (2016) 647-659.

[123] A.J. Mahiny, A. Dewerth, L.E. Mays, M. Alkhaled, B. Mothes, E. Malaeksefat, B. Loretz, J. Rottenberger, D.M. Brosch, P. Reautschnig, In vivo genome editing using nuclease-encoding mRNA corrects SP-B deficiency, Nature biotechnology, 33 (2015) 584-586.

[124] Y. Zhou, X. Chen, J. Cao, H. Gao, Overcoming the biological barriers in the tumor microenvironment for improving drug delivery and efficacy, Journal of Materials Chemistry B, (2020).

[125] C.A. Ruge, J. Kirch, C.-M. Lehr, Pulmonary drug delivery: from generating aerosols to overcoming biological barriers—therapeutic possibilities and technological challenges, The lancet Respiratory medicine, 1 (2013) 402-413.

[126] M. Schneider, M. Windbergs, N. Daum, B. Loretz, E.-M. Collnot, S. Hansen, U.F. Schaefer, C.-M. Lehr, Crossing biological barriers for advanced drug delivery, in, Elsevier, 2013.

[127] C.A. Stein, D. Castanotto, FDA-approved oligonucleotide therapies in 2017, Molecular Therapy, 25 (2017) 1069-1075.

[128] L. Pray, Discovery of DNA structure and function: Watson and Crick, Nature Education, 1 (2008).

[129] Y. Zhang, J. Ge, Green nanoparticles for oligonucleotide delivery, Gene Therapy, (2020) 1-2.

[130] D. Bonn, Prospects for antisense therapy are looking brighter, The Lancet, 9004 (1996) 820.

[131] V.S. Group, A randomized controlled clinical trial of intravitreous fomivirsen for treatment of newly diagnosed peripheral cytomegalovirus retinitis in patients with AIDS, American journal of ophthalmology, 133 (2002) 467-474.

[132] R.S. Geary, S.P. Henry, L.R. Grillone, Fomivirsen, Clinical pharmacokinetics, 41 (2002) 255-260.

[133] T.C. Roberts, R. Langer, M.J. Wood, Advances in oligonucleotide drug delivery, Nature Reviews Drug Discovery, 19 (2020) 673-694.

[134] A. Aartsma-Rus, D.R. Corey, The 10th oligonucleotide therapy approved: golodirsen for Duchenne muscular dystrophy, Nucleic acid therapeutics, 30 (2020) 67-70.

[135] J. Kim, C. Hu, C. Moufawad El Achkar, L.E. Black, J. Douville, A. Larson, M.K. Pendergast, S.F. Goldkind, E.A. Lee, A. Kuniholm, Patient-customized oligonucleotide therapy for a rare genetic disease, New England Journal of Medicine, 381 (2019) 1644-1652.

[136] V. Baldo, C. Reno, S. Cocchio, M.P. Fantini, SARS-CoV-2/COVID-19 Vaccines: The Promises and the Challenges Ahead, in, Multidisciplinary Digital Publishing Institute, 2021.

[137] W.H. Organization, Background document on the mRNA vaccine BNT162b2 (Pfizer-BioNTech) against COVID-19: background document to the WHO interim recommendations for use of the Pfizer–BioNTech COVID-19 vaccine, BNT162b2, under emergency use listing, 14 January 2021, in, World Health Organization.

[138] A. Flemming, mRNA vaccine shows promise in autoimmunity, Nature Reviews Immunology, 1-1.

[139] F.P. Polack, S.J. Thomas, N. Kitchin, J. Absalon, A. Gurtman, S. Lockhart, J.L. Perez, G. Pérez Marc, E.D. Moreira, C. Zerbini, Safety and efficacy of the

BNT162b2 mRNA Covid-19 vaccine, New England Journal of Medicine, 383 (2020) 2603-2615.

[140] S. Van Lint, D. Renmans, K. Broos, H. Dewitte, I. Lentacker, C. Heirman, K. Breckpot, K. Thielemans, The ReNAissanCe of mRNA-based cancer therapy, Expert review of vaccines, 14 (2015) 235-251.

[141] U. Sahin, E. Derhovanessian, M. Miller, B.-P. Kloke, P. Simon, M. Löwer, V. Bukur, A.D. Tadmor, U. Luxemburger, B. Schrörs, Personalized RNA mutanome vaccines mobilize poly-specific therapeutic immunity against cancer, Nature, 547 (2017) 222-226.

[142] O.M. Merkel, I. Rubinstein, T. Kissel, siRNA delivery to the lung: what's new?, Advanced drug delivery reviews, 75 (2014) 112-128.

[143] N. Agrawal, P. Dasaradhi, A. Mohmmed, P. Malhotra, R.K. Bhatnagar, S.K. Mukherjee, RNA interference: biology, mechanism, and applications, Microbiology and molecular biology reviews, 67 (2003) 657-685.

[144] D.-H. Kim, M.A. Behlke, S.D. Rose, M.-S. Chang, S. Choi, J.J. Rossi, Synthetic dsRNA Dicer substrates enhance RNAi potency and efficacy, Nature biotechnology, 23 (2005) 222-226.

[145] S.M. Hammond, S. Boettcher, A.A. Caudy, R. Kobayashi, G.J. Hannon, Argonaute2, a link between genetic and biochemical analyses of RNAi, Science, 293 (2001) 1146-1150.

[146] R. Kole, A.R. Krainer, S. Altman, RNA therapeutics: beyond RNA interference and antisense oligonucleotides, Nature reviews Drug discovery, 11 (2012) 125-140.

[147] R.L. Juliano, The delivery of therapeutic oligonucleotides, Nucleic acids research, 44 (2016) 6518-6548.

[148] A. Khvorova, J.K. Watts, The chemical evolution of oligonucleotide therapies of clinical utility, Nature biotechnology, 35 (2017) 238-248.

[149] D.A. Glazier, J. Liao, B.L. Roberts, X. Li, K. Yang, C.M. Stevens, W. Tang, Chemical synthesis and biological application of modified oligonucleotides, Bioconjugate chemistry, 31 (2020) 1213-1233.

[150] D. Lochmann, E. Jauk, A. Zimmer, Drug delivery of oligonucleotides by peptides, European journal of pharmaceutics and biopharmaceutics, 58 (2004) 237-251.

[151] Y. Wang, L. Miao, A. Satterlee, L. Huang, Delivery of oligonucleotides with lipid nanoparticles, Advanced drug delivery reviews, 87 (2015) 68-80.

[152] L. Huang, Y. Liu, In vivo delivery of RNAi with lipid-based nanoparticles, Annual review of biomedical engineering, 13 (2011) 507-530.

[153] H. Yin, R.L. Kanasty, A.A. Eltoukhy, A.J. Vegas, J.R. Dorkin, D.G. Anderson, Non-viral vectors for gene-based therapy, Nature Reviews Genetics, 15 (2014) 541-555.

[154] A.K. Leung, Y.Y.C. Tam, P.R. Cullis, Lipid nanoparticles for short interfering RNA delivery, Advances in genetics, 88 (2014) 71-110.

[155] G. Ozcan, B. Ozpolat, R.L. Coleman, A.K. Sood, G. Lopez-Berestein, Preclinical and clinical development of siRNA-based therapeutics, Advanced drug delivery reviews, 87 (2015) 108-119.

[156] S. Wilhelm, A.J. Tavares, Q. Dai, S. Ohta, J. Audet, H.F. Dvorak, W.C. Chan, Analysis of nanoparticle delivery to tumours, Nature reviews materials, 1 (2016) 1-12.

[157] A. George, P.A. Shah, P.S. Shrivastav, Natural biodegradable polymers based nano-formulations for drug delivery: A review, International journal of pharmaceutics, 561 (2019) 244-264.

[158] L. Ding, S. Tang, T.A. Wyatt, D.L. Knoell, D. Oupický, Pulmonary siRNA delivery for lung disease: Review of recent progress and challenges, Journal of Controlled Release, (2020).

[159] T. Fischer, T. Tschernig, F. Drews, K. Brix, C. Meier, M. Simon, R. Kautenburger, M. Schneider, siRNA delivery to macrophages using aspherical, nanostructured microparticles as delivery system for pulmonary administration, European Journal of Pharmaceutics and Biopharmaceutics, (2020).

[160] G. Decher, Fuzzy nanoassemblies: toward layered polymeric multicomposites, science, 277 (1997) 1232-1237.

[161] M.P. Aljoscha Koenneke, Marc Schneider, Nanostructured microparticles for inhalation, in: R. Shegokar (Ed.) Delivery of Drugs, Elsevier, 2020, pp. 119 - 160.

[162] A. Akinc, M. Thomas, A.M. Klibanov, R. Langer, Exploring polyethylenimine-mediated DNA transfection and the proton sponge hypothesis, The Journal of Gene Medicine: A cross-disciplinary journal for research on the science of gene transfer and its clinical applications, 7 (2005) 657-663.

[163] D.R. Hess, Nebulizers: principles and performance, Respiratory care, 45 (2000) 609-622.

[164] D. Prime, P.J. Atkins, A. Slater, B. Sumby, Review of dry powder inhalers, Advanced drug delivery reviews, 26 (1997) 51-58.

[165] M.J. Telko, A.J. Hickey, Dry powder inhaler formulation, Respiratory care, 50 (2005) 1209-1227.

[166] L. Gradon, T.R. Sosnowski, Formation of particles for dry powder inhalers, Advanced Powder Technology, 25 (2014) 43-55.

[167] A. Ziaee, A.B. Albadarin, L. Padrela, T. Femmer, E. O'Reilly, G. Walker, Spray drying of pharmaceuticals and biopharmaceuticals: Critical parameters and experimental process optimization approaches, European Journal of Pharmaceutical Sciences, 127 (2019) 300-318.

[168] B. Chaurasiya, Y.-Y. Zhao, Dry Powder for Pulmonary Delivery: A Comprehensive Review, Pharmaceutics, 13 (2021) 31.

[169] M.S. Hassan, R.W.M. Lau, Effect of particle shape on dry particle inhalation: study of flowability, aerosolization, and deposition properties, Aaps Pharmscitech, 10 (2009) 1252.

[170] Q.T. Zhou, T. Gengenbach, J.A. Denman, H.Y. Heidi, J. Li, H.K. Chan, Synergistic antibiotic combination powders of colistin and rifampicin provide high aerosolization efficiency and moisture protection, The AAPS journal, 16 (2014) 37-47.

[171] W. Kaialy, A review of factors affecting electrostatic charging of pharmaceuticals and adhesive mixtures for inhalation, International Journal of Pharmaceutics, 503 (2016) 262-276.

[172] T.T. Thorben Fischer, Franziska Drews, Kristina Brix, Carola Meier, Martin Simon, Ralf Kautenburger, Marc Schneider, European Journal of Pharmaceutical Sciences, (accepted).

[173] N. Daum, C. Tscheka, A. Neumeyer, M. Schneider, Novel approaches for drug delivery systems in nanomedicine: effects of particle design and shape, Wiley Interdisciplinary Reviews: Nanomedicine and Nanobiotechnology, 4 (2012) 52-65.

[174] D.A.L. Kohler, Asymmetric particles for pulmonary drug delivery, (2010).

[175] T. Tschernig, T. Fischer, A. Grissmer, A. Beckmann, C. Meier, P. Lipp, M. Schneider, Silica nanoparticles of microrods enter lung epithelial cells, Biomedical reports, 9 (2018) 156-160.

[176] R. Aquino, L. Prota, G. Auriemma, A. Santoro, T. Mencherini, G. Colombo, P. Russo, Dry powder inhalers of gentamicin and leucine: formulation parameters, aerosol performance and in vitro toxicity on CuFi1 cells, International journal of pharmaceutics, 426 (2012) 100-107.

[177] C. Weiler, M. Egen, M. Trunk, P. Langguth, Force control and powder dispersibility of spray dried particles for inhalation, Journal of pharmaceutical sciences, 99 (2010) 303-316.

[178] L. Borgström, On the use of dry powder inhalers in situations perceived as constrained, Journal of aerosol medicine, 14 (2001) 281-287.

[179] S.P. Newman, F. Morén, E. Trofast, N. Talaee, S.W. Clarke, Terbutaline sulphate Turbuhaler: effect of inhaled flow rate on drug deposition and efficacy, International journal of pharmaceutics, 74 (1991) 209-213.

[180] M.E. Abdelrahim, H. Chrystyn, Aerodynamic characteristics of nebulized terbutaline sulphate using the next generation impactor (NGI) and CEN method, Journal of aerosol medicine and pulmonary drug delivery, 22 (2009) 19-28.

[181] A. Torge, G. Pavone, M. Jurisic, K. Lima-Engelmann, M. Schneider, A comparison of spherical and cylindrical microparticles composed of nanoparticles for pulmonary application, Aerosol Science and Technology, 53 (2019) 53-62.

[182] C. Darquenne, J.S. Fleming, I. Katz, A.R. Martin, J. Schroeter, O.S. Usmani, J. Venegas, O. Schmid, Bridging the gap between science and clinical efficacy: physiology, imaging, and modeling of aerosols in the lung, Journal of aerosol medicine and pulmonary drug delivery, 29 (2016) 107-126.

[183] M. Geiser, W.G. Kreyling, Deposition and biokinetics of inhaled nanoparticles, Particle and fibre toxicology, 7 (2010) 2.

[184] J. Heyder, Deposition of inhaled particles in the human respiratory tract and consequences for regional targeting in respiratory drug delivery, Proceedings of the American Thoracic Society, 1 (2004) 315-320.

[185] C. Graf, Silica, Amorphous, Kirk-Othmer Encyclopedia of Chemical Technology, (2000) 1-43.

[186] J. Bousquet, R. Dahl, N. Khaltaev, Global Alliance against Chronic Respiratory Diseases, Eur Respir J, 29 (2007) 233-239.

[187] C.M. Greene, P.S. Hiemstra, Innate Immunity of the Lung, Journal of Innate Immunity, 12 (2020) 1-3.

[188] S. Gordon, Alternative activation of macrophages, Nature reviews immunology, 3 (2003) 23-35.

[189] P.R. Taylor, L. Martinez-Pomares, M. Stacey, H.-H. Lin, G.D. Brown, S. Gordon, Macrophage receptors and immune recognition, Annu. Rev. Immunol., 23 (2005) 901-944.

[190] B.A. Lubamba, L.C. Jones, W.K. O'Neal, R.C. Boucher, C.M. Ribeiro, X-box–binding protein 1 and innate immune responses of human cystic fibrosis alveolar macrophages, American journal of respiratory and critical care medicine, 192 (2015) 1449-1461.

[191] J.B. Rubins, Alveolar macrophages: wielding the double-edged sword of inflammation, in, American Thoracic Society, 2003.

[192] L.M. Sedger, M.F. McDermott, TNF and TNF-receptors: From mediators of cell death and inflammation to therapeutic giants–past, present and future, Cytokine & growth factor reviews, 25 (2014) 453-472.

[193] I. Striz, E. Brabcova, L. Kolesar, A. Sekerkova, Cytokine networking of innate immunity cells: a potential target of therapy, Clinical science, 126 (2014) 593-612.

[194] J. Sznitman, Respiratory microflows in the pulmonary acinus, Journal of biomechanics, 46 (2013) 284-298.

[195] A. Ari, J.B. Fink, Recent advances in aerosol devices for the delivery of inhaled medications, Expert Opinion on Drug Delivery, 17 (2020) 133-144.

[196] A. de Fougerolles, T. Novobrantseva, siRNA and the lung: research tool or therapeutic drug?, Current opinion in pharmacology, 8 (2008) 280-285.

[197] M. Thomas, J.J. Lu, J. Chen, A.M. Klibanov, Non-viral siRNA delivery to the lung, Advanced drug delivery reviews, 59 (2007) 124-133.

[198] B. Yu, X. Zhao, L.J. Lee, R.J. Lee, Targeted delivery systems for oligonucleotide therapeutics, The AAPS journal, 11 (2009) 195-203.

[199] R. Juliano, J. Bauman, H. Kang, X. Ming, Biological barriers to therapy with antisense and siRNA oligonucleotides, Molecular pharmaceutics, 6 (2009) 686-695.

[200] M. Cascella, M. Rajnik, A. Cuomo, S.C. Dulebohn, R. Di Napoli, Features, evaluation and treatment coronavirus (COVID-19), in: Statpearls [internet], StatPearls Publishing, 2020.

[201] Y.-C. Chang, Y.-A. Tung, K.-H. Lee, T.-F. Chen, Y.-C. Hsiao, H.-C. Chang, T.-T. Hsieh, C.-H. Su, S.-S. Wang, J.-Y. Yu, Potential therapeutic agents for COVID-19 based on the analysis of protease and RNA polymerase docking, (2020).

[202] A.A. Elfiky, Anti-HCV, nucleotide inhibitors, repurposing against COVID-19, Life sciences, (2020) 117477.

[203] D. Zhou, S.-M. Dai, Q. Tong, COVID-19: a recommendation to examine the effect of hydroxychloroquine in preventing infection and progression, Journal of Antimicrobial Chemotherapy, (2020).

[204] M. Zheng, D. Librizzi, A. Kılıç, Y. Liu, H. Renz, O.M. Merkel, T. Kissel, Enhancing in vivo circulation and siRNA delivery with biodegradable polyethylenimine-graft-polycaprolactone-block-poly (ethylene glycol) copolymers, Biomaterials, 33 (2012) 6551-6558.

[205] N. Durcan, C. Murphy, S.-A. Cryan, Inhalable siRNA: potential as a therapeutic agent in the lungs, Molecular pharmaceutics, 5 (2008) 559-566.

[206] R. Mathaes, G. Winter, A. Besheer, J. Engert, Influence of particle geometry and PEGylation on phagocytosis of particulate carriers, International journal of pharmaceutics, 465 (2014) 159-164.

[207] J. Wong, B.E. Magun, L.J. Wood, Lung inflammation caused by inhaled toxicants: a review, International journal of chronic obstructive pulmonary disease, 11 (2016) 1391.

[208] R. Mohamud, S.D. Xiang, C. Selomulya, J.M. Rolland, R.E. O'Hehir, C.L. Hardy, M. Plebanski, The effects of engineered nanoparticles on pulmonary immune homeostasis, Drug metabolism reviews, 46 (2014) 176-190.

[209] D.M. Smith, J.K. Simon, J.R. Baker Jr, Applications of nanotechnology for immunology, Nature Reviews Immunology, 13 (2013) 592-605.

[210] I. Esteban-Gorgojo, D. Antolin-Amerigo, J. Dominguez-Ortega, S. Quirce, Non-eosinophilic asthma: current perspectives, J Asthma Allergy, 11 (2018) 267-281.

[211] A.A. and, D.M. Underhill, MECHANISMS OF PHAGOCYTOSIS IN MACROPHAGES, Annual Review of Immunology, 17 (1999) 593-623.

[212] P.O. Andersson, C. Lejon, B. Ekstrand-Hammarström, C. Akfur, L. Ahlinder, A. Bucht, L. Österlund, Polymorph-and size-dependent uptake and toxicity of TiO2 nanoparticles in living lung epithelial cells, Small, 7 (2011) 514-523.

[213] D.A. Kuhn, D. Vanhecke, B. Michen, F. Blank, P. Gehr, A. Petri-Fink, B. Rothen-Rutishauser, Different endocytotic uptake mechanisms for nanoparticles in epithelial cells and macrophages, Beilstein journal of nanotechnology, 5 (2014) 1625-1636.

[214] L. Shachar-Berman, Y. Ostrovski, K. Koshiyama, S. Wada, S.C. Kassinos, J. Sznitman, Targeting inhaled fibers to the pulmonary acinus: Opportunities for augmented delivery from in silico simulations, European Journal of Pharmaceutical Sciences, 137 (2019) 105003.

[215] S. Murugadoss, D. Lison, L. Godderis, S. Van Den Brule, J. Mast, F. Brassinne, N. Sebaihi, P.H. Hoet, Toxicology of silica nanoparticles: an update, Arch Toxicol, 91 (2017) 2967-3010.

[216] H.J. Park, J.-H. Sohn, Y.-J. Kim, Y.H. Park, H. Han, K.H. Park, K. Lee, H. Choi, K. Um, I.-H. Choi, J.-W. Park, J.-H. Lee, Acute exposure to silica nanoparticles aggravate airway inflammation: different effects according to surface characteristics, Experimental & Molecular Medicine, 47 (2015) e173-e173.

[217] S. Brennan, P. Sly, C. Gangell, N. Sturges, K. Winfield, M. Wikstrom, S. Gard, J. Upham, Alveolar macrophages and CC chemokines are increased in children with cystic fibrosis, European Respiratory Journal, 34 (2009) 655-661.

[218] E. Berg, P. Lamb, A. Ali, J. Dennis, M. Tservistas, J. Mitchell, Assessment of the need to coat particle collection cups of the NGI to mitigate droplet bounce when evaluating nebuliser-produced droplets, Pharmeuropa scientific notes, 2008 (2008) 21-25.

[219] L. Li, S.S.Y. Leung, T. Gengenbach, J. Yu, G.F. Gao, P. Tang, Q.T. Zhou, H.-K. Chan, Investigation of L-leucine in reducing the moisture-induced deterioration of spray-dried salbutamol sulfate power for inhalation, International Journal of Pharmaceutics, 530 (2017) 30-39.

[220] A.T. Lada, L.L. Rudel, R.W.S. Clair, Effects of LDL enriched with different dietary fatty acids on cholesteryl ester accumulation and turnover in THP-1 macrophages, Journal of lipid research, 44 (2003) 770-779.

[221] A. Stefaniak, R. Guilmette, G. Day, M. Hoover, P.N. Breysse, R. Scripsick, Characterization of phagolysosomal simulant fluid for study of beryllium aerosol particle dissolution, Toxicology in vitro, 19 (2005) 123-134.

[222] H. Goldshtein, M.J. Hausmann, A. Douvdevani, A rapid direct fluorescent assay for cell-free DNA quantification in biological fluids, Annals of clinical biochemistry, 46 (2009) 488-494.

[223] W. Finlay, K. Stapleton, P. Zuberbuhler, Fine particle fraction as a measure of mass depositing in the lung during inhalation of nearly isotonic nebulized aerosols, Journal of aerosol science, 28 (1997) 1301-1309.

[224] V. Marple, B. Olson, K. Santhanakrishnan, D. Roberts, J. Mitchell, B. Hudson-Curtis, Calibration of the archival next generation pharmaceutical impactor (NGI) at 15 L/min, Drug Deliv Lung, 14 (2003) 37-40.

[225] W. Liang, A.Y. Chan, M.Y. Chow, F.F. Lo, Y. Qiu, P.C. Kwok, J.K. Lam, Spray freeze drying of small nucleic acids as inhaled powder for pulmonary delivery, asian journal of pharmaceutical sciences, 13 (2018) 163-172.

[226] R.S. Tuma, M.P. Beaudet, X. Jin, L.J. Jones, C.-Y. Cheung, S. Yue, V.L. Singer, Characterization of SYBR Gold nucleic acid gel stain: a dye optimized for use with 300-nm ultraviolet transilluminators, Analytical biochemistry, 268 (1999) 278-288.

[227] E.C. Dreaden, S.W. Morton, K.E. Shopsowitz, J.-H. Choi, Z.J. Deng, N.-J. Cho, P.T. Hammond, Bimodal tumor-targeting from microenvironment responsive hyaluronan layer-by-layer (LbL) nanoparticles, ACS nano, 8 (2014) 8374-8382.

[228] E. Ansoborlo, M. Henge-Napoli, V. Chazel, R. Gibert, R. Guilmette, Review and critical analysis of available in vitro dissolution tests, Health Physics, 77 (1999) 638-645.

[229] S.M. Levitz, S.-H. Nong, K.F. Seetoo, T.S. Harrison, R.A. Speizer, E.R. Simons, Cryptococcus neoformans resides in an acidic phagolysosome of human macrophages, Infection and immunity, 67 (1999) 885-890.

[230] K. Yoshida, K. Sato, J.-i. Anzai, Layer-by-layer polyelectrolyte films containing insulin for pH-triggered release, Journal of Materials Chemistry, 20 (2010) 1546-1552.

[231] D.K. Armstrong, S. Cunningham, J.C. Davies, E.W.F. Alton, Gene therapy in cystic fibrosis, Archives of disease in childhood, 99 (2014) 465-468.

[232] M. Lieber, G. Todaro, B. Smith, A. Szakal, W. Nelson-Rees, A continuous tumor-cell line from a human lung carcinoma with properties of type II alveolar epithelial cells, International journal of cancer, 17 (1976) 62-70.

[233] M. Oberhofer, Q. Tian, S. Ruppenthal, S. Wegener, J.-C. Reil, C. Körbel, K. Hammer, M. Menger, H.-R. Neuberger, L. Kaestner, Calcium dysregulation in ventricular myocytes from mice expressing constitutively active Rac1, Cell Calcium, 54 (2013) 26-36.

[234] J.E. Rash, H.S. Duffy, F.E. Dudek, B.L. Bilhartz, L.R. Whalen, T. Yasumura, Grid-mapped freeze-fracture analysis of gap junctions in gray and white matter of adult rat central nervous system, with evidence for a "panglial syncytium" that is not coupled to neurons, Journal of Comparative Neurology, 388 (1997) 265-292.

[235] E. Diler, M. Schwarz, R. Nickels, M.D. Menger, C. Beisswenger, C. Meier, T. Tschernig, Influence of external calcium and thapsigargin on the uptake of polystyrene beads by the macrophage-like cell lines U937 and MH-S, BMC Pharmacology and Toxicology, 15 (2014) 1-11.

[236] S. Mirza, R.D. Clay, M.A. Koslow, P.D. Scanlon, COPD guidelines: a review of the 2018 GOLD report, in: Mayo Clinic Proceedings, Elsevier, 2018, pp. 1488-1502.

[237] G.J. Rodrigo, C. Rodrigo, J.B. Hall, Acute asthma in adults: a review, Chest, 125 (2004) 1081-1102.

[238] S.D. Strausbaugh, P.B. Davis, Cystic fibrosis: a review of epidemiology and pathobiology, Clinics in chest medicine, 28 (2007) 279-288.

[239] L.H. Chin, C.M. Hon, D.K. Chellappan, J. Chellian, T. Madheswaran, F. Zeeshan, R. Awasthi, A.A. Aljabali, M.M. Tambuwala, H. Dureja, Molecular mechanisms of action of naringenin in chronic airway diseases, European Journal of Pharmacology, (2020) 173139.

[240] T.I. Lee, R.A. Young, Transcriptional regulation and its misregulation in disease, Cell, 152 (2013) 1237-1251.

[241] S. Rezaei, M. Mahjoubin-Tehran, S.H. Aghaee-Bakhtiari, A. Jalili, A. Movahedpour, H. Khan, M. Moghoofei, Z. Shojaei, M.R. Hamblin, H. Mirzaei, Autophagy-related MicroRNAs in chronic lung diseases and lung cancer, Critical Reviews in Oncology/Hematology, (2020) 103063.

[242] D.R. Samuelson, D.A. Welsh, J.E. Shellito, Regulation of lung immunity and host defense by the intestinal microbiota, Frontiers in microbiology, 6 (2015) 1085.

[243] D.K. Singh, R.K. Thakur, Dry Powder Inhalers, Journal of Critical Reviews, 7 (2020) 915-920.

[244] Nanologica, NLAB Spiro™, (2020).

[245] R. Narayan, U.Y. Nayak, A.M. Raichur, S. Garg, Mesoporous silica nanoparticles: A comprehensive review on synthesis and recent advances, Pharmaceutics, 10 (2018) 118.

[246] M. Manzano, M. Vallet-Regí, Mesoporous silica nanoparticles for drug delivery, Advanced Functional Materials, 30 (2020) 1902634.

[247] R.R. Castillo, D. Lozano, M. Vallet-Regí, Mesoporous silica nanoparticles as carriers for therapeutic biomolecules, Pharmaceutics, 12 (2020) 432.

[248] A. Mehmood, H. Ghafar, S. Yaqoob, U.F. Gohar, B. Ahmad, Mesoporous silica nanoparticles: a review, J. Dev. Drugs, 6 (2017).

[249] F.N. Crespilho, V. Zucolotto, O.N. Oliveira Jr, F.C. Nart, Electrochemistry of layer-by-layer films: a review, Int. J. Electrochem. Sci, 1 (2006) 194-214.

[250] S.K. Sadozai, S.A. Khan, N. Karim, D. Becker, N. Steinbrück, S. Gier, A. Baseer, F. Breinig, G. Kickelbick, M. Schneider, Ketoconazole-loaded PLGA nanoparticles and their synergism against Candida albicans when combined with silver nanoparticles, Journal of Drug Delivery Science and Technology, 56 (2020) 101574.

[251] P. Anand, A.B. Kunnumakkara, R.A. Newman, B.B. Aggarwal, Bioavailability of curcumin: problems and promises, Molecular pharmaceutics, 4 (2007) 807-818.

[252] M. Kharat, Z. Du, G. Zhang, D.J. McClements, Physical and chemical stability of curcumin in aqueous solutions and emulsions: impact of pH, temperature, and molecular environment, Journal of agricultural and food chemistry, 65 (2017) 1525-1532.

[253] B. Hu, L. Zhong, Y. Weng, L. Peng, Y. Huang, Y. Zhao, X.-J. Liang, Therapeutic siRNA: state of the art, Signal transduction and targeted therapy, 5 (2020) 1-25.

[254] D. Tracey, L. Klareskog, E.H. Sasso, J.G. Salfeld, P.P. Tak, Tumor necrosis factor antagonist mechanisms of action: a comprehensive review, Pharmacology & therapeutics, 117 (2008) 244-279.

[255] K.N. Pham, D. Fullston, K. Sagoe-Crentsil, Surface charge modification of nano-sized silica colloid, Australian Journal of Chemistry, 60 (2007) 662-666.

[256] G. Xie, J. Sun, G. Zhong, L. Shi, D. Zhang, Biodistribution and toxicity of intravenously administered silica nanoparticles in mice, Archives of toxicology, 84 (2010) 183-190.

[257] P. Chenebault, A. Schürenkämper, The Measurement of Small Surface Areas by the BET Adsorption Method1, The Journal of Physical Chemistry, 69 (1965) 2300-2305.

[258] G. Decher, J.D. Hong, Buildup of ultrathin multilayer films by a self-assembly process, 1 consecutive adsorption of anionic and cationic bipolar amphiphiles on charged surfaces, in: Makromolekulare Chemie. Macromolecular Symposia, Wiley Online Library, 1991, pp. 321-327.

[259] T. Benhalima, H. Ferfera-Harrar, Eco-friendly porous carboxymethyl cellulose/dextran sulfate composite beads as reusable and efficient adsorbents of cationic dye methylene blue, International journal of biological macromolecules, 132 (2019) 126-141.

[260] R. Heo, D.G. You, W. Um, K.Y. Choi, S. Jeon, J.-S. Park, Y. Choi, S. Kwon, K. Kim, I.C. Kwon, Dextran sulfate nanoparticles as a theranostic nanomedicine for rheumatoid arthritis, Biomaterials, 131 (2017) 15-26.

[261] R. Vehring, Pharmaceutical particle engineering via spray drying, Pharmaceutical research, 25 (2008) 999-1022.

[262] P.C. Seville, T. Learoyd, H.-Y. Li, I. Williamson, J.C. Birchall, Amino acid-modified spray-dried powders with enhanced aerosolisation properties for pulmonary drug delivery, Powder technology, 178 (2007) 40-50.

[263] A. Feng, M. Boraey, M. Gwin, P. Finlay, P. Kuehl, R. Vehring, Mechanistic models facilitate efficient development of leucine containing microparticles for pulmonary drug delivery, International journal of pharmaceutics, 409 (2011) 156-163.

[264] K.A. Foster, C.G. Oster, M.M. Mayer, M.L. Avery, K.L. Audus, Characterization of the A549 cell line as a type II pulmonary epithelial cell model for drug metabolism, Experimental cell research, 243 (1998) 359-366.

[265] J.C. Stockert, R.W. Horobin, L.L. Colombo, A. Blázquez-Castro, Tetrazolium salts and formazan products in Cell Biology: Viability assessment, fluorescence imaging, and labeling perspectives, Acta histochemica, 120 (2018) 159-167.

[266] Y. Fu, W.J. Kao, Drug release kinetics and transport mechanisms of non-degradable and degradable polymeric delivery systems, Expert opinion on drug delivery, 7 (2010) 429-444.

[267] C.F. Barbas, D.R. Burton, J.K. Scott, G.J. Silverman, Quantitation of DNA and RNA, Cold Spring Harbor Protocols, 2007 (2007) pdb. ip47.

[268] R.M. Lequin, Enzyme immunoassay (EIA)/enzyme-linked immunosorbent assay (ELISA), Clinical chemistry, 51 (2005) 2415-2418.

[269] J. Sun, H. Shigemi, M. Cao, E. Qin, J. Tang, J. Shen, H. Iwasaki, Minocycline induces autophagy and inhibits cell proliferation in LPS-stimulated THP-1 cells, BioMed Research International, 2020 (2020).

[270] C.S. Clay, G.W. Peace, Ion beam sputtering: an improved method of metal coating SEM samples and shadowing CTEM samples, Journal of Microscopy, 123 (1981) 25-34.

[271] P.G. Jeelani, P. Mulay, R. Venkat, C. Ramalingam, Multifaceted application of silica nanoparticles. A review, Silicon, 12 (2020) 1337-1354.

[272] Y. Hurtado, C. Beltrán, R.D. Zabala, S.H. Lopera, C.A. Franco, N.N. Nassar, F.B. Cortés, Effects of surface acidity and polarity of SiO2 nanoparticles on the foam stabilization applied to natural gas flooding in tight gas-condensate reservoirs, Energy & fuels, 32 (2018) 5824-5833.

[273] L. Slika, D. Patra, A short review on chemical properties, stability and nano-technological advances for curcumin delivery, Expert Opinion on Drug Delivery, 17 (2020) 61-75.

[274] A. Aderem, D.M. Underhill, Mechanisms of phagocytosis in macrophages, Annual review of immunology, 17 (1999) 593-623.

[275] D. Alkekhia, P.T. Hammond, A. Shukla, Layer-by-layer biomaterials for drug delivery, Annual review of biomedical engineering, (2020).

[276] K.C. Wood, J.Q. Boedicker, D.M. Lynn, P.T. Hammond, Tunable drug release from hydrolytically degradable layer-by-layer thin films, Langmuir, 21 (2005) 1603-1609.

[277] Y. Wang, Q. Zhao, N. Han, L. Bai, J. Li, J. Liu, E. Che, L. Hu, Q. Zhang, T. Jiang, Mesoporous silica nanoparticles in drug delivery and biomedical applications, Nanomedicine: Nanotechnology, Biology and Medicine, 11 (2015) 313-327.

[278] S. Hassanzadeh, M.I. Read, A.R. Bland, M. Majeed, T. Jamialahmadi, A. Sahebkar, Curcumin: an inflammasome silencer, Pharmacological Research, (2020) 104921.

[279] Z. Tang, Y. Wang, P. Podsiadlo, N.A. Kotov, Biomedical applications of layer-by-layer assembly: from biomimetics to tissue engineering, Advanced materials, 18 (2006) 3203-3224.

[280] M.I. Sajid, M. Moazzam, S. Kato, K. Yeseom Cho, R.K. Tiwari, Overcoming Barriers for siRNA Therapeutics: From Bench to Bedside, Pharmaceuticals, 13 (2020) 294.

[281] D.M. Soni, Strategies and Approaches for siRNA Delivery, Journal of Drug Delivery and Therapeutics, 10 (2020) 239-250.

[282] F. Pittella, G.A.V. Abcs, G. Acm, Short Interfering RNA (siRNA) based Medicines and the Future of RNAi Therapy: A Mini Review, Current Trends in Biomedical Engineering & Biosciences, 19 (2020) 116-121.

[283] A.J. Hibbitts, J.M. Ramsey, J. Barlow, R. MacLoughlin, S.-A. Cryan, In Vitro and In Vivo Assessment of PEGylated PEI for Anti-IL-8/CxCL-1 siRNA Delivery to the Lungs, Nanomaterials, 10 (2020) 1248.

[284] M. Möhwald, Aspherical, Nanostructured Microparticles For Pulmonary Gene Delivery To Alveolar Macrophages, (2017).

[285] S.K. Natarajan, S. Selvaraj, Mesoporous silica nanoparticles: importance of surface modifications and its role in drug delivery, RSC advances, 4 (2014) 14328-14334.

[286] A.B. Nik, H. Zare, S. Razavi, H. Mohammadi, P.T. Ahmadi, N. Yazdani, M. Bayandori, N. Rabiee, J.I. Mobarakeh, Smart drug delivery: Capping strategies for mesoporous silica nanoparticles, Microporous and Mesoporous Materials, 299 (2020) 110115.

[287] F.R. Wibowo, O.A. Saputra, W.W. Lestari, M. Koketsu, R.R. Mukti, R. Martien, pH-triggered drug release controlled by poly (styrene sulfonate) growth hollow mesoporous silica nanoparticles, ACS omega, 5 (2020) 4261-4269.

[288] A.F. Moreira, D.R. Dias, I.J. Correia, Stimuli-responsive mesoporous silica nanoparticles for cancer therapy: A review, Microporous and Mesoporous Materials, 236 (2016) 141-157.

10. Scientific output

Articles

T. Tschernig*, **T. Fischer***, A. Grissmer, A. Beckmann, C. Meier, P. Lipp, M. Schneider
Silica nanoparticles of microrods enter lung epithelial cells, Biomedical reports, 9 (**2018**) 156-160.

A.-V. Weiss, **T. Fischer**, J. Iturri, R. Benitez, J.L. Toca-Herrera, M. Schneider
Mechanical properties of gelatin nanoparticles in dependency of crosslinking time and storage, Colloids and Surfaces B: Biointerfaces, 175 (**2019**) 713-720.

T. Fischer, T. Tschernig, F. Drews, K. Brix, C. Meier, M. Simon, R. Kautenburger, M. Schneider
siRNA delivery to macrophages using aspherical, nanostructured microparticles as delivery system for pulmonary administration, European Journal of Pharmaceutics and Biopharmaceutics, 158 (**2021**) 284-293.

T. Fischer, A. Koenneke, M. Schneider
Comparison between the aerodynamic properties of cylindrical, aspherical microparticles and their spherical counterparts using Next Generation Impactor
(submitted)

T. Fischer, I. Winter, R. Drumm, M. Schneider
Cylindrical microparticles composed of mesoporous silica nanoparticles for the targeted delivery of curcumin and siRNA to the lungs: exemplified with curcumin and siRNA
(submitted)

*contributed equally

Oral presentations

Specific targeting of human macrophages using aspherical microparticles as gene delivery system

T. Fischer, T. Tschernig, F. Drews, M. Simon, J. Metz, M. Schneider

12th International Conference and Workshop on Biological Barriers, Saarbrücken, Germany, **2018** (Best oral presentation award).

Aspherical microparticles composed from nanoparticles for gene delivery to alveolar macrophages

T. Fischer, M. Schneider

2nd Annual Inhalation and Respiratory, Drug Development Summit, Barcelona, Spain, **2018**.

Cytokine inhibition by aspheric drug carriers for pulmonary administration

T. Fischer, T. Tschernig, F. Drews, M. Simon, M. Schneider

23rd annual meeting, CRS Germany Local Chapter, Leipzig, Germany, **2019**.

Poster presentations

Development of nanostructured, aspherical microparticles for pulmonary application

T. Fischer, M. Schneider

22nd annual meeting, CRS Germany Local Chapter, Halle, Germany, **2018**.

Pulmonary gene delivery by aspherical microparticles

T. Fischer, T. Tschernig, F. Drews, M. Simon, M. Schneider

6th Galenus Workshop, Development & Translation of Bioresponsive Drug Delivery Systems & Medical Devices, Würzburg, Germany, **2018**.

Specific targeting of human macrophages using aspherical microparticles as gene delivery system

T. Fischer, T. Tschernig, F. Drews, M. Simon, J. Metz, M. Schneider

12th International Conference and Workshop on Biological Barriers, Saarbrücken, Germany, **2018**.

Development of a novel drug carrier system for specific targeting of human macrophages

T. Fischer, S. Al-Fityan, A. Dembek, B. Diesel, A. K. Kiemer, M. Schneider

8th HIPS Symposium on pharmaceutical sciences devoted to infection research, Saarbrücken, Germany, **2018**.

Evaluating the mechanical Properties of Gelatin Nanoparticles and the Influence on cellular Uptake

A.-V. Weiss, **T. Fischer**, M. Schneider

45th Annual Meeting Exposition of the Controlled Release Society, New York, **2018**.

Nanoindentation in Scanning Probe Microscopy – A powerful Tool to determine mechanical Properties of Gelatin Nanoparticles

A.-V. Weiss, **T. Fischer**, M. Schneider

International PhD students/Postdocs meeting 2018 of the German Pharmaceutical Society (DPhG), Bad Dürkheim, Germany, **2018**.

Novel drug carrier systems for the specific repolarization of human macrophages

S. Al-Fityan, **T. Fischer,** B. Diesel, Schneider, A. K. Kiemer

9th HIPS Symposium on pharmaceutical sciences devoted to infection research, Saarbrücken, Germany, **2019**.

Aspherical silica microparticles as drug delivery system: Effects on viability and primary human macrophages polarisation

S. Al-Fityan, B. Diesel, **T. Fischer,** M. Schneider, A. K. Kiemer

Nanosafety virtual conference, **2020**.

Downregulation of TNF-alpha levels in lung disease using aspheric microparticles as gene delivery system to alveolar macrophages

T. Fischer, T. Tschernig, F. Drews, M. Simon, M. Schneider

24th annual meeting, CRS Germany Local Chapter, München, Germany, **2020**.

11. Curriculum vitae

Thorben Fischer

*November 9, 1992 in Saarbrücken

Nov. 2020 – April 2021   Practical training in public pharmacy
Paracelsus Apotheke, Saarbrücken

Mai 2017 – Oct. 2020   Doctoral Thesis, Saarland University
Working group: Prof. Dr. Schneider
Biopharmaceutics and Pharmaceutical Technology
Topic: Development of novel nanostructured drug carrier systems for targeting of human macrophages for inhalation treatment

Oct. 2017   Diploma - Pharmacist

Nov. 2016 – April 2017   Diploma Thesis, Saarland University
Working group: Prof. Dr. Schneider
Biopharmaceutics and Pharmaceutical Technology
Topic: Untersuchung der zellulären Aufnahme von Gelatinenanopartikeln in Abhängigkeit der Elastizität

March 2015 – April 2018   Student assistant at RpDoc® Solutions GmbH, Saarbrücken

April 2012 – Sep. 2016   Studies in Pharmacy, Saarland University

Oct. 2011 – March 2012   Studies in Chemistry, Saarland University

June 2011   General qualification for university entrance (Abitur)
Warndtgymnasium Geislautern

12. Acknowledgement

Furthermore, I would like to thank PD Dr. Anette Kraegeloh and Dr. Jana Fleddermann from the Institute of New Materials for allowing me to use their CLSM when ours was broken.

I thank the whole DDEL and BION group of HIPS for the exciting and scientific PhD seminars both in Saarbrücken and in Bacharach. Here I would like to emphasize Justus and remind of the legendary Bierkönig visits, as well as the trip to Malle.

Then I would also like to mention my students who have accompanied me in the lab either in the form of the elective internship or as master student. Tim, Sonja and Inga, you have done a really good job, thank you.

Here I would like to thank Peter, Marijas and Isabelle in special, who were always there with help and advice when organizational or lab-specific problems arose. You really made the work at the institute easier and supported me in many situations. Thank you.

A very special thanks goes to all former and current colleagues of the Schneider Group. Here I want to highlight Sarah, Tamara, Afra, Daniel P., Alina, Enkeleda, Camilla, Nesma, Salma AbdelHafez, Baseer, Michi, Mohammad, Daniel S., Marie-Sophie, Sabrina, Jörg, Sonia, Karola, Elena, Tom and Julia.

I would especially like to thank my long-time office colleague Alexandra, who always had an open ear for the ups and downs of the PhD and who was always on hand for a convivial drink ;-) Thank you Alex.

Then I would also like to thank Johannes for the interesting and absolutely non-aggressive soccer talk :D. It was always very exhilarating to chat with you about God and the world. Of course, the grandiose trip to Malle must be mentioned here, which was still brilliant despite little legroom of Spain. Thank you.

Then I would like to thank especially my friends Joschi, Marci, Caro and Agnes. With you I could experience many crazy trips, like the life-threatening ski vacations with the subsequent highlight in the ''Après-Ski Pilz'', as well as the vice-championship in an international frisbee tournament :D I am very happy to have met you in the working group. This made the long way of the PhD much easier. Thank you, guys.

I especially want to thank Agnes, for her great support during the writing of the thesis, both with the language check and with all questions around the work. Thank you, Agnes.

The opportunity to go this long way was only possible with the help of my family, who always supported me. Therefore, I would like to especially thank my parents Roman and Ulrike, as well as my brother Eric. All this would not have been possible without you.

Finally, I would like to thank Maria, who was always by my side and accompanied me through all the ups and downs. Thank you for your loving support and patience for me during this long time.